EVOLUTION OF THE FLAMMABILITY ENVIRONMENT SURROUNDING LITHIUM-ION BATTERY FAILURES

by

SIMONE MARIE MUEHLHAUSEN HILL

Submitted in Partial Fulfillment
of the Requirements for the Degree of
Master of Science in Mechanical Engineering
with Specialization in Mechatronics

New Mexico Institute of Mining and Technology
Socorro, New Mexico
November, 2022

ABSTRACT

Failure of lithium-ion batteries can result in venting of gases which pose a significant flammability risk. As a failing cell vents, the flammability of the surrounding environment changes, and the composition of the vented gases determines the flammability risks. The flammability environment surrounding the failing 18650 format cells was studied here through both analytical and experimental methods. An analytical reduced-order model was built to simulate the venting of the failing cell and study the evolution of the environment flammability as a function of time. The model compares the system composition to the flammability limits of species vented out of the cell. Experimental thermal abuse testing was performed on individual cells to dynamically capture gaseous samples vented from the cells. Two analytical chemistry techniques were used to analyze the collected samples: Fourier-Transform Infrared Spectroscopy (FTIR) and Mass Spectrometry (MS). From the experimental testing, it was found that the majority of the vented material was dimethyl carbonate, a component from the liquid electrolyte solvent which is flammable, and water vapor. After determining the mean partial pressures for both dimethyl carbonate and water from the mass spectrometry data, the upper and lower limits of these partial pressures were also determined using 95% confidence intervals. Simulations were then performed using the analytical model incorporating the different partial pressures for the two species. From the model simulations, it was found that no volume above 1.1275 m^3 should become flammable for a single failing cell. It was also found that any volume less than or equal to 0.3695 m^3 reaches a dimethyl carbonate to air mass ratio that surpasses the upper flammability limit. The model provides a foundation for safety assessment that could easily be built upon. The experimental test method developed allowed for the chemical composition of the vented material from the failing cells to be studied, which lent to the risk assessment from the model. The methods developed here could be applied to other cell geometries and chemistries.

Keywords: Lithium-ion battery; Flammability environment; Flammability limit; Vacuum grab sampling; Dimethyl carbonate

ACKNOWLEDGMENTS

I would like to thank my research adviser Dr. Michael Hargather for his support throughout my graduate and undergraduate careers. Thank you for the guidance with my research and with my academic path and for providing me with so many opportunities.

I want to thank Dr. Joshua Lamb and Dr. Loraine Torres-Castro at Sandia National Laboratories for counsel and funding through PO 1989037, PO 2201527, and PO 2371397, which allowed this research to be possible. I would also like to thank Dr. Gayan Rubasinghege for his assistance throughout this research.

To all of the members of the Shock and Gas Dynamics Laboratory, thank you for your assistance and support throughout this research. Thank you all for being wonderful lab mates and friends.

I want to thank Isaiah for being by my side. You are such an amazing partner and your dedicated support means so much to me. Thank you for always having my back and looking out for me.

I also want to thank all of my family for their constant encouragement and love. I am eternally grateful for my parents, Mike and Shanon, for supporting me throughout everything, for pushing me to pursue my passions, and for always being there for me. Thank you both for your love and patience as I grew into who I am today. I also want to thank Dan for being a part of my support system. The three of you have allowed me to follow such a wonderful path and to continue to do so. I dedicate this work to my parents as well as to Linda Egge, and I am so thankful that I have such amazing people to dedicate this work to.

CONTENTS

LIST OF TABLES

LIST OF FIGURES

This thesis is accepted on behalf of the faculty of the Institute by the following committee:

Michael Hargather

Academic and Research Advisor

Andrei Zagrai

Loraine Torres-Castro

Gayan Rubasinghege

I release this document to the New Mexico Institute of Mining and Technology.

SIMONE MARIE MUEHLHAUSEN HILL November 29, 2022

CHAPTER 1

INTRODUCTION

1.1 Research motivation

The increase in lithium-ion battery (LIB) use in the consumer market and in general energy storage poses the need for safety assessments of these energy storage devices. LIBs have a wide range of applications and are being adopted or have been used in different systems including: electric vehicles, consumer electronics, and grid-scale energy storage [15, 22, 38]. Lithium-ion batteries are highly beneficial due to their high specific energy, energy density, efficiency, and life span.

Although LIBs are becoming more widely used and show promise for further wide-spread use, they also pose a safety risk as the failure of these cells is often volatile and dangerous. The flammability risks present at failure have been studied in literature [7, 30, 38]. During failure, lithium-ion batteries often vent out flammable mixtures caused by the break-down of the cell components. These mixtures are easily ignited and can cause catastrophic failure, especially in grid-storage applications. The break-down of the cells has been studied, and the general composition of the mixture can be predicted, but based on manufacturing and chemical differences in the cell components, the exact make-up can be difficult to determine [12, 15, 19, 34].

Studying the evolving flammability environment surrounding failing cells could provide necessary information for risk management. Therefore, research to characterize the chemical composition of the environment around failing cells, and development of tools to simulate the environment with the inclusion of the chemistry are the primary focus of this work.

1.2 Details of lithium-ion batteries

1.2.1 Lithium-ion battery anatomy and failure mode

The cell anatomy is essential to understand the failure modes and mechanics of LIBs. LIBs are composed of an anode, cathode, separator material, and electrolyte mixture inside a casing [12]. The cell casing also consists of terminals and safety mechanisms like current interrupt devices [22]. The main components of an LIB in a cylindrical configuration is shown below in Figure 1.1.

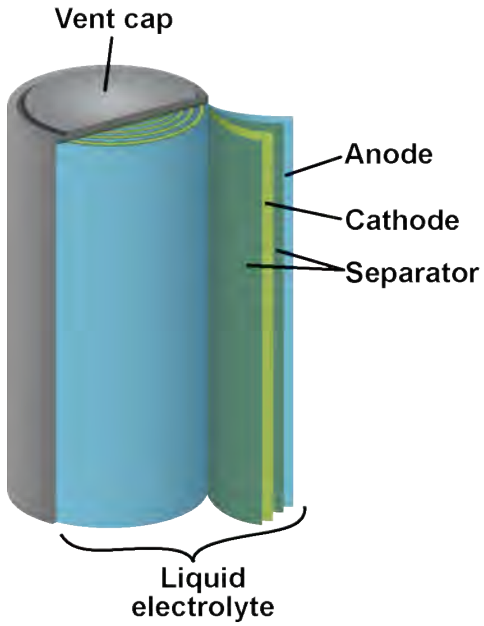

Figure 1.1: Schematic of a lithium-ion battery in a cylindrical configuration

Some common cathode configurations include lithium layered oxides (LCO - lithium cobalt oxide, NMC - lithium nickel cobalt manganese oxide, NCA - lithium nickel cobalt aluminum oxide), lithium manganese oxide (LMO), and lithium iron phosphate (LFP) [12, 21, 38]. The cathode material is the typical identifier used in LIBs, as it is the main factor in battery performance. The anodes in LIBs are often made of one of the following materials: graphite, graphene, lithium titanate, lithium metal, or titanium niobium oxides [12]. The separators usually consist of: polyolefin separators (polyethylene, polypropylene) or polyvinulidene fluoride (PVdF). Separators assist battery operation by holding electrolyte liquid between the two electrodes [12]. The electrolyte mixture is often composed of carbonate solvents, including some common ones such as: ethylene carbonate (EC), diethyl carbonate (DEC), dimethyl carbonate (DMC), and ethyl methyl carbonate (EMC) [15]. The electrolyte also often contains Lithium hexafluorophosphate ($LiPF_6$).

Certain scenarios can cause thermal runaway in LIBs: overcharging, over dis-charging, thermal abuse of both high and low temperatures, mechanical abuse, electric abuse, manufacturing defects, age or normal wear, and combinations of these scenarios [12, 22, 38]. Operating conditions to prevent all failure modes are thus limited. Even with ideal operating conditions, LIBs have the chance of failure, presenting flammability and safety hazards. The sensitivity of the cells to these failure modes is still relatively unknown, which delivers an even greater necessity for the assessment of failure scenarios and hazards.

Each potential failure scenarios causes failure due to certain components of the cell. Each component - the cathode, anode, electrolyte, and separator - can contribute to failure through different scenarios. Many of these failure modes result in thermal runaway. When LIBs go into thermal runaway, gases are produced from the decomposition of the electrolyte liquid in the cells. The gases produced build up pressure in the cell, which could cause the case to rupture violently. Because of this, battery vent caps are built into most cells. These vent caps are a safety device that allows the built-up gases to rupture a small disk and flow out of the cell, relieving the pressure [22]. The rupture of the disk also breaks the circuit within the battery. Although this prevents energetic failure of the cell casing, the vented gases are often flammable and, if allowed to ignite, can still cause extremely dangerous failure situations.

The general composition of the cell electrolyte is often known to the manufacturer, but may not be explicitly published or available to users due to proprietary considerations. Additionally, reactions between the electrolyte, separator, and electrode materials may produce additional components due to the abuse process. Thus, the exact composition of the vented gases is unknown. The gas composition contributes directly to the flammability hazard of the failure, and information on the composition is crucial to flammability assessment.

1.2.2 Lithium-ion battery abuse testing

Different types of lithium-ion battery abuse testing have been developed to study the many different failure modes of the cells. Some of the main types of abuse testing used to research LIB failure are: mechanical abuse (i.e., bending, compression, and puncturing), thermal abuse (i.e., external heating), and electric abuse (i.e., overcharge, over-discharge, internal short circuit) [18, 22, 23, 35]. Testing using a combination of testing types is often conducted [35].

Certain types of abuse testing can also result in other types of failures in the cell. An example of this is electric abuse which generates heat and can produce some of the same failure modes as thermal abuse. Thermal abuse can lead to the collapse of the separator and decomposition of the electrolyte as well as thermal runaway. Although it causes these failure modes, thermal abuse does not cause some of the failure modes that other testing may, such as separator tearing. Therefore, thermal abuse is desired for the study of electrolyte decomposition and thermal runaway without the added failure modes that come with other types of cell abuse.

For thermal abuse, the state of charge (SOC) and the heating rate of the battery can affect the time and temperature of thermal runaway onset. The temperature of thermal runaway can occur anywhere between 71 and 170°C [7, 23]. The increase in heating rate seems to increase the temperature at which venting and thermal runaway begin, but it also occurs faster due to the faster heating rate [23].

1.2.3 Risk assessment of failure

An understanding of gas environment properties and flammability limits is necessary to assess flammability risk. When a flammable gas is present in a volume, the flammability of the volume is determined by comparing the amount of oxidizing gas in the system to the amount of flammable gas [8]. Each flammable gas species has flammability limits which specify a range of flammable gas to oxidizer ratios that allow the gas to combust. Typically the flammability range is defined by lower and upper flammability limits. If the ratio of flammable gas to oxidizer is less than the lower flammability limit (LFL) of the flammable species, the mixture is not flammable due to a lack of fuel. If the ratio is larger than the LFL but less than the upper flammability limit (UFL) of the species, the mixture is flammable. This also means that if the ratio is larger than the UFL of the species, the mixture is over-saturated with fuel (too little oxidizer) and is nonflammable. Every flammable gas has a unique set of flammability limits that are a chemical property of the species. Flammability limits for many gas species are well documented and can be found in reports such as Coward's [8].

1.3 Chemical analysis techniques

Many different techniques can be used to analyze the chemical compositions of a mixture. Each type of analysis method provides different information about the composition. Due to this, there were two main types of analysis that were desirable for this research: Fourier-transform infrared spectroscopy and mass spectrometry. The coupling of the two different data-sets will allow for a better understanding of the makeup of the sample, and for a more accurate risk assessment.

1.3.1 Fourier-transform infrared spectroscopy

Fourier-transform infrared spectroscopy (FTIR) is an analytical chemistry technique that is based on the absorption or reflection of infrared radiation [25, 31]. The radiation is in the electromagnetic radiation range of frequencies from 14300 to 20 cm^{-1}, and the absorption is measured based on the wavelengths (0.7 to 500 μm). A spectrum of absorption versus wavelength is produced by obtaining an interferogram and performing a Fourier transform of the data [2]. An interferogram is collected by measuring the interference of radiation difference between a reference beam and a measurement beam. An example of a background FTIR spectrum is shown in Figure 1.2. Background spectra are obtained and used as a control to determine the data from a sample spectrum by comparison to the background.

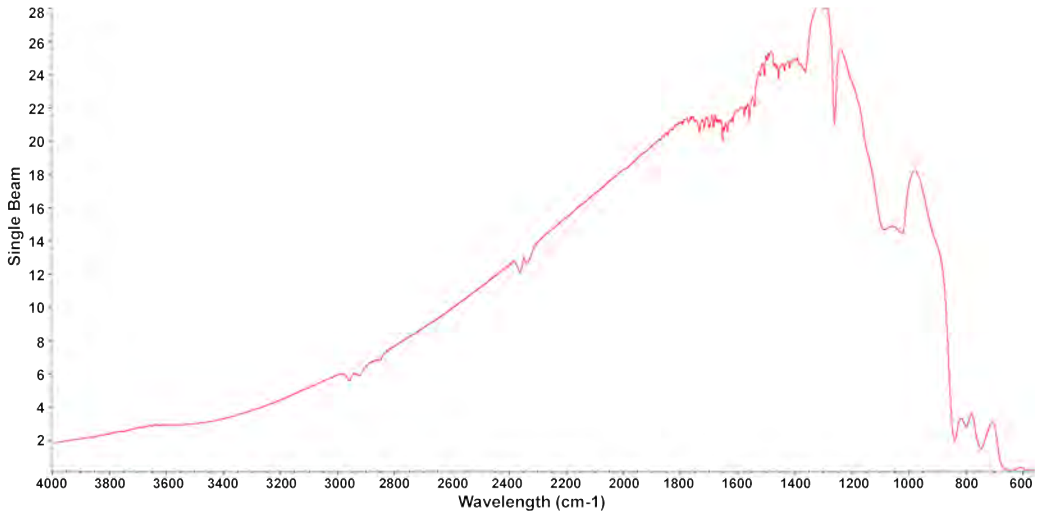

Figure 1.2: A representative Fourier-Transform Infrared background spectrum

The peaks in the spectrum relate to the functional groups of the species present in the sample. For example, the peak structure at around 2350 cm^{-1} in the spectrum in Figure 1.2 is the peak formation that represents the presence of carbon dioxide, and the many peaks between 1800 and 1300 cm^{-1} indicates the presence of water vapor. This data is useful on its own, but combined with the data from other chemical analysis techniques can give a comprehensive analysis on the species present.

Since FTIR measures the transmittance or absorbance of the sample being analyzed, one of the base methods for measuring this is passing the source light directly through the sample and measuring the wavelengths of light not absorbed. This method is called the transmission technique and can be used for solid, liquid, or gas samples. The Attenuated Total Reflection (ATR) method uses a reflective accessory that is a crystal often made of ZnSe, Ge, or diamond [16]. These crystals have a high refractive index. Infrared light is directed out of the source of the system and is split and condensed by the beveled edges of the crystal. The light reflects inside the crystal and interacts with the solution that is in contact with the surface. The light is then directed back out into the system's detector. A schematic showing the light in the system is shown in Figure 1.3 [17] .

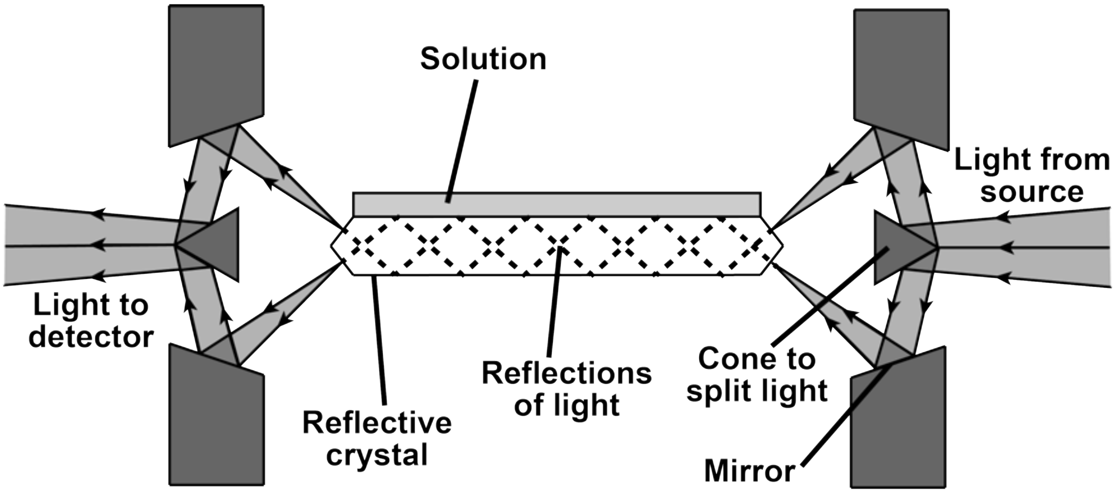

Figure 1.3: Schematic of the Fourier-transform infrared spectroscopy method using Attenuated Total Reflection

Knowing functional groups from FTIR can be informative but does not give a good representation on its own of the full composition, including species identification or partial pressures of the species. For that reason, other analytic chemistry techniques need to be implemented.

1.3.2 Mass spectrometry

Mass spectrometry is a chemical analysis technique that determines molecular masses and abundances of species in a sample [9, 31]. It is a commonly used method due to its high molecular specificity, high detection sensitivity, versatility, and its ability to be applicable across many applications [9].

Analysis using mass spectrometry is broken down into three steps: ionization to convert molecules into gas-phase ionic species, separation and analysis of the ions by mass, and measurement and amplification of current from the mass-separated ions. The system is pulled to a high vacuum for the ionization and separation processes to avoid interactions between species [9]. The main components of a spectrometer include: an inlet system, and ion source, a mass analyzer, a detector, a data system, a vacuum system, and electronics. The data produced from mass spectrometers is the relative abundance of a species as a function of mass-to-charge ratio, where the mass-to-charge ratio is the ratio of the mass of the ion (m) to number of charges (z). The total ion charge is the number of charges multiplied by the charge on an electron. The mass-to-charge ratio can then be converted to molecular mass (in amu).

Results are produced with mass-to-charge ratio along the x-axis and relative abundance along the y-axis, and is presented as a mass spectrum. The software that is used with mass spectrometers can have data processing features integrated into them. Some software, such as Process Eye Professional [24], produces results that are represented in molecular mass rather than mass-to-charge ratio and in pressure instead of relative abundance. An example of a spectrum produced by the system and software used in this research is shown in Figure 1.4. The different peaks relate to the different species in the sample and the heights are their pressure.

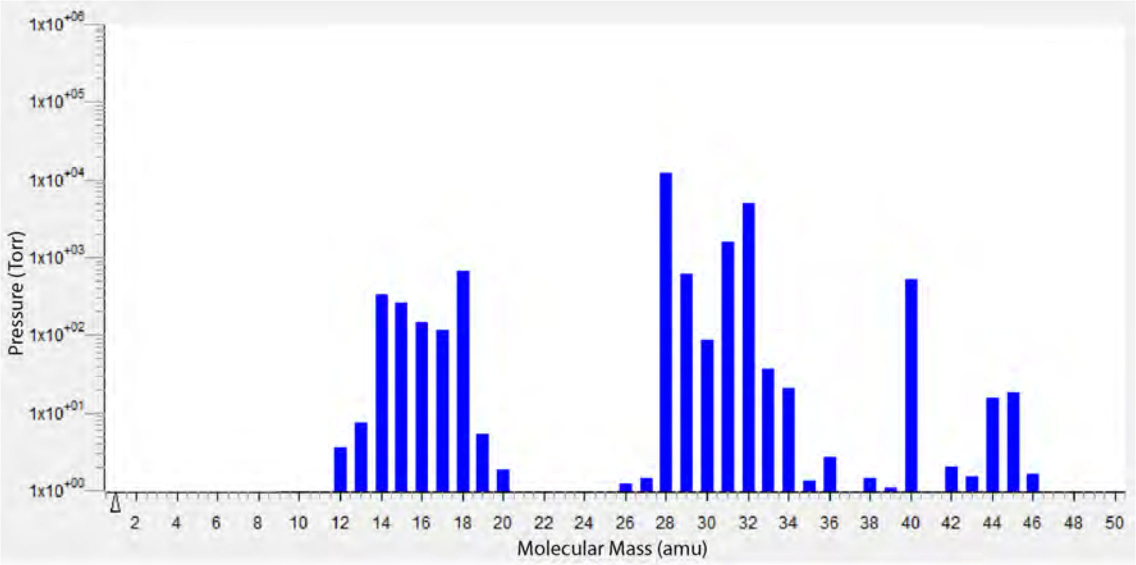

Figure 1.4: Example mass spectrum of a gaseous sample

There are many different types of mass spectrometers that allow different analyses to be conducted. The system that is utilized in this research is a quadrupole mass spectrometer. A quadrupole spectrometer consists of four rod electrodes that are configured in a parallel assembly. Two of the four poles are positively charged electrodes that are paired across while the other two are negatively charged. A potential is supplied to the electrodes, generating an oscillating field in the space between the rods, where ions from a source are passed through [9, 31]. A diagram of the quadrupoles, their charge, and their configuration is shown in Figure 1.5. The ions are separated through paths of different stability throughout the field. Quadruapole mass spectrometers also contain detectors to measure the separation of these ions at the opposite end of the field from the source. From there, a spectrum is produced.

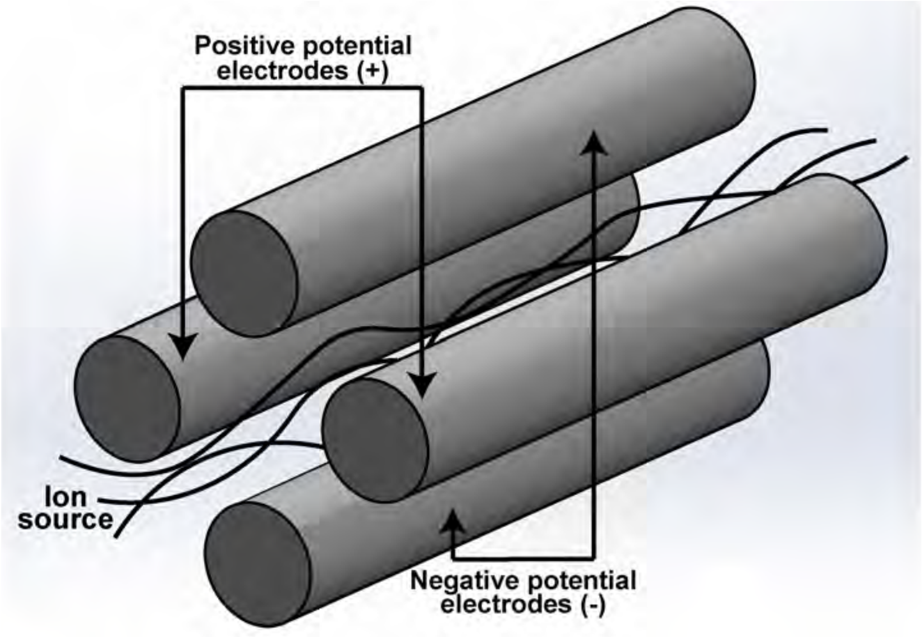

Figure 1.5: Quadrupole mass spectrometer schematic

1.4 Schlieren Refractive Imaging Technique

Refractive imaging is an imaging method that visualizes differences in refractive index in transparent media [32]. Schieren imaging is a type of refractive imaging that visualizes the gradient of the refractive index field and allows idenitification of regions of different refractive index or ”schliere.” Refractive index gradients can occur in materials for many different reasons, including density or temperature differences and mixing of non-homogeneous materials.

Typical schlieren imaging systems utilize a pair of parabolic lenses, a camera, a knife edge, and some light source. The light from a point source is directed into the first parabolic lens, which turns the diverging light into parallel light. If the light source is not a point source, a condensing lens and an iris assist in creating a point source. The flow or objects of interest are placed in the parallel light section. On the other side of the test section is the second matching parabolic lens. This turns the parallel light into converging light toward the camera and knife edge. At the focal point of the converging light, a knife edge is placed, and the camera is placed immediately behind it. Schlieren imaging is unique because a knife edge is used to block some of the light refracted from the object in the test section, yielding the schlieren image. Without the knife edge, the same optical setup yields a focused shadowgraph image.

The parallel light rays in the testing section are bent at an angle due to the object in the field. This causes areas to either be brighter or darker depending on which way the rays are bent. If the light rays are bent toward the knife edge they are obstructed, causing dark areas, but if they are bent away from it they land on the camera sensor away from the light focal point and cause brighter areas. A schlieren imaging setup with a condensing lens and iris is shown in Figure 1.6 with examples of bent light rays.

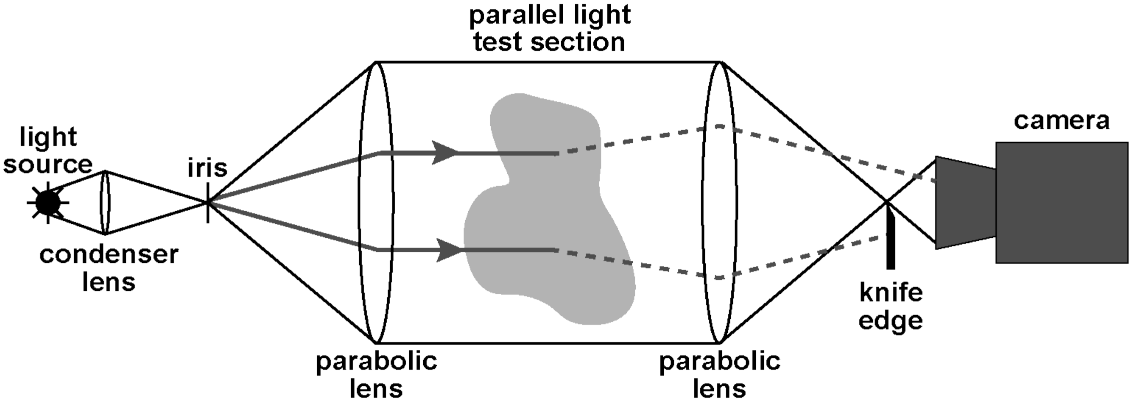

Figure 1.6: Schematic of a schlieren imaging setup

Pairing schlieren imaging techniques with high-speed imaging equipment allows for the timing of events to be determined and documented. High-speed imaging equipment often includes: high-speed cameras, function delay generators, and computers to communicate with the cameras. Using these techniques can help with the refinement of processes through the visualization of events.

1.5 Present research objectives

The present research focuses on the development of methods to assess the risks posed by flammable environments surrounding failing lithium-ion batteries. The temporally-resolved flammability environment around the failing cells is investigated here through simulations and experimental testing. Previous works for studying failing cells focused on characterizing the fluid dynamics of the vented electrolytes for safety assessment [22, 23]. While this research continues to focus on lithium-ion battery failures for safety assessment, the investigation is shifted to the characterization of the chemical composition of the electrolyte mixture.

The goals of this research aim to successfully characterize this gas mixture chemical composition and understand its effect on the flammability environment around the cells. The goals are to:

- Assess the flammability risks of lithium-ion battery failures through the characterization of the chemical composition of vented electrolyte mixtures.

- Develop a reduced-order model to simulate the temporally-evolving flammability environment around failing cells.
- Design and construct of a vacuum grab sampling test method to characterize temporally-resolved chemical profiles of vented materials.
- Determine the vented electrolyte composition through experimental testing and chemical analysis techniques.

CHAPTER 2

REDUCED-ORDER MODEL

The theoretical assessment of flammability environments will be conducted using a reduced-order mathematical model developed for this research. This model was built using MATLAB and simulates the flow out of failing cells into a specified environment. The mass ratio (ϕ) of flammable gas to air is compared to the flammability limits of the species to characterize the temporally evolving environments. The outputs for the model include: the time at which the defined system becomes flammable (if this occurs), the time at which the system surpasses the upper flammability and is no longer flammable (if this occurs), plots showing mass ratio ϕ as a function of time, and flammability curves showing lower and upper flammability limits as a function of time and gas species.

2.1 Assumptions, Variables, and Equations

To simulate the venting process, a number of variable are defined and stored in the work-space. The variables used for calculations have been categorized into three types: user-defined properties based on the system and experiment, test-specific properties, and user-defined properties to be changed across experiments. The user-defined properties that are based on the system are: atmospheric temperature, atmospheric pressure, system volume, and a time increment. The model allows for multiple system volumes to be defined to compare results for a range of spaces. Most of the values used for properties that are test-specific come from Mier's experimental data [23], and these variables include: initial internal battery stagnation pressure, internal battery stagnation temperature, vent cap burst pressure, battery exit area, and Mach number at the battery exit during venting. Lastly, there are variables in the model that the user defines to produce the desired results. These variables are: the number of cells in the system and the gas species vented. A schematic of the simulation with the system variables is shown in Figure 2.1.

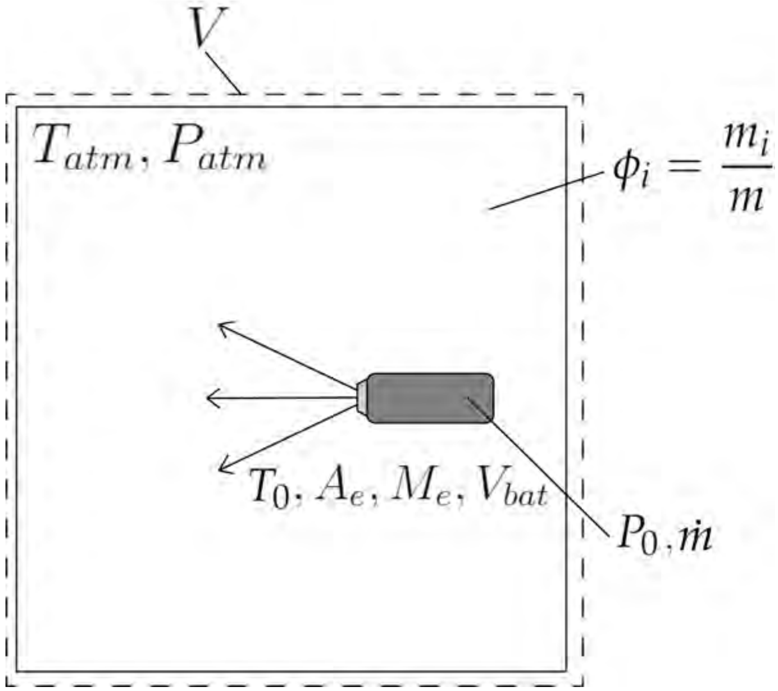

Figure 2.1: Schematic of the reduced order model

The reduced-order model is based off certain assumptions and equations. The first assumption used for the model is that all gases in the system are ideal gases. The ideal gas law and its relations to it are also used in the model. Another assumption is that the gases vented out of the cell mix instantaneously and disperse evenly throughout the volume. The flow of the gases out of the battery is also assumed to be isentropic and one-dimensional. The last assumption that the model is based on is that all cells in the volume begin venting simultaneously at the start of the simulation.

There are many equations that the model is built on. The first set of equations are those for properties of a mixture of ideal gases [3, 28]. The partial fraction or mass fraction ratio x_i is calculated using the pressure P or the mass m for each species i:

$$\frac{P_i}{P} = \frac{m_i}{m} = x_i \tag{2.1}$$

Using this ratio, the molecular weight of the mixture MW_{mix} can be found:

$$MW_{mix} = \sum_{i=1}^{n} x_i MW_i \tag{2.2}$$

The gas constant R_{mix}, density ρ_{mix}, and specific heat ratio γ_{mix} for the mixture are all calculated:

$$R_{mix} = \frac{R_U}{MW_{mix}} \tag{2.3}$$

$$\rho_{mix} = \sum_{i=1}^{n} x_i \rho_i \tag{2.4}$$

$$\gamma_{mix} = \frac{\bar{c_p}}{\bar{c_v}} = \frac{\sum_{i=1}^{n} x_i c_{p,i}}{\sum_{i=1}^{n} x_i c_{v,i}} \tag{2.5}$$

The gas constant of the mixture is calculated using Equation 2.3 with the universal gas constant R_U of 8.314 kJ/kg-K and the molar mass of the mixture M_{mix}. The density of the mixture ρ_{mix} is calculated with the partial pressure ratio and individual densities with Equation 2.4. Using Equation 2.5, the specific heat ratio for the mixture is determined using the specific heat ratios for each species and the mass fractions. The properties and values for individual gases used in the model are listed in Table 2.1.

Table 2.1: Gas properties for ideal gases

Gas Species	Gas Constant - R (kJ/kg-K)	Specific Heat Ratio - γ	Density - ρ (kg/m^3)	Molecular Mass - M (g/mol)
Acetylene	0.3192	1.232	1.092	26.00
Air	0.2870	1.4	1.205	28.97
Ammonia	0.4882	1.31	0.717	17.031
Argon	0.2081	1.667	1.661	39.948
Butane	0.1433	1.091	2.489	58.124
Carbon Dioxide	0.1889	1.289	1.842	44.01
Carbon Monoxide	0.2968	1.4	1.165	28.011
Chlorine	0.1173	1.34	2.994	70.906
Ethane	0.2765	1.186	1.264	30.07
Helium	2.0769	1.667	0.1664	4.003
Hydrogen	4.124	1.405	0.0899	2.016
Methane	0.5182	1.299	0.668	16.043
Neon	0.412	1.667	0.8999	20.179
Nitrogen	0.2968	1.4	1.165	28.013
Oxygen	0.2598	1.395	1.331	31.999
Propane	0.1885	1.126	1.882	44.097

Mier [23] derived an equation to estimate mass flow out of a failing cell:

$$\dot{m} = C_d \frac{P_0}{\sqrt{RT_0}} A_e \sqrt{\gamma} M_e (1 + \frac{\gamma - 1}{2} M_e^2)^{\frac{\gamma+1}{2-2\gamma}} \tag{2.6}$$

This equation is used as the basis of this model. The equation contains parameters that relate to the internal battery properties and exit geometry: discharge coefficient C_d, stagnation pressure P_0, stagnation temperature T_0, area of exit A_e, and exit Mach number M_e. The discharge coefficient is determined based on the ratio of stagnation pressure to atmospheric pressure (P_0/P_{atm}). For a ratio P_0/P_{atm} less than 2.2, the discharge coefficient is a constant of $C_d = 0.75$, and for a ratio greater than 3.2, it is a constant of 0.95 [23]. Between 2.2 and 3.2, the discharge coefficient is a linear relationship. The mass flow equation is also built upon properties of the vented gases: the gas constant R, and the specific heat ratio γ.

Mass ratios for each species (ϕ_i) can then be found:

$$dm_i = x_i \dot{m} dt \tag{2.7}$$

$$\phi_i = \frac{m_i}{m} \tag{2.8}$$

where dm$_i$ is the mass of a species entering the system, x_i is the mass ratio of that species, $\dot{m}$ is the mass flow, dt is the time step, m_i is the total mass of a species in the environment, and m is the system mass.

From the mass flow equation, the change in internal stagnation pressure in the cell can be calculated using:

$$\frac{dP_0}{dt} = -\frac{RT_0}{V}\dot{m} \tag{2.9}$$

This includes the parameters previously mentioned as well as the volume of the cell V.

2.2 Modeling process

The venting of the cells is simulated with the use of Equations 2.1-2.9. At the initialization of the model, after all previously saved data had been cleared, tabulated data for flammable gases is imported into MATLAB. This data includes the values presented in Table 2.1, as well as the lower flammability limit (LFL) and upper flammability limit (UFL) of each species which are listed in Table 2.2. The flammability limits are obtained from the 2021 ASHRAE Fundamentals Handbook [1], Coward [8], and Rhodes [29].

Table 2.2: Flammability limits for gases

Gas Species	Lower Flammability Limit (%)	Upper Flammability Limit (%)
Acetylene	2.5	100
Ammonia	15	28
Butane	1.86	8.41
Carbon Monoxide	12	75
Ethane	3	12.4
Hydrogen	4	75
Methane	4.4	16.4
Propane	2.1	10.1
Dimethyl Carbonate	4.2	12.9

Next, the user is prompted to select the species that make up the vented mixture, and the ratios of each species in the mixture. Any number of species can be selected. The properties for each of the selected species are then written into variables for gas properties in the model. The values for these properties were found from Kobe [14], Borgnakke [3], and Zhou [39]. Using Equations 2.3, 2.4, and 2.5, the gas mixture properties for the selected mixture are calculated and defined.

After the properties for the gas mixture are determined, other variables are initialized. These variables include a mixture of all three types of parameters and include: system volume (or range of volumes), number of cells, time step value, initial battery stagnation pressure at failure, internal battery stagnation temperature at failure, cell exit area, exit Mach number, battery volume, and pressure. The last part of the setup is setting the mass of each species in the chamber volume and the time equal to zero.

Once all variables have been defined or initialized, the venting process is simulated through a step-wise process at each time step. At each time step, the mass flow ($\dot{m}$) out of the battery is first calculated based on the current state. The mass flow is then turned into mass into the system of each species (dm_i) using the defined time step (dt) and partial pressures (x_i) of the gas species. The mass of each species (m_i) is updated with this change in mass. The system volume is assumed to be filled with air. The total mass of each species in the system is then divided by the mass of air in the volume to give a mass ratio (ϕ_i) which is compared to the flammability limits of each species. If the mass ratio of a species is greater than its LFL, the system is flammable. If this occurs during the current time step, that time is recorded as the flammability time. If the mass ratio then exceeds the UFL, that current time is saved as the nonflammable time (the time at which the system is no longer flammable).

The next step in the simulation is updating the internal stagnation pressure (P_0) from the change in pressure equation and the mass flow out of the cell. Using the new pressure, the pressure ratio is recalculated and a new discharge coefficient (C_d) for the mass flow equation is determined based on the new pressure ratio. Time is then increased, and a new iteration begins. The process continues until the end time is reached.

When the end time is reached, if multiple system volumes have been defined, the next volume is set as the new volume, and the simulation process is restarted. The variables are reinitialized, and the entire step-wise process is repeated until the end time is again reached. This continues for all defined system volumes. Once the venting process is simulated for all volumes, results from the model can be plotted.

The model produces the following results for every volume simulated: the time at which the system became flammable by surpassing a species' lower flammability limit (if this occurs within the time limit), and the time at which the system surpasses a species' upper flammability limit and is no longer flammable (if this occurs in the time limit). The model also produces a flammability map showing lower and upper flammability limits for the species as a function of time over the range of volumes.

A visual schematic of the simulation process from start to finish is shown in Figure 2.2

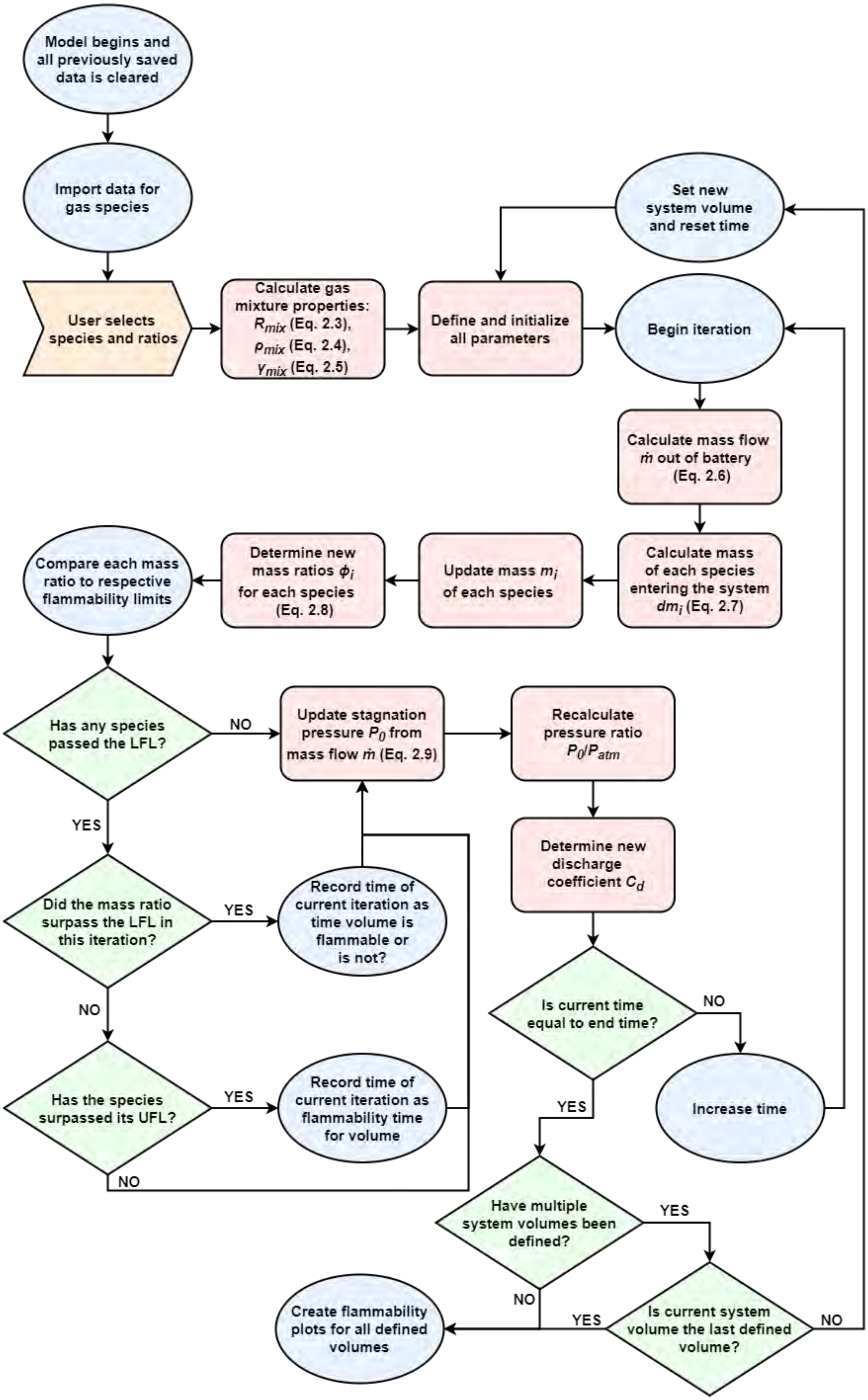

Figure 2.2: Flow chart of simulation process and the steps involved

2.3 Model Testing

Testing with the model consists of adjustments to variables such as system volume, vented species, and number of cells in the system. The changes to the system are indicated in Figure 2.3. The adjustment of these variables allow for a range of scenarios to be simulated.

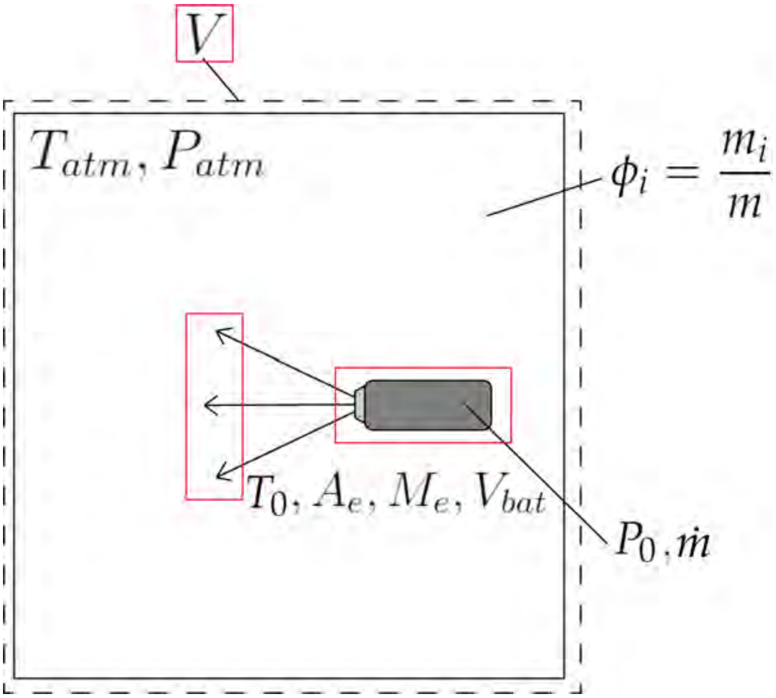

Figure 2.3: Schematic of changed variables for model testing

A series of preliminary tests were run with the model using pure hydrogen as the vented species. The tests were run with one cell in the system over a range of system volumes from 0.001 to 0.1 m^3. These tests guided the construction of the experimental testing enclosure discussed in Chapter 3. It was determined that for this scenario, which represents the most flammable situation due to the low flammability limit and explosive hazard of hydrogen, any volume above 0.0413 m^3 does not become flammable. As discussed in Chapter 3, the experimental chamber volume was selected to be approximately 0.223 m^3 to prevent a flammable environment from being achieved. Figure 2.4 shows the flammability map produced by the model from these preliminary tests. The chemical composition of the vented gases from failing a cell directly impacts the evolution of the flammability environment surrounding the cell. The identification of the composition is then crucial for accurate safety assessment. Due to this direct effect, experimental abuse testing was conducted to determine the composition.

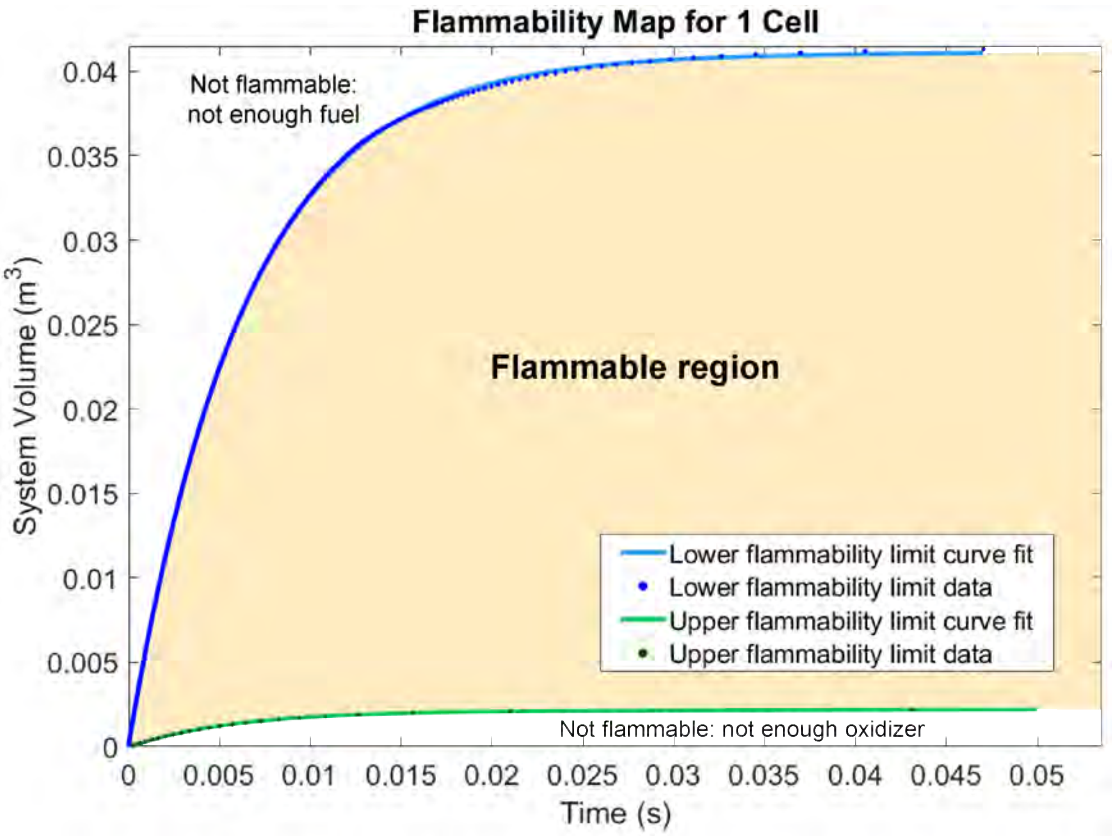

Figure 2.4: Flammability map for 1 cell venting hydrogen

CHAPTER 3

EXPERIMENTAL METHODS

An experimental testbed was developed to capture and analyze the gases vented from failing batteries. The experimental setup included dynamic vacuum samplers, a heater block for thermally loading a battery cell, a chamber into which the gases were vented, and a control system to perform data acquisition and control. Chemical analysis methods, including FTIR and mass spectrometry, were established for analyzing the collected samples.

3.1 Battery Thermal Abuse Testbed

A system for thermal abuse testing of battery cells was designed and constructed. The overall system includes a holder for the battery cell under test, a large volume into which the gases are vented, vacuum grab samplers, and a control system. Two samplers were built to allow for time-resolved samples to be captured.

A mount for the battery cell being tested was designed and machined out of a 7.62 cm (3 inch) cube of aluminum to hold one 18650 format cell, four cartridge heaters, and two thermocouples, as seen in Figure 3.1. The battery is inserted from the front of the block and the vent cap face is flush with the front of the block. The voltage of the cell is measured before being placed into the block. The cartridge heaters and thermocouples are inserted from the back of the block. The heaters lie along the entire length, while the thermocouples are located at the midway point of the cell. Thermal paste was used on all components mounted in the block. The design of this block enabled uniform, steady heating of the cell. The placement of the thermocouples in the block allows for not only temperature monitoring but also for the calculation of an estimated cell temperature based on their location between one heater and the edge of the cell. The cartridge heaters are connected in parallel to a variable transformer and to a Solid-State Relay (SSR). The variable transformer allows power across the system to be adjusted. The SSR connects and disconnects power to the heaters when power is supplied to it.

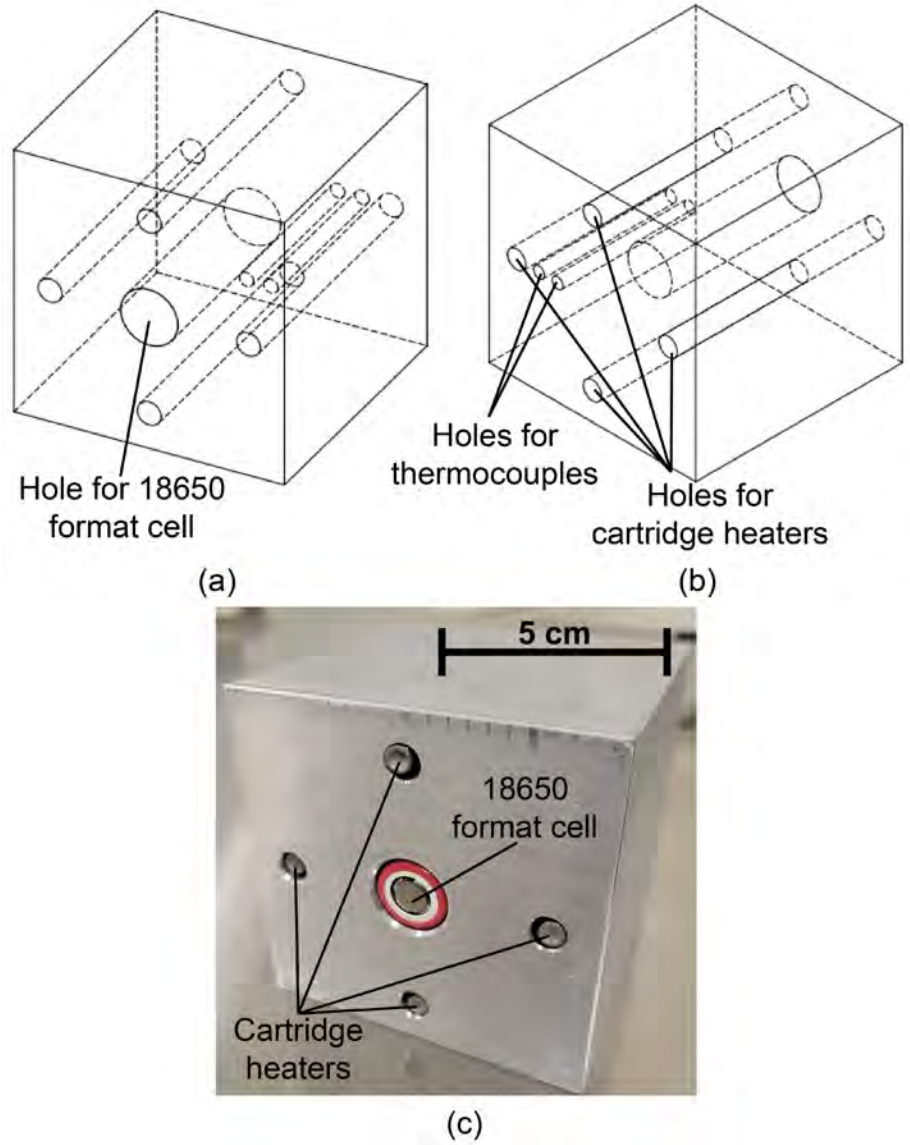

Figure 3.1: Aluminum block mount: (a) design as seen from front of block, (b) design as seen from back of block, (c) image of the front of block with heaters and a cell in place

The mounting block and the grab samplers are integrated into a testing enclosure. The enclosure for testing is made of 0.61 m (2 foot) sections of 2.53 cm (1 inch) t-slotted aluminum framing with 0.61 by 0.61 m sheets of 6.35 mm (1/4 inch) thick acrylic acting as walls. The testing enclosure can be seen in Figure 3.2. A ventilation system was integrated into the test apparatus to mitigate the flammability risk of the failures. The venting duct in the enclosure as well as the other main testing components can be seen in Figure 3.3. Four different cameras were used to monitor and record the abuse event.

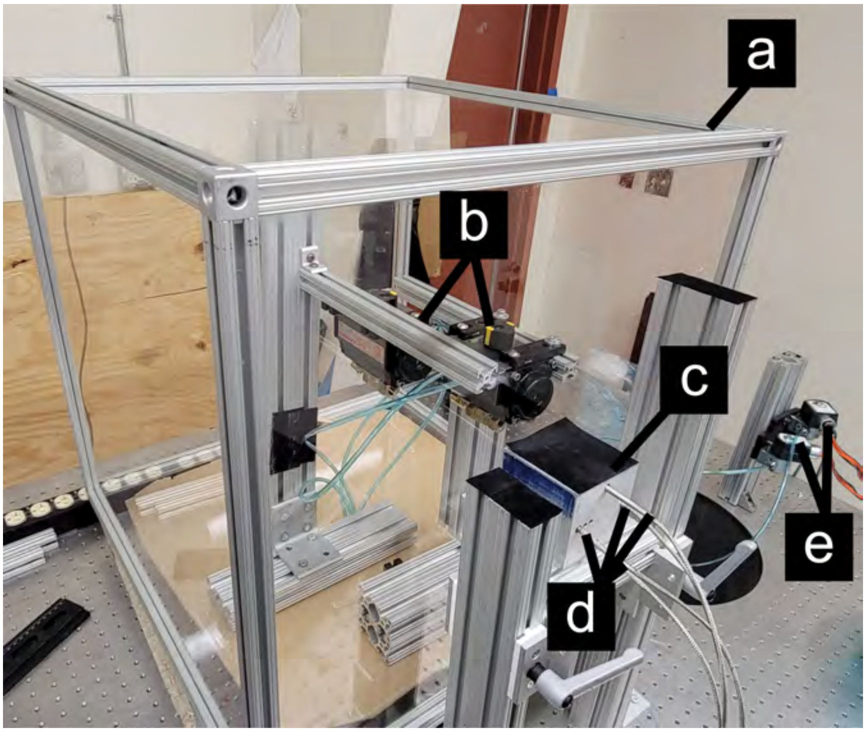

Figure 3.2: Testing setup with components (a) test enclosure, (b) pneumatic valves for grab samplers, (c) aluminum mounting block, (d) cartridge heaters, (e) electric solenoid valves

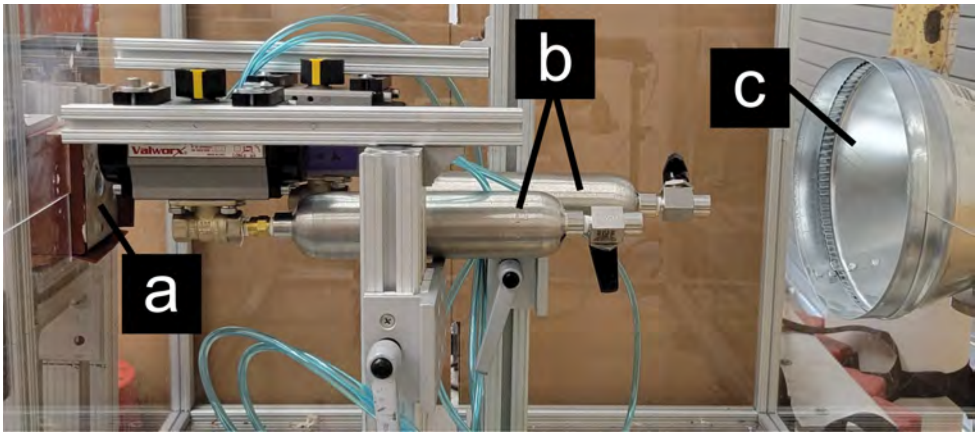

Figure 3.3: Image of testing setup with (a) aluminum mounting block, (b) grab samplers, and (c) venting system

A National Instruments compact data acquisition (cDAQ) unit is used to connect multiple National Instruments modules that are used in the testing setup. In the cDAQ, four modules were used: NI 9212, NI 9482, NI 9205, and NI 9269. The

NI 9212 module is used to read data from the two thermocouples in the mounting block. The NI 9482 module is a relay module that connects and disconnects power to the two electric solenoid valves. Each valve is connected to a different terminal in the module allowing each to be turned on separately. The NI 9205 module reads analog inputs and is used to monitor the analog microphone. Lastly, the NI 9269 module outputs voltages from -10 to 10 volts. This module is used to trigger other components, which is discussed later, and to power on the SSR for the heaters.

A LabVIEW Virtual Instrument (VI) was developed for this research to communicate with the cDAQ for control of the electronic components and reading sensors within the testing setup. The VI communicates with the cDAQ and the modules that are in it. The front panel of the VI is shown in Figure 3.4. The front panel consists of many switches to control different aspects of the setup, variables for the sensors, the channels that each component is connected to in the modules of the cDAQ, and plots of sensor data.

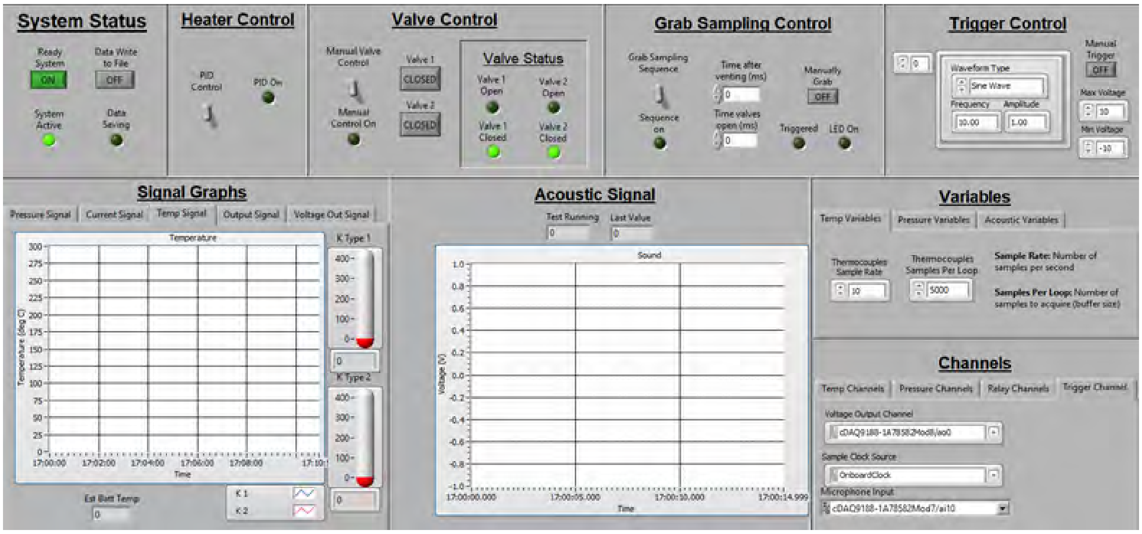

Sample Rate: Number of samples per second

Samples Per Loop: Number of samples to acquire (buffer size)

Figure 3.4: LabVIEW VI Front Panel

In the VI, a sequence was programmed to power and open the samplers with pre-defined time delays. The time delays consist of: the time after venting, which is how long the system waits once triggered to power on one or both samplers; the time the samplers are open, which specifies the duration of the sample; and the time between samples, which can be set to 0 for simultaneous sampling or nonzero for sequential sampling. The time between samples indicates the time between the opening of the first sampler and that of the second. This means that samples may overlap in time, or the second sample may begin sampling after the first has closed. When triggered, the sampling sequence first waits the time specified as the time after venting, then turns on the relays for both samplers for simultaneous sampling or one sampler for sequential. The system waits until the sample duration has passed to close the samplers.

The sampling sequence is initiated with a trigger input signal. For testing here, an analog microphone trigger was implemented. When the vent cap ruptures, acoustic emission is detected with the microphone, which initiates the grab sampling sequence. The sampling sequence can also be triggered manually via a button in the VI front panel. If the cell failed and sampling was not triggered acoustically, the system was manually triggered through the VI.

A heating sequence was also programmed into the VI. This sequence powers the SSR to connect the power for the heaters. Minimum and maximum temperatures are specified by the user and the sequence keeps the temperature of the block between these values by powering on and off the heaters based on the measurements of the thermocouples.

3.2 Vacuum Grab Sampling

A vacuum grab sampler was designed and implemented to dynamically collect a sample of the gases vented from a cell during failure. Each setup consists of two main components: a double-ended stainless steel sample cylinder (part f in Figure 3.5), and a pneumatic ball valve (part a). A check valve (part b) is used between the sample cylinder and the pneumatic valve. On the far end of the cylinder is a ball valve (part g). Pneumatic valves were chosen due to their low actuation time, which allows for a short sample duration to be obtained. The check valve allows flow into the cylinder while preventing the release of gases. The ball valve is used to connect the sample cylinders to the chemical analysis and vacuum systems.

For preliminary testing, a pressure transducer (part c) was incorporated into the sampler using a tee-connector and a straight-connector (parts d and e, respectively). The inclusion of these parts allowed the pressure inside the cylinder to be monitored, which assisted in sampling time determination. For final tests, these parts were not used, and only the base sampler components (parts a, b, f, and g) were included.

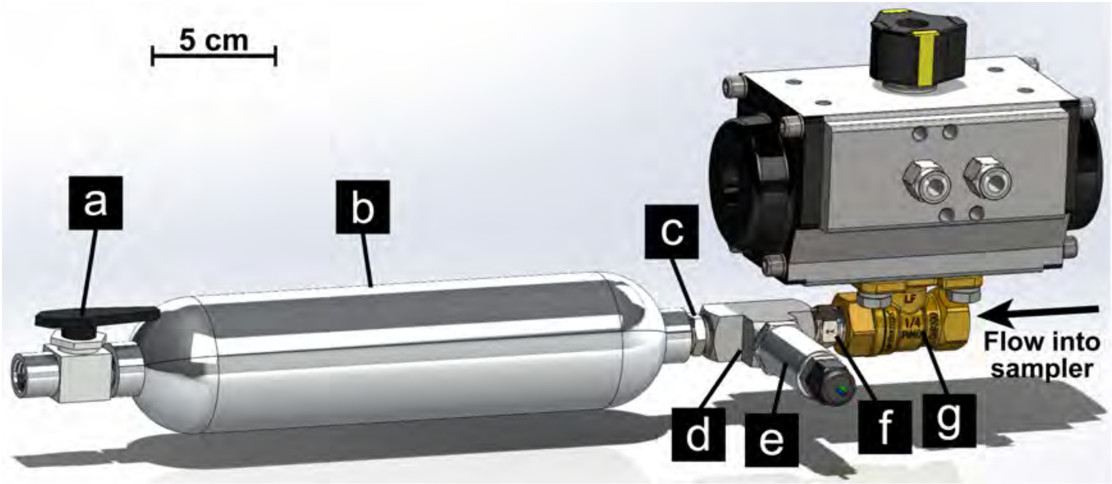

Figure 3.5: Model of extended grab sampler with individual parts including (a) pneumatic valve, (b) check valve, (c) pressure transducer, (d) tee-connector, (e) straight connector, (f) sample cylinder, (g) ball valve

Before attaching the cylinders to the grab samplers, each cylinder was cleaned to reduce the residual gases that might have been absorbed into the inside surface. This was completed by first thoroughly rinsing and agitating each cylinder with reverse osmosis (RO) water. The water was then poured out, and methanol was added. The methanol was swirled around and then agitated vigorously before also being disposed. The cylinders were then allowed to drain and dry while the rest of the test was set up.

To prepare the grab sampler, the clean cylinder is attached, the pneumatic valve is closed, and the cylinder is pulled to vacuum through the ball valve using a vacuum pump. Air from a compressor is supplied at approximately 689.5 kPa (100 psi) to the inlet of a three-way electric solenoid valve which controls air flow to the pneumatic valve. While there is no power supplied to the solenoid valve, the air flows out of one outlet through a muffler. Once power is switched on, the valve opens, and the air is directed to the input of the pneumatic valve allowing it to open and for a sample to be pulled into the cylinder. Incorporating the electric solenoid valves allowed for the pneumatic valves to be controlled electronically. The two grab samplers and the electric solenoid valves can be seen in Figures 3.2 and 3.3. To trigger the samplers, an analog microphone is used to detect acoustic emissions of the vent cap rupture.

3.3 Schlieren Imaging Setup

In order to visualize the operation of the samplers, a high-speed schlieren imaging setup was built around the testing enclosure, as shown in Figure 3.6. Light from a Sugar Cube LED is directed through a light guide (part A) and then condensed to a point light source using a 50 mm condensing lens (part b). The light is directed through an iris (part c), then directed to an in-line 127-mm-diameter collimating lens just outside the testing chamber (part d). On the opposite side of the chamber, another 127-mm-diameter collimating lens condenses the light back down toward the Photron SA-X2 high-speed camera (part f). At the focal point of the light, just in front of the camera lens, a horizontal knife edge is placed (part e). The Photon camera is triggered through a Stanford Research Systems Digital Delay Generator (part g). For tests that incorporate schlieren imaging, the grab sampling sequence is programmed to include a voltage output from the NI 9269 module. The voltage is sent to the delay generator which triggers the camera when the sampling is triggered.

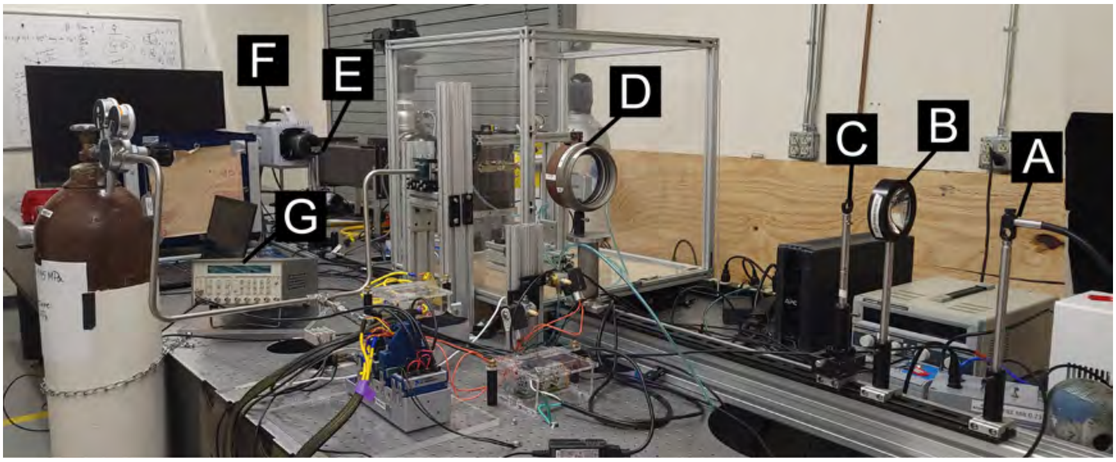

Figure 3.6: Schlieren imaging setup around the testing enclosure with components including (a) light source, (b) condensing lens, (c) iris, (d) collimating lens, (e) knife edge, (f) high-speed camera, (g) digital delay generator

3.4 Chemical Analysis methods

The two main chemical analysis techniques used for determining mixture composition were FTIR and MS. These techniques were used to determine the composition of the samples collected throughout the abuse tests.

The FTIR system used was a Thermo Fisher Nicolet iS50. This system was used for both analysis of liquid electrolyte samples and gaseous samples from the battery abuse tests. For liquid samples, an ATR crystal was used as the analysis accessory, while the transmission technique was used for the gases. For both types of tests, a background spectrum was collected before the sample was introduced. For the ATR crystal, this consisted of collecting a spectrum for the bare crystal. For the gas samples, the gas test chamber was pulled to vacuum before a sample was introduced, and a background spectrum was taken of the gas chamber at vacuum and the purged chamber surrounding it. Chambers around the testing area in both systems were constantly purged with dry air to reduce the detection of carbon dioxide and moisture in the chamber. In both methods, species in the chamber (such as carbon dioxide and water) were still detected when purged with dry air. Even with the constant purging with dry air, levels of CO_2 and water can fluctuate in the chamber. Due to this, the chamber often needed to be scanned multiple times until the levels of the spectra were not fluctuating between scans.

Once the background spectrum was obtained, a sample was introduced into the system and analyzed. For electrolyte baseline tests, once the electrolyte was extracted from the battery into a test tube, it was transferred to the surface of the ATR crystal. The electrolyte was spread to cover the entire surface of the crystal to ensure maximum sample area. To analyze the gaseous samples, the grab sampler cylinders were heated to the battery failure temperature for that test using a ribbon heater. Once heated, the cylinder was opened to allow flow into the vacuum chamber, and the spectrum was measured. For the two baseline air samples, the cylinders were not heated, but were analyzed the same way for all FTIR analyses. In the FTIR system, 250 scans were taken before the software produced the spectra.

The MS system was only used for gaseous samples and was connected to the sample cylinder and the FTIR system. The device used for MS analysis was a Cirrus 3-XD, V-lens, Quadrupole Mass Spectrometer. This system has a maximum molecular weight that it can detect of 100 amu. Chambers around the testing area in both systems were constantly purged with dry air to reduce the detection of carbon dioxide and moisture in the chamber. For the MS data, the gas present in the empty device was measured for approximately 25 scans, which represents about 5 minutes of time. Once these scans were completed, along with the FTIR background spectrum, the sample cylinder was opened which introduced the sample into both systems. MS data was collected for around 25 more scans with the gas. The scanning was completed with the Process Eye Professional software.

The data from both FTIR and MS were analyzed using literature and chemical databases [5, 6, 10, 13, 27] to identify chemical species. The MS data from the software is a table containing the pressures of each molecular weight (from 1 to 100) at each scan. A simple code was written using MATLAB to display the pressure data across the scans for each molecular weight one at a time. For each plot, the user is able to indicate whether that dataset is to be included in analysis (deciding if that species is present in the sample) based on values across the scans and if there is a significant pressure increase at the time of gas introduction. The total pressure in the system was calculated for each scan time by summing the pressure of every molecular weight. The scan with the maximum pressure was determined and used for calculating pressure measurements. Once all of the present molecular weights had been identified, the partial pressure of each weight was determined by dividing the pressure of that species by the total scan pressure. The tabulated data of molecular weight and their partial pressures is then produced. The code was run on the MS data sets for each gaseous sample.

The molecular weights specified were searched in the National Institute of Standards and Technology (NIST) Chemistry WebBook [5, 6] and the PubChem data base from the National Institute of Health's National Library of Medicine [13], and all species possibilities for each were recorded.

The FTIR scans were plotted against one another to compare the sample data and find average relative intensities and wavelengths of peaks. Then, using these intensities and locations, functional group possibilities for each peak were determined. These were determined using the Sigma Aldrich IR Spectrum data base [33]. Next, the spectral data for the MS species possibilities were searched in the NIST and PubChem databases [5, 6, 13]. The spectra of these species were compared to the FTIR spectra of the samples both visually and through spectra subtraction to determine which MS species possibilities matched the sample data.

CHAPTER 4

VALIDATION TESTS

After the completion of testing method development, a range of tests were conducted. Validation tests assisted in understanding the testing process and grab sampling event more accurately. Base-line experiments were also conducted to compare data from the abuse tests

4.1 Timing validation tests

A tabulated list of the validation experiments completed, the test method and triggering mode used, and the desired analysis for the tests can be seen in Table 4.1. Once validation experiments were complete, abuse tests were run based on the findings from the validation tests.

Table 4.1: Validation tests conducted for grab sampling

Validation test	Test method	Trigger mode	Validation target
Test 1	vertical and horizontal jets	manual trigger	sample timing
Test 2	vent cap rupture	acoustic trigger	sample timing with acoustic trigger
Test 3	vertical jet and vent cap rupture	acoustic trigger	sample timing with acoustic trigger

To validate and refine the testing setup and procedure, three different types of experiments were conducted before battery abuse testing began. The goal of these tests were to ensure that all electronics and hardware were working properly and to determine the timing of the sampling sequence. The timing parameters to be observed were the delays in the system and the time it takes for the cylinders to equalize pressure and finish sampling from the time they were opened. For all validation tests, only one sampler was used, and the heaters were not used. The timing across all validation tests was consistent with a time delay after venting of 1 ms and a sample duration of 2 seconds. These tests used a combination of manual and acoustic triggering.

The first set of trials was completed using carbon dioxide and helium jets. Tests with carbon dioxide jets were used initially before switching to helium to increase the visibility of the jet in the schlieren imaging. Tests were conducted with both vertical and horizontal placement of the jets, and high-speed schlieren imaging was used to visualize the sampling of these jets. An image of the horizontal jet test setup is shown in Figure 4.1 with a grab sampler placed in line with the jet. The jet and edge of the sampler were both placed in the field of view of the schlieren imaging setup. When testing, the jet was adjusted to be close to laminar and was flowing for the entire test. Then, when the sampler was manually activated, the jet was pulled into the sampler and the imaging system was triggered.

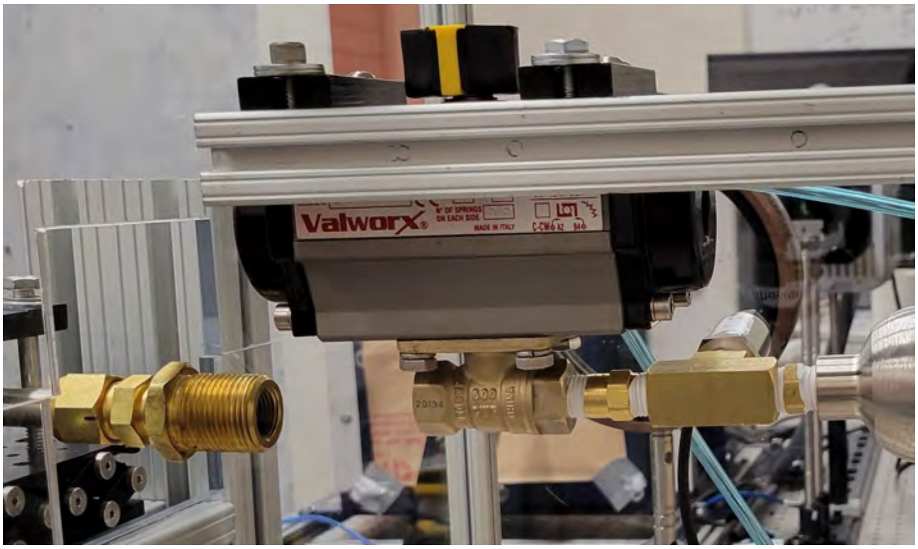

Figure 4.1: Setup picture for the horizontal jet test with grab sampler and schlieren

Schlieren images from one of the vertical CO_2 jet test before and during the sampling are shown in Figure 4.2. In the image during the sampling event, vortices are seen at the top of the flow as it is pulled into the pneumatic valve. The light area below the top portion of the pneumatic valve is where the CO_2 had collected from the vertical jet flowing before the sampler was opened. This set of trials was manually triggered because there was no abrupt sound in the test to initiate the acoustic triggering in the system. From this test, the timing of the grab sampler was investigated, and it was determined that from the vacuum, the sampler was able to collect gas for approximately 100 ms before the pressure equalized and gas was not sampled anymore. These tests were not able to determine timing with acoustic triggering which lead to further validation tests.

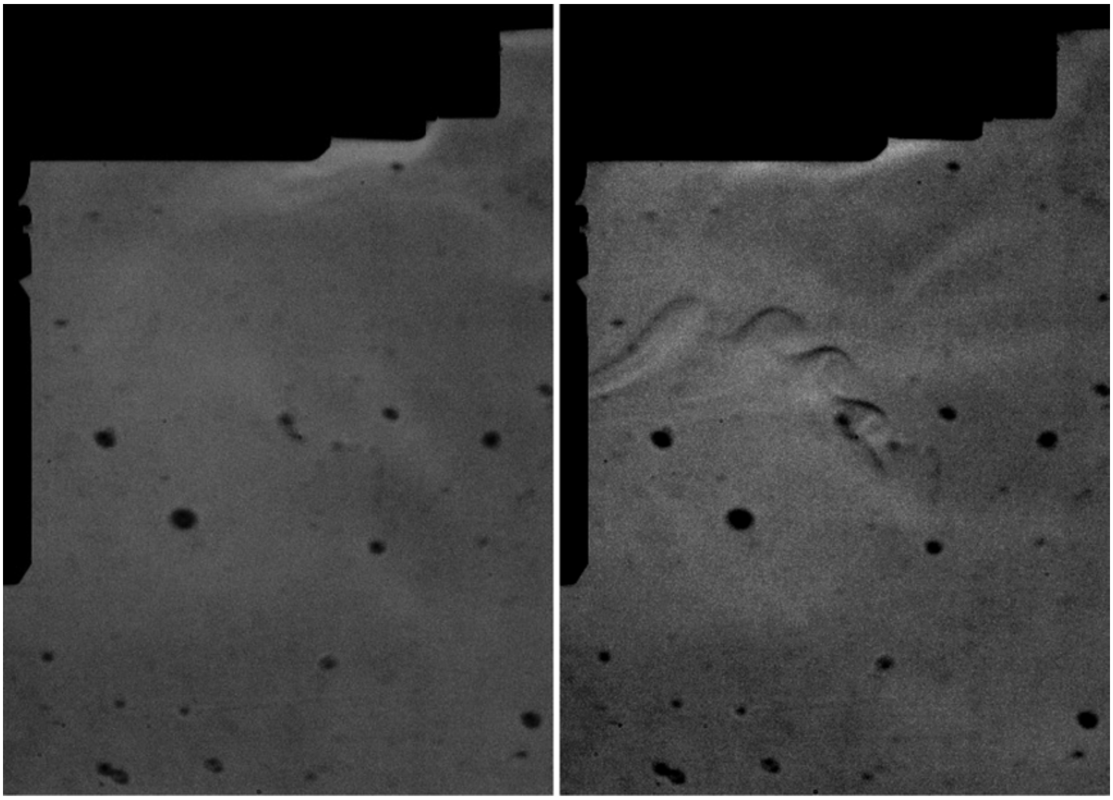

Figure 4.2: (a) Schlieren image of vertical CO_2 jet before sampling, (b) Schlieren image of CO_2 jet being pulled into the sampler

The second set of validation tests consisted of vent cap burst tests to further refine timing and procedures with acoustic triggering. Vent caps were pressurized and ruptured using a vent cap burst fixture that was attached to a compressed CO_2 bottle source. The apparatus used for the horizontal jet in the previous validation tests was used to attach the vent cap burst fixture. The sampling process was initiated through the acoustic detection of the rupture. Schlieren imaging was used to visualize the timing between the rupture and the sampling. These tests allowed the determination of acoustic triggering levels and timing for the vent cap bursts.

From this test series, it was determined that the system was able to be triggered acoustically, but schlieren imaging showed that the vent cap rupture (which occurred at approximately 1.92 MPa [22]) caused too much turbulent flow to capture the sampling event. Figure 4.3 shows the turbulent flow in the field of view after the vent cap ruptures. Due to this, another set of validation tests was deemed necessary to image the sampling event while triggering acoustically with a vent cap rupture.

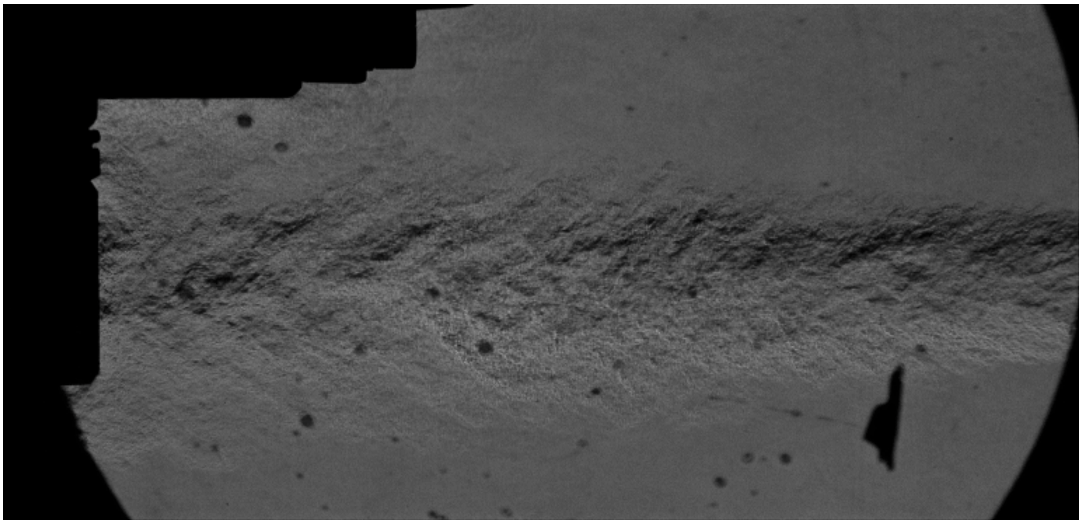

Figure 4.3: Schlieren image vent cap rupture with grab sampler

The last set of validation tests was a combination of the first two sets. A vertical helium jet was sampled in the imaging field to see the sampling process, while a vent cap was ruptured separately to incorporate acoustic detection triggering. This set of validation tests aimed to analyze the sampling process more closely with the inclusion of acoustic triggering. The vent caps tend to rupture at approximately 1.92 MPa (278.5 psi) [22], which causes a lot of turbulent flow once ruptured that can be difficult to image. Because of this, the vent cap burst fixture was placed below the field of view for the camera, while the helium jet was imaged and sampled. Images from the test before and after the vent cap ruptured can be seen in Figure 4.4.

Although the helium jet is clearly seen in the schlieren image before the vent cap rupture, and the rupture event did occur outside of the field of view, the flow out of the vent cap still caused the air in the field of view to be disrupted. This meant that even though the system was triggered, the sampling process was still unable to be visualized. The helium jet continued to flow through the entire test but was disrupted by the vent cap flow and cannot be seen in the schlieren image. The turbulent flow in the images was significantly less than the tests with the vent cap in view, but the sampling event was still unable to be visualized.

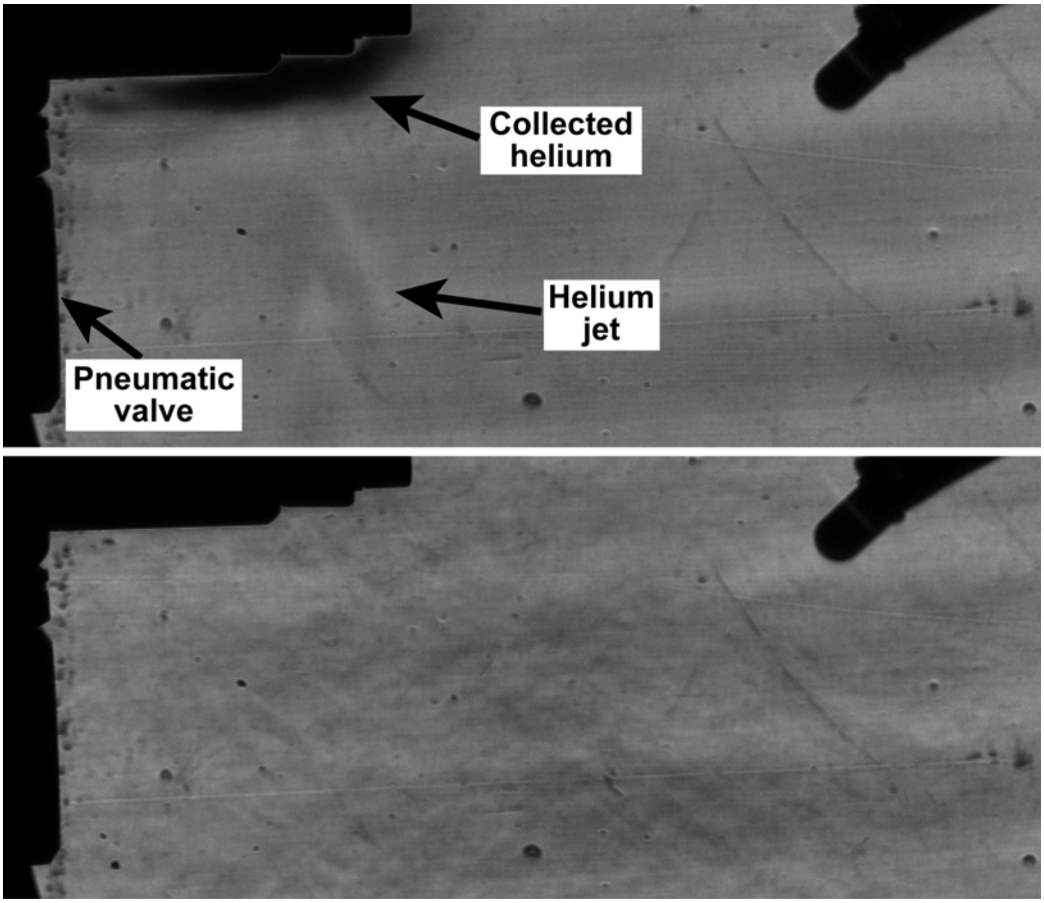

Figure 4.4: (a) Schlieren image of vertical helium jet before vent cap rupture and sampling, (b) Schlieren image of air flow in testing enclosure after vent cap rupture

4.2 Baseline chemical analysis tests

Two baseline tests were also completed and analyzed to compare to the sample data. The first baseline was a sample of the air in the testing enclosure before any abuse tests were conducted. The grab samplers were used to sample the air, and the samples were analyzed using the same process used for the abuse test samples.

The second set of baseline tests aimed to quantify the electrolyte makeup and breakdown separate from abuse tests. There were two sets of electrolyte tests: a baseline, and a heating test. The baseline tests were to determine the chemical make-up of the liquid electrolyte before any chemical reaction might have occurred due to heating. For this, batteries were drained to 0% SOC (around 2.8 volts) before a hole was drilled in one end of the cell. Once a hole was made, the batteries were each placed in a 3D-printed mount into a test tube as shown in

Figure 4.5, and were then centrifuged at 7830 revolutions per minute for 5 minutes. The cell and mount were then removed from the tube, and the electrolyte was analyzed.

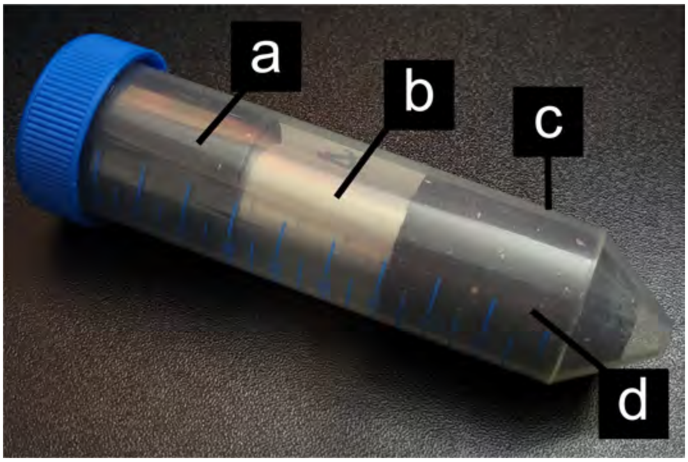

Figure 4.5: Setup for battery electrolyte extraction with (a) the top part of 3D-printed mount, (b) a drilled cell, (c) the bottom part of 3D-printed mount, and (c) a 50 mL test tube

The heating tests consisted of the same procedure as the baseline, with the exception that after the sample was collected in the tube, it was transferred to a cleaned sample cylinder and heated before analysis.

Another baseline test was completed to validate the cleaning process of the abuse tests procedure. To study the cleaning process, a sample cylinder that had been used for abuse tests was cleaned using the procedures used in abuse testing. Then, the cylinder was connected to the grab sampler and air in the enclosure was sampled. The air was then analyzed and the results were compared to those of the abuse test samples.

CHAPTER 5

BATTERY ABUSE TESTS

A summary of all of the abuse tests and their settings is shown in Table 5.1. The summarized findings from each experiment and resulting adjustments are listed in Table 5.2. The chemistry of the samples from the abuse tests was analyzed immediately following each test.

Table 5.1: Variables for battery abuse tests with grab sampling

Test	Cell voltage (V)	Approximate power to each heater (W)	Heat rate (C/min)	Time after venting (ms)	Time between samples (ms)	Sample duration (ms)
1	3.8	75	2-2.5	100	2000	100
2	3.83	80	5	100	2000	100
3	3.83	155	12.3	100	2000	100
4	4.12	155	12.0	100	2000	100
5	4.15	155	12.0	100	2000	100
6	3.81	155	11.9	100	2000	1000
7	3.83	155	11.5	100	2000	1000
8	3.83	155	11.6	100	2000	1000
9	3.83	155	11.7	100	2000	1000
10	3.83	155	11.4	100	2000	1000
11	3.83	155	12.2	100	2000	1000

Table 5.2: Battery abuse test results

Test	Result	Notes	Sampling process
1	No vent cap rupture	Heating rate increased for future test	No sample taken
2	No vent cap rupture	Heating rate increased further	No sample taken
3	Vent cap ruptured, but valve did not open fully	Sampling duration increased	Sampled with manual triggering
4	No vent cap rupture	Tested again without sampling	Sampled with manual triggering
5	No vent cap rupture with no samplers	All future tests kept at nominal voltage	No sample taken
6	Vent cap ruptured and vented gas sampled	Kept settings for future tests; Test A in final series	Sampled with manual triggering
7	Vent cap ruptured and vented gas sampled	Test 2 of final test series	Sampled with acoustic triggering
8	Vent cap ruptured and vented gas sampled	Test 3 of final test series	Sampled with manual triggering
9	Vent cap ruptured and vented gas sampled	Test 4 of final test series	Sampled with acoustic triggering
10	Vent cap ruptured and vented gas sampled	Test 5 of final test series	Sampled with manual triggering
11	Vent cap ruptured and vented gas sampled	Test 6 of final test series	Sampled with manual triggering

The initial battery abuse experiments consisted of adjustments to variables to find the most desirable settings for these experiments. Once the settings had been determined, the final series of tests was run with these variables to study the statistical differences in data sets. Schlieren imaging was not used for the battery abuse tests, and the grab samplers were modified to just the base components.

The two grab samplers were placed at two locations of approximately 4 cm and 14 cm from the cell face, which were consistent across all tests, and were centered radially around the cell in the aluminum block. The samplers were triggered sequentially, with the closer sampler triggering first and the further next.

Certain time variables were kept constant throughout all abuse tests, while certain time settings changed until the final experiment series. The time at which the first sampler opened after the system was triggered stayed constant at 100 ms. The time between the opening of the first and second samplers also stayed the same at 2000 ms. The duration of the sample, or the time that each sampler was open, was adjusted throughout the tests, with the preliminary tests running at a duration of 100 ms and the final tests at 1000 ms.

The heaters were run between 75 and 200 Watts each for a total system power of between 300 and 800 Watts. The heaters were measured at 48 Ohms, so the total system resistance with the heater configuration was 12.25 Ohms. The necessary voltage from the variable controller was calculated based on the desired power for the heaters. The voltage powered for the 75 W setting, was around 60 Volts, while for the 200 W output, the voltage was 99 Volts.

For the first battery abuse experiment, a cell at nominal voltage (3.8 Volts) was heated with an approximate heater power of 75 Watts each, resulting in an average heating rate of between 2 and 2.5 °C/min. This heating rate was used based on the low heating rate tests completed in Mier's work [23]. For this test, the failure temperature was unknown due to a monitoring camera malfunction, but the failure of this cell consisted of a small amount of liquid electrolyte leaking out of the bottom of the vent cap with no audible vent cap rupture. This was believed to be due to the low heating rate causing the vent cap to fail without the energetic rupture and spray of gases. Due to this, the heating rate was then increased for further testing. Figure 5.1 shows a cell and the samplers in place during an experiment before the heating and sampling process was started.

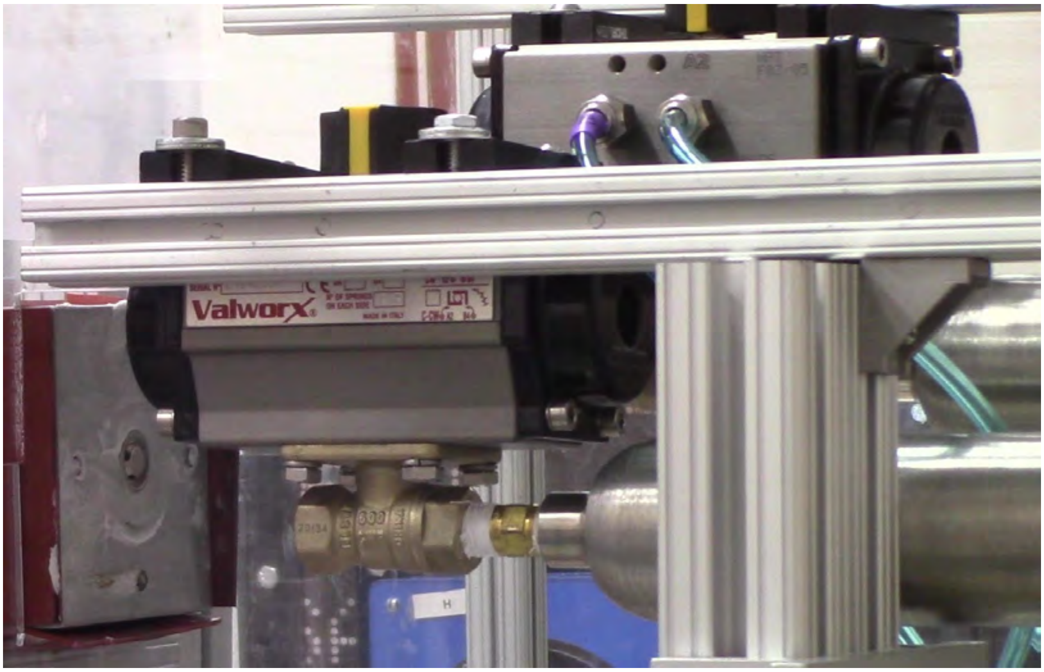

Figure 5.1: Testing components in place for battery abuse tests

For the second battery abuse test, the heater power, and consequently the heating rate, was increased. For this trial, a cell with nominal voltage (measured at 3.83 volts) was heated at a rate of approximately 5.5°C/min from heaters at approximately 80 Watts each. This test resulted in the same type of vent cap failure and electrolyte extrusion as the previous test, with a heating rate of 2.5°C/min, so another test was conducted with an even higher heating rate. Due to the failure event that occurred with this test and the previous, samples were not taken or analyzed.

For the third test, the heater power was increased to approximately 155 Watts each, resulting in a heating rate of approximately 12.3 °C/min. In this test, the vent cap ruptured abruptly and vented out gases while the liquid electrolyte poured out was minimal. Although it did not pour out electrolyte, it sprayed liquid on the testing enclosure walls. Two frames from the test video for this trial can be seen in Figure 5.2, with the cell in the mounting block before and after the vent cap rupture. The droplets from the spray on the wall and gas exiting the cell can be seen in Frame b of Figure 5.2. Because the abuse settings from this test produced the desired failure outcome, the heating settings used were used for the remainder of the experiments.

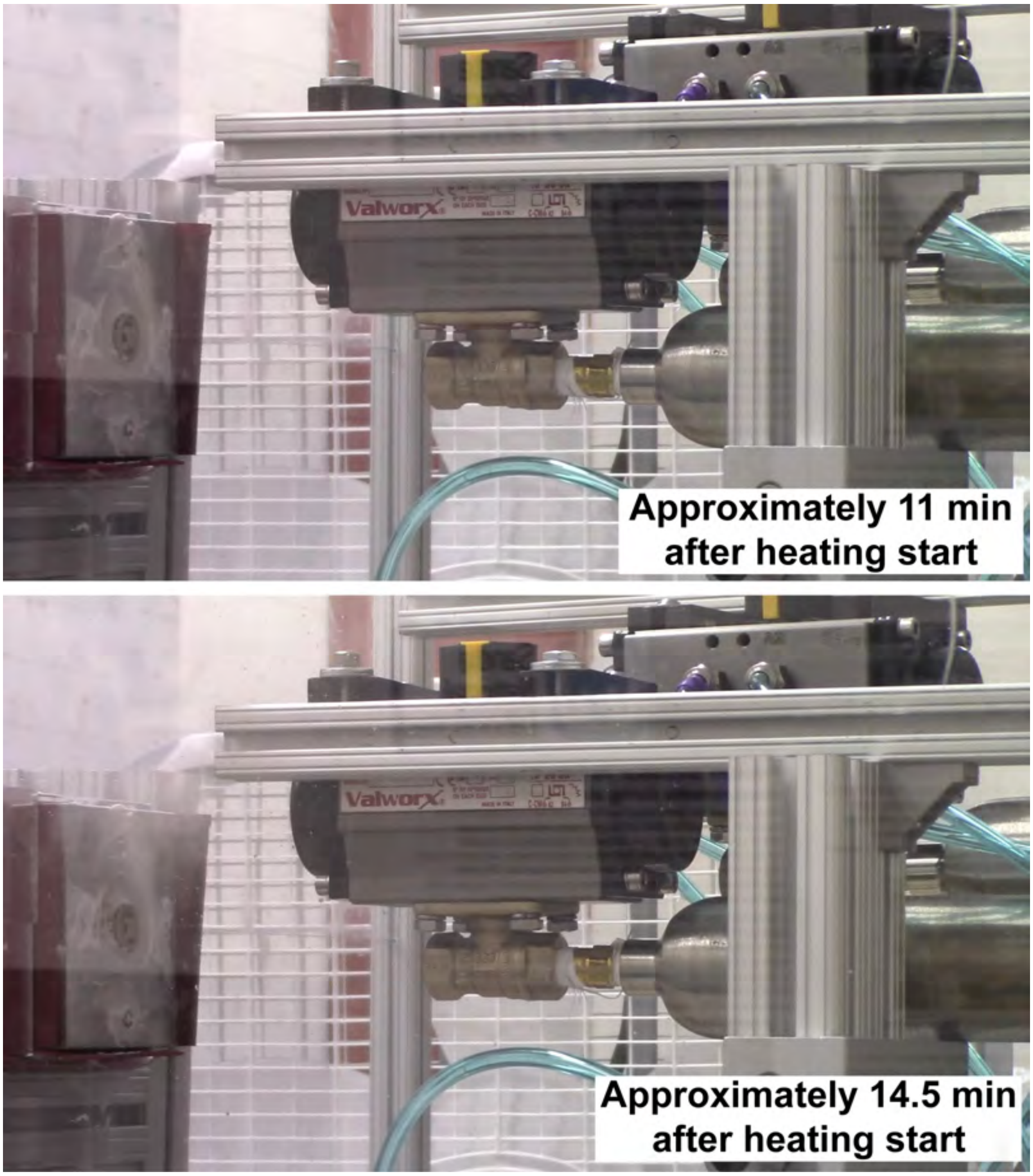

Figure 5.2: (a) Image from battery abuse test during the heating process, (b) Image from battery abuse test after vent cap rupture

The timing settings for this experiment consisted of the following: 100 ms delay after vent cap rupture, 100 ms sample duration, and 2000 ms delay between two samples. When analyzing the video of the failure event, it was observed that the sampling duration length did not allow the pneumatic valves to fully open. Due to this, the sampling duration for future tests was increased to 1000 ms.

Before a test was run with a longer sample duration, the effect of the state of charge on the failure mode and sample quantity was investigated. To study this, a cell was charged to 4.12 volts (around 100% SOC) to use for an abuse test. The power supplied to the heaters in this experiment was consistent with the previous test at nominal charge at approximately 155 Watts each for a heating rate of around 12°C/min. This test had the same timing settings as the previous test. During this trial, similar to the first two abuse experiments with lower heating rates, the vent cap did not rupture. This also means that the system did not trigger acoustically. In this failure event, gases were vented out of the cell, but there was a much smaller quantity of gas than in the previous test. The cell also poured out much more liquid electrolyte than the first two abuse tests. The failed cell and the leaked liquid electrolyte in a frame from the test are shown in Figure 5.3. Although less gas was vented out of this cell from failure than the previous abuse test, and the system did not trigger acoustically, samples were taken through manual triggering when gas was seen venting.

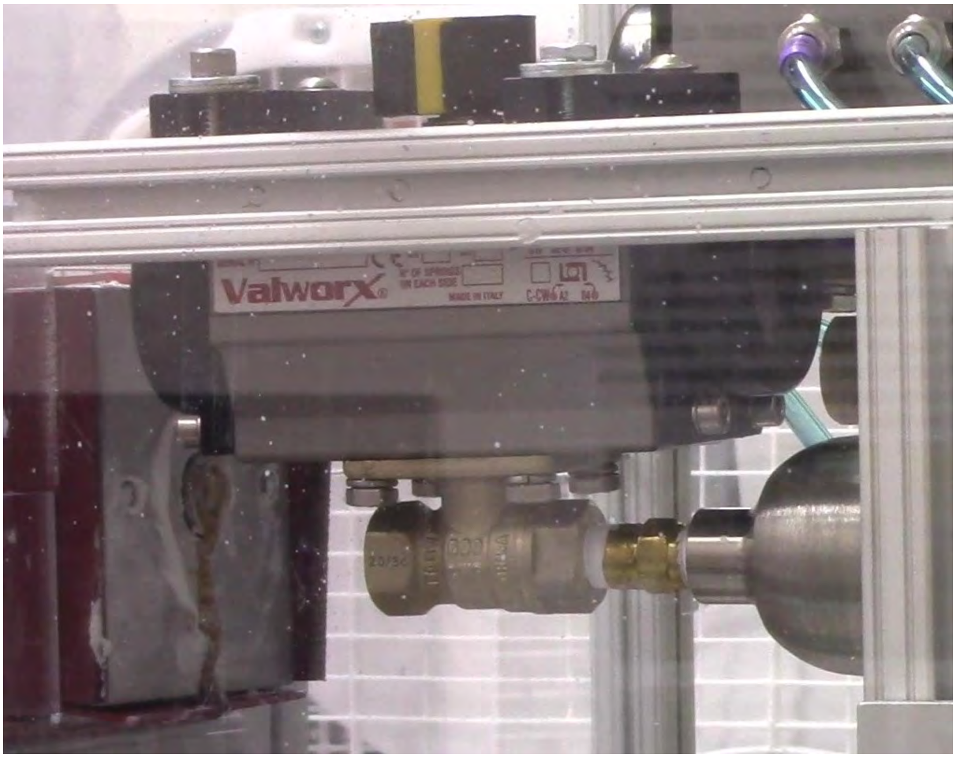

Figure 5.3: Frame from abuse test after failure with a cell at 100% SOC

To test the failure mechanism of a 100% SOC cell again, another cell was charged to around 100% SOC (4.15 volts) and failed with no samplers in use. In this test, the heater power was kept constant from the previous charged cell test. This cell had the same failure mechanism as the last, with no vent cap rupture, a small amount of vented gas, and a large amount of liquid electrolyte pouring out. Due to these test results, all further abuse tests were continued using cells at a nominal voltage of around 3.8 volts.

The final series of abuse experiments was then conducted. The series consisted of 6 abuse tests with cells at nominal voltage, a heating power of approximately 155 Watts each, and an increased sample duration of 1000 ms. All tests in this series failed with a loud vent cap rupture, but some tests still required manual sampling through LabVIEW. This was due to inconsistencies in the microphone data, including voltage drift, possibly due to increased sensor temperature.

CHAPTER 6

CHEMICAL ANALYSIS RESULTS

The samples collected from each of the experiments were processed to study the chemical composition and the effectiveness of the grab sampling method. The baseline experiments were analyzed first to obtain an understanding of the baseline materials and composition. Next, the abuse tests were analyzed to determine species and ratios of the gas mixture vented from the failing cells. Statistical differences in the data from the tests were used as error bounds for species ratios. Once the ratios were determined, the values were used in the reduced-order model to simulate a cell venting with more accuracy.

6.1 Baseline test results

From the Material Safety Data Sheet (MSDS) for the battery cells, certain components of the cell composition are known [36]. The cathode material for the cell is lithium nickel manganese cobalt oxide (LiNiMnCoO), and the anode material is graphite (carbon). The cell also contains copper and aluminum. The electrolyte salt, lithium hexafluorophosphate ($LiPF_6$), is dissolved in the electrolyte solvent which is made up of at least one of the following (not specified on MSDS): ethylene carbonate ($C_3H_4O_3$), propylene carbonate ($C_4H_6O_3$), dimethyl carbonate ($C_3H_6O_3$), and diethyl carbonate ($C_5H_{10}O_3$).

To understand the chemical changes in the electrolyte during thermal abuse, the baseline electrolyte chemistry was analyzed. The extracted samples of electrolyte were analyzed using the ATR method of FTIR analysis to produce FTIR spectra. The spectra results from three battery cells were plotted and the results had a good agreement, as seen in Figure 6.1.

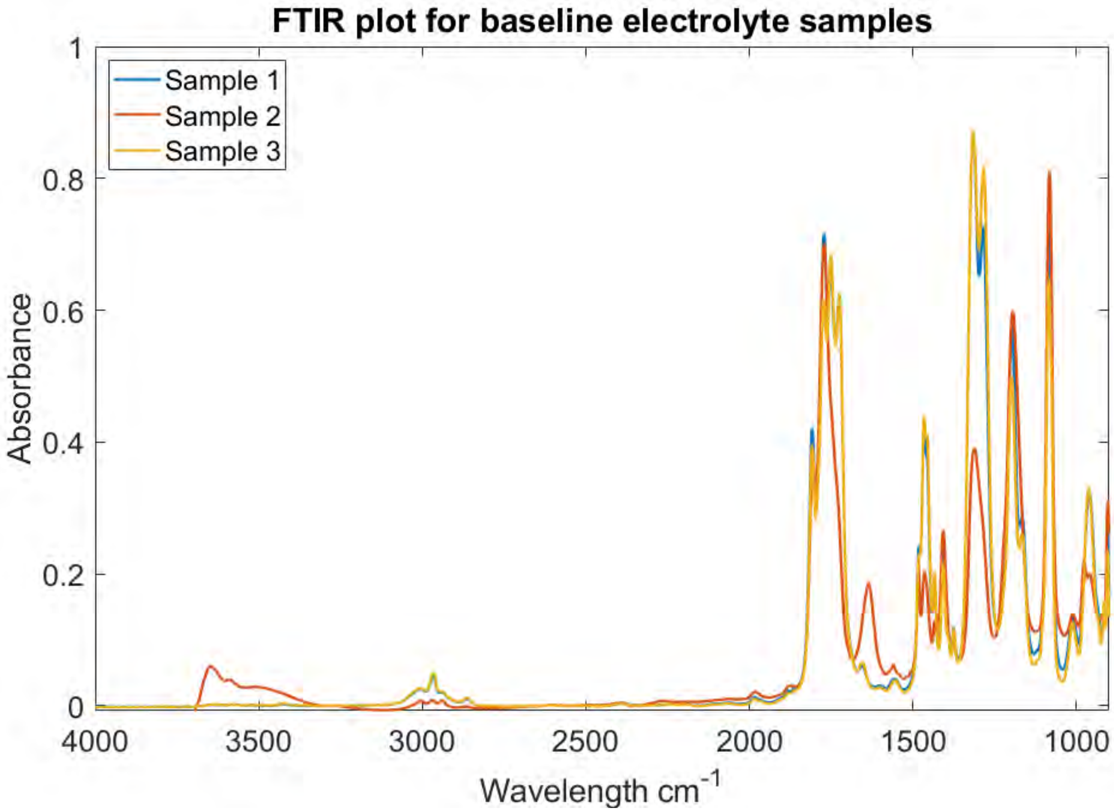

Figure 6.1: FTIR spectra for the three baseline electrolyte samples

Because these samples were not able to be analyzed with mass spectrometry, the composition of the samples was difficult to determine. Therefore the spectra were compared to one of the heated electrolyte samples where the electrolyte was heated after being extracted from a drained cell. The three electrolyte spectra compared to the heated electrolyte spectrum can be seen in Figure 6.2. The region in an FTIR spectrum below 1400 cm^{-1} is often considered the fingerprint region [37], and can be difficult to analyze. Taking this into consideration, the location of the major peaks from the baseline electrolyte spectra outside of the fingerprint region seems to stay fairly consistent. The heated electrolyte spectrum also had good agreement with the sample spectra, so it is assumed that the liquid electrolyte has the same composition as the sample after heating.

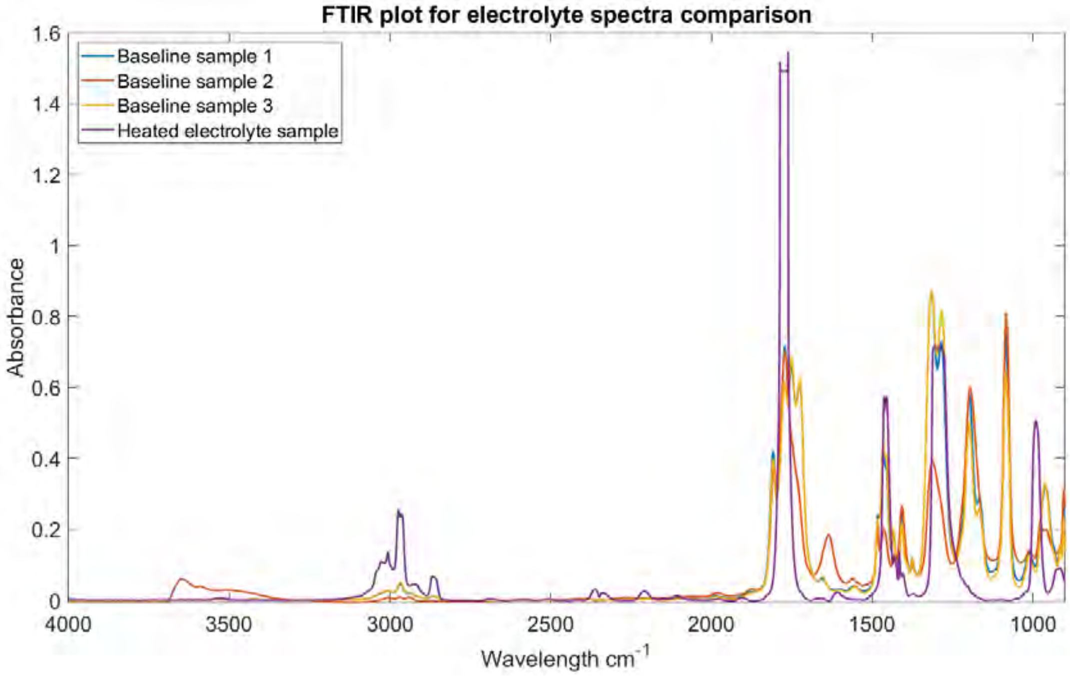

Figure 6.2: FTIR spectra for the three baseline electrolyte samples and the heated electrolyte sample

Baseline samples of the air in the testing enclosure were analyzed using FTIR and MS. Figure 6.3 shows the FTIR spectra for the air samples. In the spectra, there are two main species that can be identified: carbon dioxide (CO_2), and water. The CO_2 can be identified through the two prominent peaks at 2361 and 2339 cm^{-1}, and the water is identified by the many peaks between 4000 and 3500 cm^{-1} and between 2000 and 1700 cm^{-1} [10, 27].

The species in the sample can be confirmed by synthesizing a synthetic FTIR spectrum from the combination of known CO_2 and water spectra. The spectra of CO2 and water are both shown in Figure 6.4. First, each spectrum was overlaid on the baseline air spectrum and scaled to match the relative absorbences (vertical intensity scaling). Then, the CO_2 and water spectra were added to create the synthetic spectrum. One of the baseline air spectra and the created spectrum are shown in Figure 6.5.

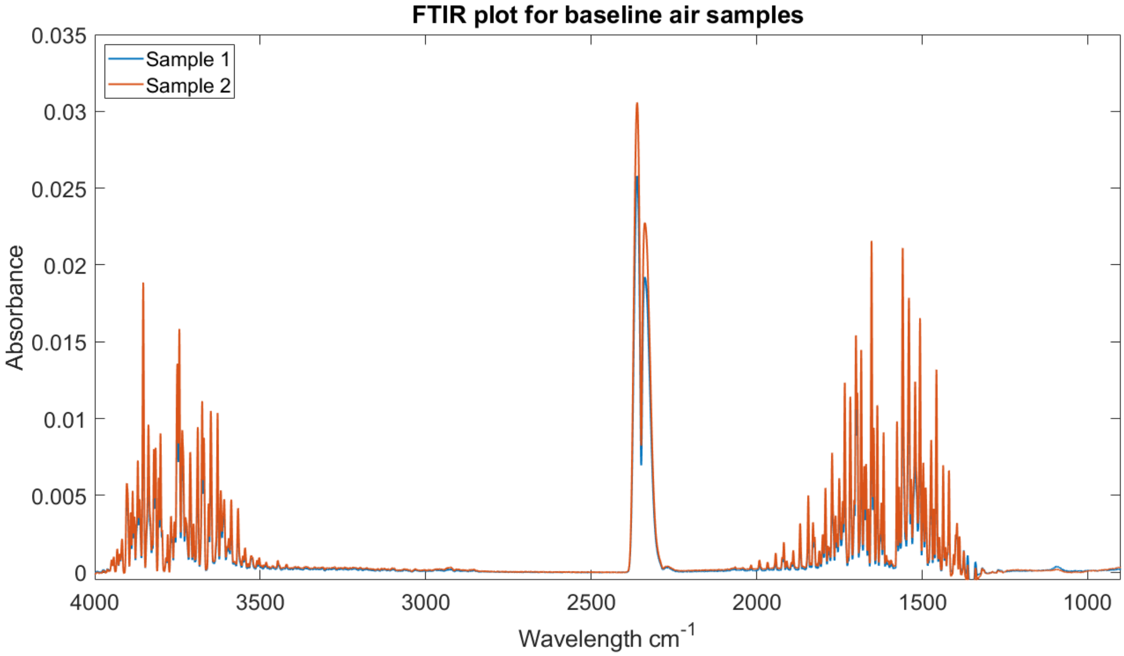

Figure 6.3: FTIR spectra of baseline air samples

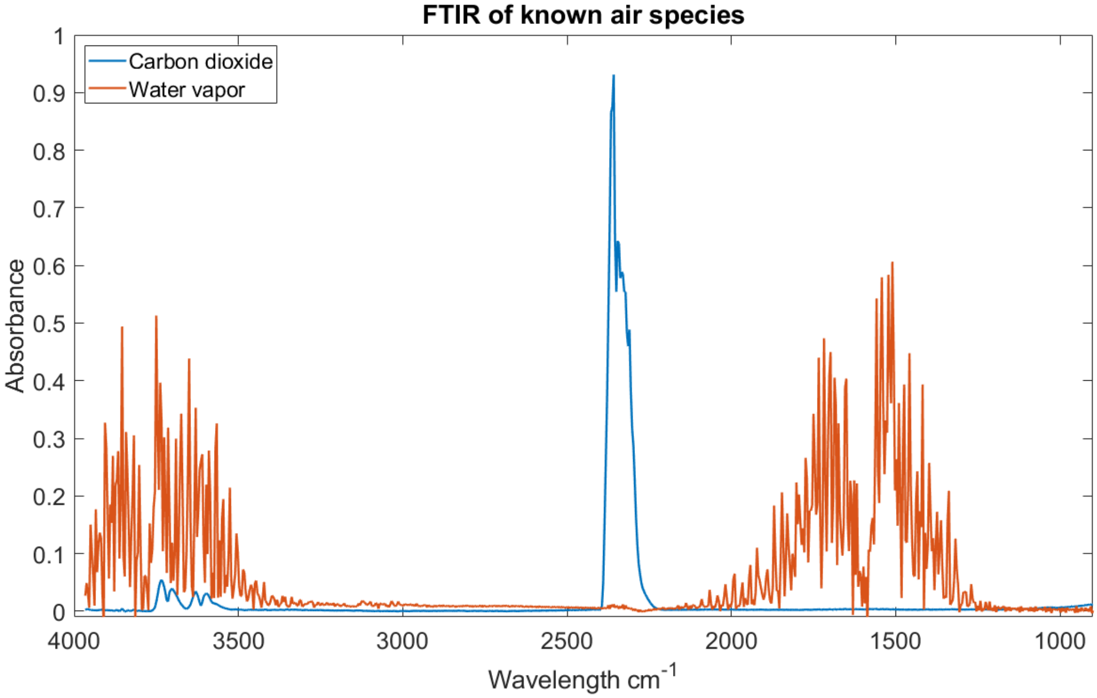

Figure 6.4: FTIR spectra of known air species

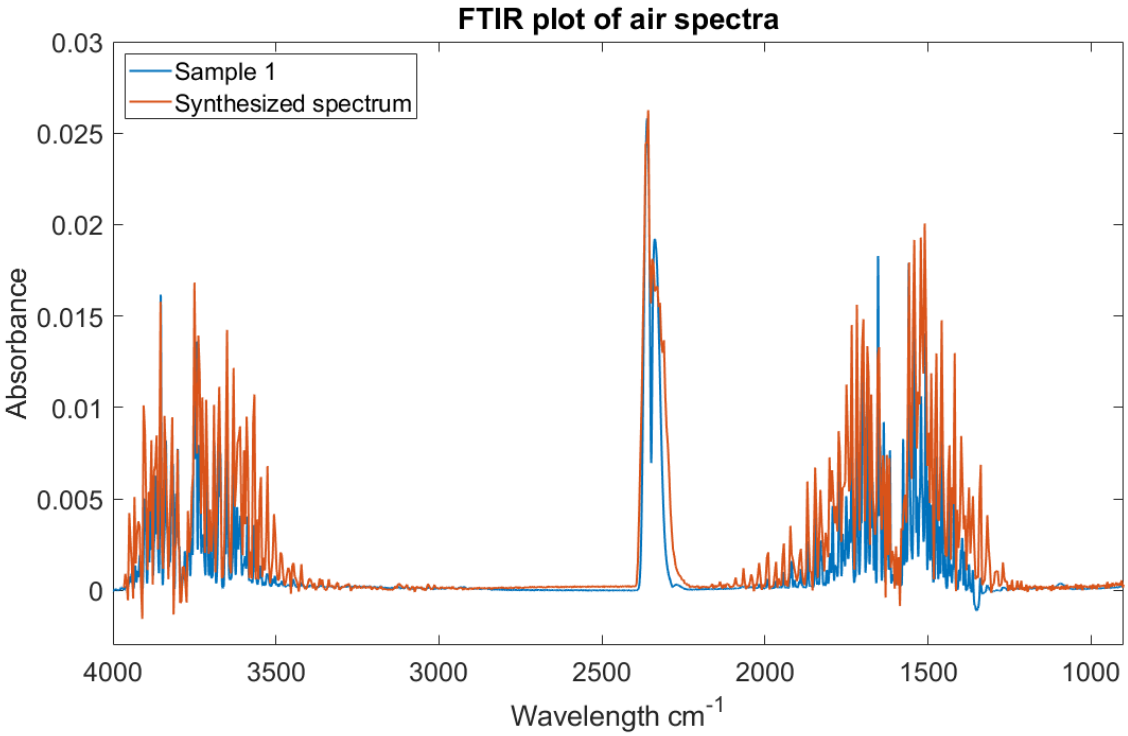

Figure 6.5: FTIR spectra of baseline air samples

In the MS data, there were two scales that species could be detected in. The first scale ranged from 35 to 100 amu, and the second scale detected species from 1 to 50 amu. The two scales result in some overlapped measurements. The masses with ”-2” after the name refer to the masses that overlap that are detected on the smaller scale (scale from 1 to 50 amu), such as ”Mass 40-2”. Some of these overlapping species, such as Mass 40 (and Mass 40-2) are detected on both scales, while some species can be detected on only one or the other.

After analyzing a sample and obtaining FTIR and MS data, the MS data set was processed using the MATLAB code. The code shows a plot of pressure versus scan for each molecular weight (35 to 100 amu and 1 to 50 amu), and the user is prompted to input if that plot is to be included in the detected masses. Figure 6.6 shows the plot for Mass 36 for baseline air with a dotted line to indicate the scan at which the sample was introduced into the MS system. It can be seen from the jump in pressure after the dotted line in the plot that Mass 36 was a mass present in the sample. The pressure plot for Mass 39 is shown in Figure 6.7, and in this plot, there is no clear increase in pressure after the introduction of the sample, which is why Mass 39 was not identified as a present mass in the sample. Once the pressure plot was analyzed visually for each mass and the detected masses were identified, a plot with the pressure versus scan data for each of the detected masses was created. Figure 6.8 shows the plot of the masses detected in the baseline air sample.

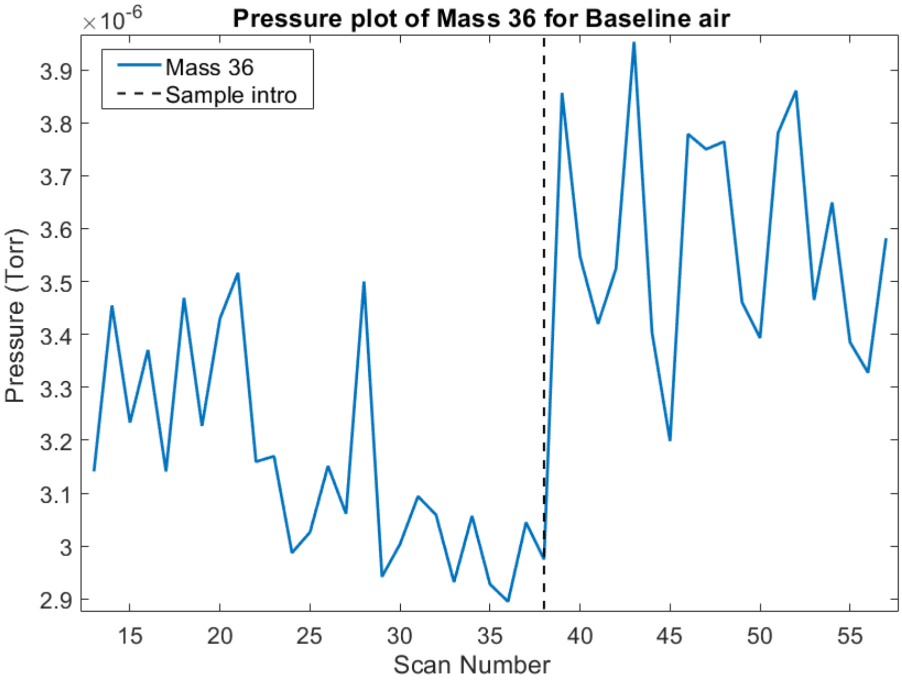

Figure 6.6: Pressure versus scan plot for Mass 36 of baseline air mass spectrometry analysis

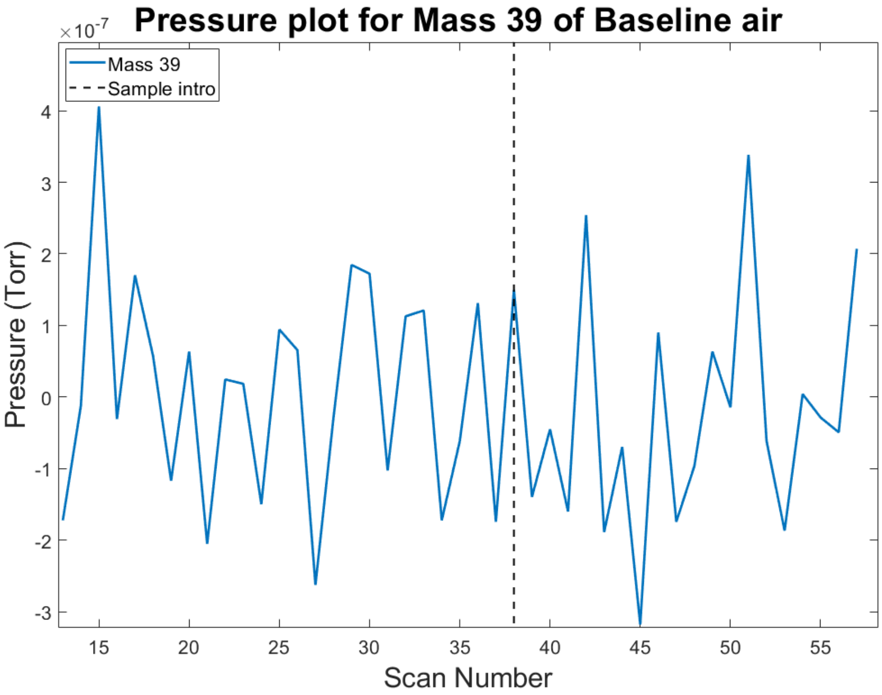

Figure 6.7: Pressure versus scan plot for Mass 39 of baseline air mass spectrometry analysis

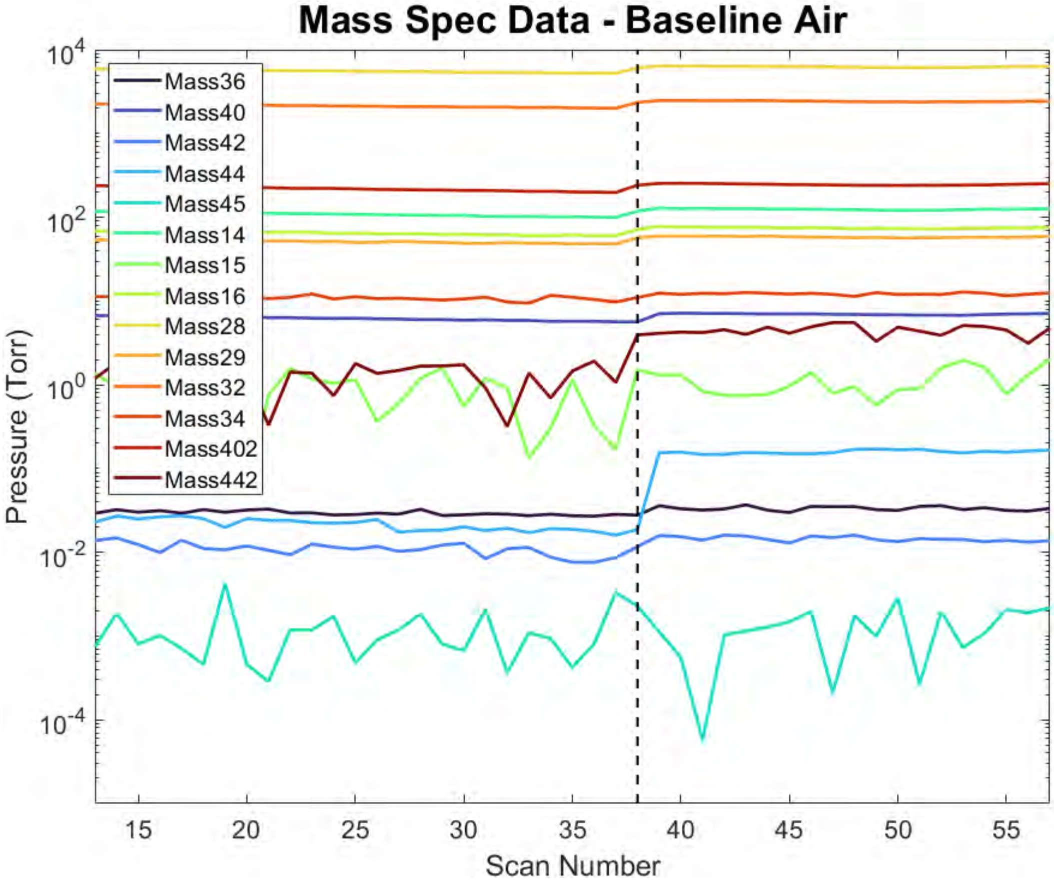

Figure 6.8: Masses detected from baseline air sample when analyzed using MS

The other results produced from the code are the tabulated masses and their partial pressures. Due to complications in the MS system, the absolute pressure values recorded were not correct, but the relative increase in pressure was accurate and partial pressures were still able to be determined. During the analysis process, the maximum total pressure was determined by calculating the total pressure at each scan using the sum of all pressures of all masses and finding the maximum pressure. The pressure of each species at the scan with the maximum partial pressure was then divided by the total pressure at that scan to find the partial pressures. Analysis was run on two separate baseline air samples. The masses detected in the MS analysis for the baseline air and the average partial pressures are listed in Table 6.4, ordered from largest partial pressure to smallest.

From these determined masses, possible species were found using the NIST Database [5, 6], and the PubChem Spectral compound database [13]. The possible species were first listed from the molecular weight found, starting at the most abundant mass (Mass 28). Then, species were eliminated based on phase and if a mass spectrum was present in the databases. The final species possibilities for each mass are listed in Table 6.1. Then species were eliminated if the species was not a common air component, and nitrous oxide was ignored because its known volume in air is 0.3 ppm [4]. This produced the final species possibility list, as shown in Table 6.2. From the species eliminations made, there were many masses determined to have no species possibilities with that molecular weight from the databases used. The masses with no known possibilities were still considered in the further analysis as possible isotopes or ions from other species.

Table 6.1: Species possibilities for each mass in the baseline air sample

Molecular mass (amu)	Species possibilities
28	Carbon monxide Nitrogen Ethylene Diborane
32	Sulfur Oxygen Silane Methyl alcohol Hydrazine
40	Argon Cyclopropene Allene Propyne
14	Unknown
16	Methane
29	Unknown
34	Hydrogen sulfide
44	Carbon dioxide Nitrous oxide Acetaldehyde Ethylene oxide Propane
15	Unknown
36	Hydrogen chloride
42	Ketene Propene Cyclopropane
45	Formamide Dimethylamine Ethylamine

Table 6.2: Refined species possibilities for each mass in baseline air sample

Molecular mass (amu)	Species possibilities
28	Nitrogen
32	Oxygen
40	Argon
14	Unknown
16	Methane
29	Unknown
34	Unknown
44	Carbon dioxide
15	Unknown
36	Unknown
42	Unknown
45	Unknown

From the species still listed as possibilities, the MS peaks present for each species from the known mass spectra were noted. The final species possibilities and the peaks from their known mass spectra as well as the relative abundances are listed in Table 6.3, with the masses of the peaks sorted from most abundant to least abundant. The relative abundance as well as the mass spectra come from the NIST database [5] and the PubChem database [13]. The known mass spectrum for nitrogen is shown in Figure 6.9, with the three peaks and their relative abundances. Note that the three different peaks represent the common diatomic nitrogen molecule at 28 amu, an isotope of the nitrogen molecule at 29, and an ionized nitrogen atom at 14.

Table 6.3: Species possibilities and their known MS data

Species	Mass of peaks (amu)	Relative abundance (%)
Nitrogen (N_2)	Mass 28	100.0
	Mass 14	13.79
	Mass 29	0.74
Oxygen (O_2)	Mass 31	100.0
	Mass 16	21.80
Argon (Ar)	Mass 40	100.0
	Mass 20	14.62
	Mass 36	0.30
	Mass 38	0.05
Methane (CH_4)	Mass 16	100.0
	Mass 15	88.79
	Mass 14	20.42
	Mass 13	10.69
	Mass 12	3.80
	Mass 17	1.64
Carbon dioxide (CO_2)	Mass 44	100.0
	Mass 28	9.81
	Mass 16	9.61
	Mass 12	8.71
	Mass 22	1.90
	Mass 45	1.20
	Mass 46	0.40
	Mass 29	0.10

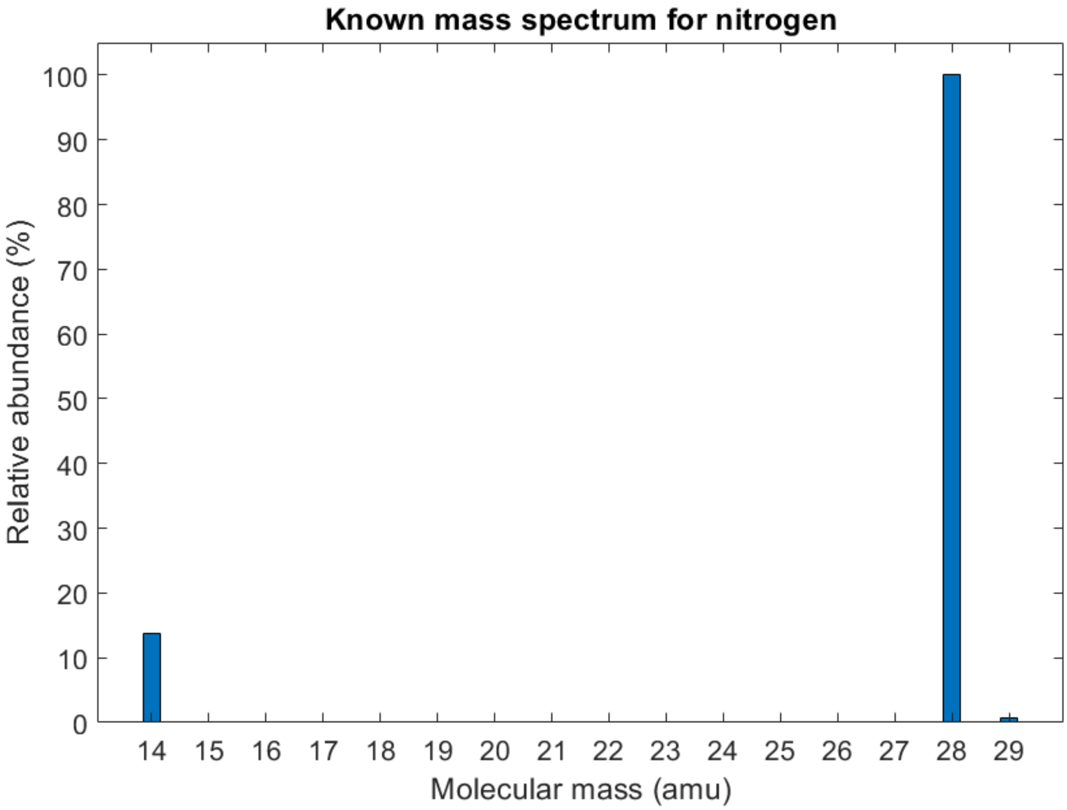

Figure 6.9: Known mass spectrum for nitrogen

From the peaks in each mass spectra, species possibilities for the detected masses could be found from the MS peaks for the species rather than the molecular weight of the species itself. The list of species possibilities with found from the MS peaks is listed in Table 6.4. The masses that were detected on both MS scales were only included once, and the values taken for these masses were from the 1 to 50 amu scale. These masses are still listed with ″-2″ after the mass (such as 40-2).

Table 6.4: Baseline air MS data and possible species

Molecular mass (amu)	Partial pressure (%)	Possible species
28	66.67	Nitrogen Carbon dioxide
32	26.62	Oxygen
40-2	2.946	Argon
14	1.250	Nitrogen Methane
16	0.7458	Oxygen Methane Carbon dioxide
29	0.6261	Nitrogen Carbon dioxide
34	0.1420	Unknown
44-2	0.04356	Carbon dioxide
15	0.01385	Methane
36	$3.62*10^{-4}$	Argon
42	$1.67*10^{-4}$	Unknown
45	$1.19*10^{-5}$	Carbon dioxide

Each species listed has a known mass spectrum obtained from the NIST database [5]. These spectra were used to analyze the experimental MS data for the baseline air sample and to determine each species' partial pressures. The partial pressures for each peak of each detected species are important to determine because it contributes to the total partial pressure for that species. Each molecule detected has contributions at multiple masses due to atomic isotopes and potential ionization in the MS system. A process was developed to calculate the contributions from each molecule at each spectral mass peak, which started with the analysis of the nitrogen present because it was the most abundant material.

The mass with the largest detected partial pressure (Mass 28) was studied first. The only species in the list that contained a peak at MW 28 were nitrogen and carbon dioxide. Because the primary peak (peak with the relative abundance of 100% in the known spectrum) for nitrogen is at Mass 28, nitrogen was studied first for Mass 28. Mass 28 in nitrogen's known spectrum is listed at 100.0% relative abundance, so the measured partial pressure for Mass 28 (66.67%) was set to be 100% relative abundance for nitrogen. This peak for nitrogen lines up with the molecular weight of the diatomic nitrogen molecule. Nitrogen's next largest peak in the known spectrum is Mass 14 at 13.79% relative abundance. If the partial pressure at Mass 28 (66.67%) is assumed to be 100% relative abundance, then the partial pressure at Mass 14, with a relative abundance of 13.79%, should be 9.194%. The actual measured partial pressure at Mass 14 was 1.250%, which is much lower than the calculated 9.194%. The peak at Mass 14 for nitrogen represents the elemental nitrogen present from the ionization of the molecule. A possible reason that the relative abundance of this peak was determined to be much lower than that in the known spectrum is the ionization process in the MS analysis for this work could have resulted in less elemental nitrogen than the system used for the spectrum from the NIST database [5]. The measured value of 1.875% (from the partial pressure of 1.250%) was therefore used as the nitrogen component at mass 14.

Nitrogen's last peak is at Mass 29, with a relative abundance in the known spectrum of 0.74%. This relative abundance with Mass 28 at 100% relative abundance would result in a partial pressure for Mass 29 of 0.4934%, which is lower than the total, partial pressure measured for Mass 29. Because of this, the relative abundance for Mass 29 was adjusted so that it would result in a partial pressure equal to that of Mass 29. This gave a relative abundance for nitrogen Mass 29 of 0.9391% to produce a partial pressure of 0.6261%. This relative abundance was much closer to that from the known spectrum, which is due to Mass 29 being an isotope for nitrogen rather than the ionization of the molecule, so the relative abundance should not vary significantly.

The mass with the next largest measured partial pressure, Mass 32, was then analyzed. The only species spectrum in the final species list to contain a peak at Mass 32 was oxygen. For the O_2 spectrum, the partial pressure at MW 32 (26.62%) was assumed to be 100% relative abundance (as Mass 28 was for N_2). The next peak in the known spectrum for O_2 (Mass 16) had a listed relative abundance of 21.80%. This relative abundance, paired with the partial pressure of Mass 32 at 100% relative abundance, would represent a partial pressure of 5.803%, This is far above the measured partial pressure for Mass 16 of 0.7458%. Therefore, a relative abundance was calculated and determined to be 2.802%, which represented a partial pressure of 0.7458%. This difference in relative abundances may also be due to the ionization process as described for nitrogen.

Then the peak at MW 40 was studied. Molecular weight 40 was detected by both ranges, but the detected MW 40 in the smaller range (1 to 50 amu) had a higher partial pressure, so that was the partial pressure used for analysis. For MW 40, argon was the only species with a peak at this location, and it is the primary peak for argon. Therefore, the partial pressure for 40-2 (2.946%) was set to 100% relative abundance. Two peaks in the argon spectrum were not detected here, at masses: 20 and 38. The relative abundance for the other peak in the spectrum, MW 36, was calculated using the maximum partial pressure measured for the weight (3.619E-4%), and it was determined to be 0.01228%.

This process was repeated to calculate the relative abundances for peaks present in the carbon dioxide spectrum. The partial pressure for the main peak for the spectrum, 0.04356% at MW 44, was set to 100% relative abundance. The next peak was at MW 28, and because the partial pressure at this location was so much larger than that at MW 44, 67.55% versus 0.04356%, respectively, the partial pressure for MW 28 could not be determined with the methods used for the other species. Therefore, the relative abundance listed in the known spectrum (9.810%) was used, which equates to a partial pressure of 4.273E-3%. Because the partial pressure at MW 28 is now used for both nitrogen and CO_2, the partial pressure of MW 28 for CO_2 was subtracted from that of N_2, but due to the low value for CO_2, it did not affect the value for N_2. The peak at MW 16 presented the same situation as the peak at MW 28, and so the partial pressure was calculated the same way. Using the relative abundance from the known spectrum (9.610%), the partial pressure was found to be 4.186E-3%. Again, this was a peak that was in multiple spectra, so the partial pressure for this peak was subtracted from that of the peak for O_2. This decreased the partial pressure for the peak in oxygen to 0.7416 which decreased the relative abundance to 2.786%. The partial pressure for peak 45 was set to the measured value (1.193E-5%), and a relative abundance of 0.02739% was calculated. Lastly, the known relative abundance was used for MW 29 (1.0E-3%), and a partial pressure of 4.356E-7% was found. Mass 29 was another peak found in multiple spectra, but this partial pressure did not affect that of the N_2 peak. The peaks in the CO_2 spectrum that were not detected in experimental testing were MW's: 12, 22, and 46.

Lastly, the relative abundances were found for methane. The main peak for methane is at MW 16, but because this mass is found in multiple species, the relative abundance and partial pressure of the next peak (MW 15) for methane were used to work backward to a partial pressure for MW 16 that represented 100% relative abundance. The partial pressure at MW 15 was 0.01385% and the relative abundance from the known spectrum was 88.79%, which produces a partial pressure for MW 16 of 0.01559% to give 100% relative abundance. This partial pressure of MW 16 further decreases the partial pressure of MW 16 for O_2 to 0.7260% and decreases the relative abundance to 2.727%. The listed relative abundance for the peak at MW 14 was 20.42% resulting in a partial pressure of 3.183E-3%, which reduced the partial pressure of MW 14 for N_2 to 1.247% and reduced the relative abundance to 1.870%.

The tabulated data of final relative abundances and partial pressures for the species is shown in Table 6.5. The final relative abundances for species were determined by summing the partial pressures of the peak within a species. The final partial pressures determined were: nitrogen at 68.54%, oxygen at 27.35%, argon at 2.946%, carbon dioxide at 0.05203%, and methane at 0.03262%. These final relative abundances for each peak and for the species will be used to calculate partial pressures for peaks in the abuse test data.

Table 6.5: Final relative abundances and partial pressures for the species in the baseline air sample

Species	MW of peak	Relative abundance from known spectrum(%)	Final calculated relative abundance (%)	Final partial pressure (%)	Notes
Nitrogen	28	100.0	100.0	66.67	
	14	13.79	1.870	1.247	
	29	0.74	0.9391	0.6261	
Oxygen	32	100.0	100.0	26.62	
	16	21.80	2.727	0.7260	
Argon	40-2	100.0	100.0	2.946	
	36	0.30	0.01228	3.6e-4	
Carbon dioxide	44	100.0	100.0	0.04356	
	28	9.81	9.810	4.27e-3	Doesn't decrease N_2 peak
	16	9.61	9.610	4.19e-3	Decreased O_2 peak partial pressure to 0.7416
	45	1.20	0.02739	1.2e-5	
	29	0.10	1.0E-3	4E-7	Doesn't decrease N_2 peak
Methane	16	100.0	100.0	0.01559	Further decreases O_2 peak to 0.7260
	15	88.79	88.79	0.01385	Used values to find partial pressure for peak 16
	14	20.42	20.42	3.18E-3	Decreased N_2 peak to 1.247

6.2 Abuse test results

Once the main baseline experiments were analyzed, chemical analysis data for the abuse tests were analyzed. Abuse tests 1 and 2 were not sampled due to the vent cap of each cell not rupturing. Therefore, the first test to be analyzed was Test 3, which consisted of a cell at nominal voltage, a heating rate of 12.3 °C/min, and a 100 ms sample duration. The produced MS plot of the determined molecular weights for the close sample of abuse Test 3 can be seen in Figure 6.10 with the dotted line representing the scan at which the sample was introduced into the MS system.

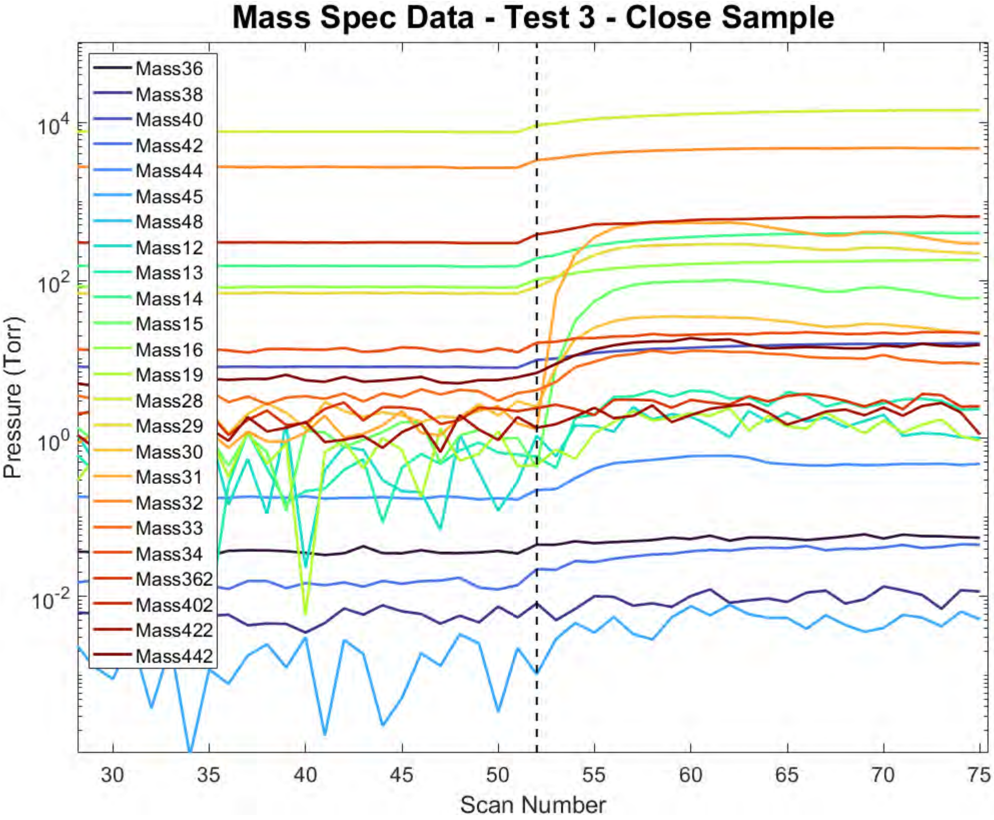

Figure 6.10: Mass spectrometry data for the close sample of test 3

This process was also completed for the far sample from the test. The data from both samples were then tabulated as shown in Table 6.6, with each species and their partial pressures sorted in descending order by pressure. The majority of the masses determined in the far sample were the same as that of the close, although some masses were detected in one sample and not the other. Also, the order of masses in relation to partial pressure differed slightly between the two.

Table 6.6: Masses from test 3 close sample and their partial pressures

Molecular weight (amu)	Partial pressure from close sample (%)	Partial pressure from far sample (%)
Mass 28	67.51	73.86
Mass 32	22.64	25.30
Mass 40-2	3.057	3.513
Mass 14	1.896	1.929
Mass 31	1.829	2.076
Mass 29	1.195	1.341
Mass 16	0.8481	0.8662
Mass 15	0.3628	0.3472
Mass 30	0.1256	0.1540
Mass 34	0.1002	0.1111
Mass 40	0.0750	0.0900
Mass 44-2	0.0685	0.0831
Mass 33	0.0474	0.0570
Mass 13	0.0148	0.0102
Mass 36-2	0.0111	0.0153
Mass 42-2	0.0092	0.0132
Mass 19	0.0056	N/A
Mass 12	0.0051	N/A
Mass 44	0.0023	0.0032
Mass 36	2.9e-4	3.2e-4
Mass 42	2.1e-4	2.6e-4
Mass 38	5.7e-4	6.6e-5
Mass 39	N/A	3.5e-5
Mass 45	2.8e-4	3.0e-5
Mass 48	1.4e-4	2.7e-5

Once the MS data were sample, the background spectrum (empty analysis chamber) for the test was subtracted from the sample spectra. This gave a spectrum of the peaks that are present in the sample but not in the background for each data set. These spectra are shown in Figure 6.11.

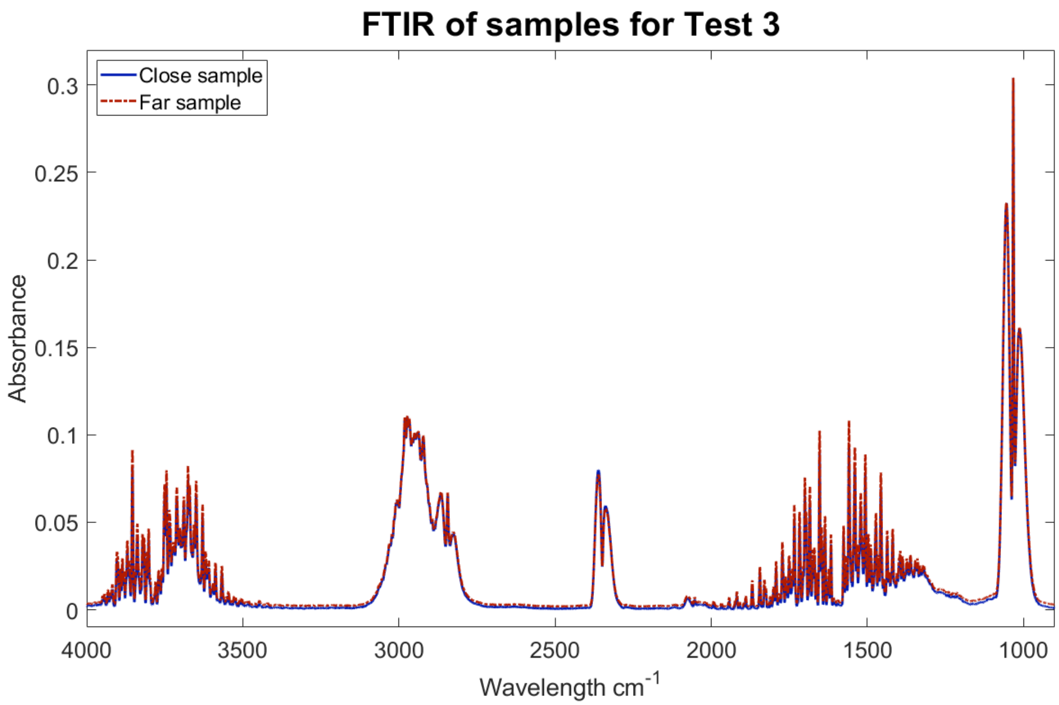

Figure 6.11: FTIR spectra for samples from test 3

The FTIR intensities were observed to be relatively low, which led to an increase in sampling time in future tests. The longer sample duration was expected to allow more mass into the sampler, resulting in higher intensity peaks in the subsequent FTIR analysis.

Two tests were conducted with cells at 100% state-of-charge (Tests 4 and 5) before increasing the sample duration. Test 5 was not sampled due to an undesirable vent cap rupture occurring and a low volume of gas exhaustion, but the samples from Test 4 were analyzed. Then the data was processed using the same method that was used for the previous test. From this processing, plots for the MS data and a list of molecular weights with their partial pressures were obtained. The MS data for the far sample was noisy and difficult to analyze accurately, so the presented data is from the close sample. The results are shown in Table 6.7.

Table 6.7: Masses from test 4 far sample and their partial pressures

Molecular weight	Partial pressure (%)
Mass 28	73.86
Mass 32	25.30
Mass 40-2	3.513
Mass 31	2.076
Mass 14	1.929
Mass 29	1.341
Mass 16	0.8662
Mass 15	0.3472
Mass 30	0.1540
Mass 34	0.1111
Mass 40	0.0900
Mass 44-2	0.0831
Mass 33	0.0570
Mass 36-2	0.0153
Mass 42-2	0.0132
Mass 13	0.0102
Mass 44	0.0032
Mass 36	3.2e-4
Mass 42	2.6e-4
Mass 38	6.6e-5
Mass 39	3.5e-5
Mass 45	3.0e-5
Mass 48	2.7e-5

Although these results are fairly consistent with the MS and FTIR results from the first experiment, the low volume of gases exhausted led to further abuse test experimentation with cells at nominal voltage and with a higher sampling duration.

After the final test series was conducted (Tests 6-11) and the samples from each test were analyzed, the data was processed. All samples were analyzed using the methods described. From this, partial pressures were obtained for all of the masses detected in each sample. The tabulated data of the masses detected, the number of samples they were found in (up to 12 from close and far samples for 6 tests), and the average partial pressure of that mass is shown in Tables 6.8 and 6.9. An example of the MS data plotted as partial pressure versus a scan from one of the tests (far sample of Test 9) can be seen in Figure 6.12.

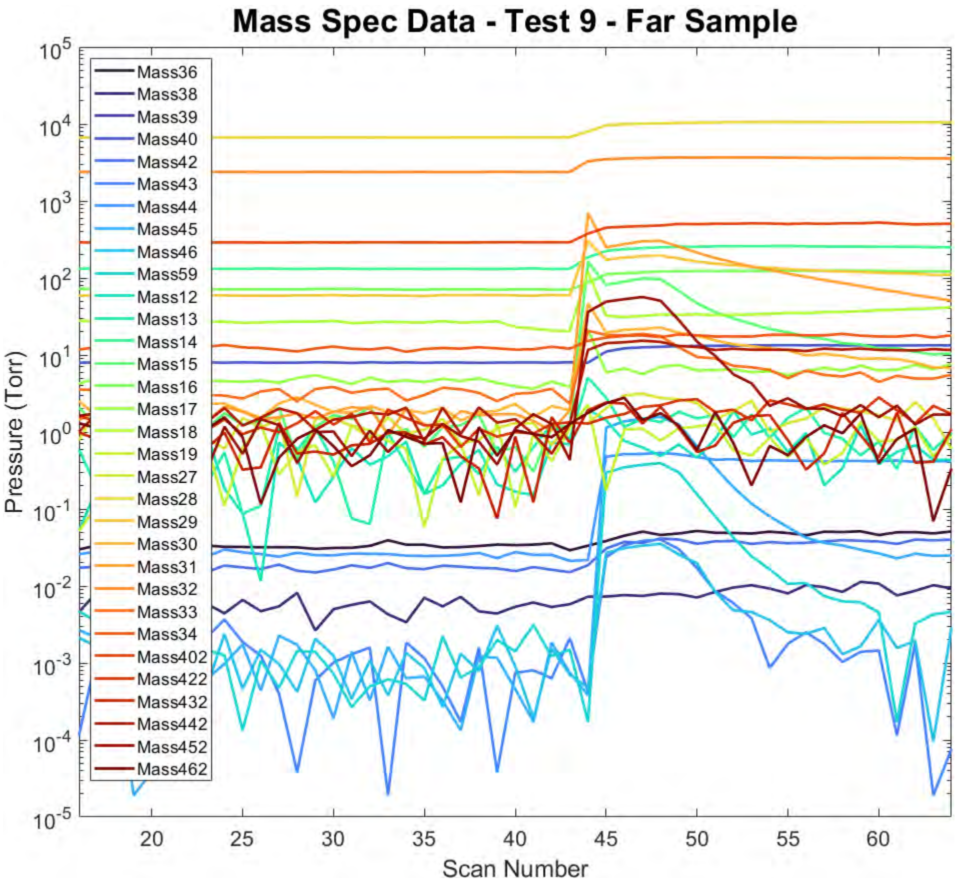

Figure 6.12: Mass spectrometry data for the far sample of Test 9

Once the means were calculated for the data, the standard deviations and 95% confidence intervals were determined and are shown in Tables 6.8 and 6.9. These ranges for the confidence interval are used as upper and lower bounds for partial pressure inputs for the model. This will give a flammability band for the range of values. The masses detected across the samples and their mean partial pressures are plotted with the 95% confidence intervals as error bars in Figure 6.13. This shows a visual representation of the tabulated data in Tables 6.8 and 6.9.

Table 6.8: Masses detected in the final test series, the number of samples that each mass was detected in, and their average partial pressures

Molecular weight	No. of samples	Mean partial pressure (%)	95% confidence interval
Mass 28	12	67.12	±0.8134
Mass 32	12	22.71	±0.6068
Mass 40-2	12	3.037	±0.1209
Mass 14	11	1.776	±0.1145
Mass 31	12	1.418	±0.5218
Mass 29	12	1.084	±0.1646
Mass 16	11	0.8252	±0.0300
Mass 18	9	0.5452	±0.3618
Mass 15	12	0.4932	±0.2180
Mass 45-2	12	0.1775	±0.1216
Mass 34	12	0.1097	±5.66e-3
Mass 30	12	0.1072	±0.02691
Mass 17	9	0.09907	±0.06158
Mass 44-2	12	0.08832	±0.01595
Mass 40	11	0.07732	±4.85e-3
Mass 33	12	0.07503	±0.01928
Mass 36-2	3	0.01659	±1.33e-3
Mass 27	9	0.01468	±3.98e-3
Mass 46-2	5	0.01228	±6.92e-3
Mass 42-2	4	0.01194	±2.44e-3
Mass 13	10	0.01098	±4.19e-3
Mass 43-2	3	0.01070	±0.01006
Mass 47-2	2	0.01066	±3.46e-3
Mass 12	4	9.46e-3	±2.53e-3
Mass 19	4	7.76e-3	±2.53e-3
Mass 45	12	5.07e-3	±3.47e-3
Mass 44	12	3.08e-3	±5.4e-4
Mass 59	8	1.24e-3	±1.16e-3
Mass 36	11	2.8e-4	±2.3e-5
Mass 42	12	2.3e-4	±2.5e-5
Mass 60	3	1.9e-4	±1.6e-4
Mass 43	12	1.3e-4	±7.6e-5
Mass 46	12	1.2e-4	±7.8e-5
Mass 62	3	1.1e-4	±8.5e-5
Mass 61	3	8.1e-5	±6.9e-5
Mass 91	2	6.5e-5	±9.1e-5
Mass 38	7	5.5e-5	±8e-6

Table 6.9: Continued masses detected in the final test series, the number of samples that each mass was detected in, and their average partial pressures

Molecular weight	No. of samples	Mean partial pressure (%)	95% confidence interval
Mass 39	4	4.9e-5	±1.1e-5
Mass 47	6	3.0e-5	±1.8e-5
Mass 48	2	2.7e-5	±3.1e-5
Mass 41	2	2.3e-5	±2.1e-5
Mass 58	1	6.9e-6	N/A

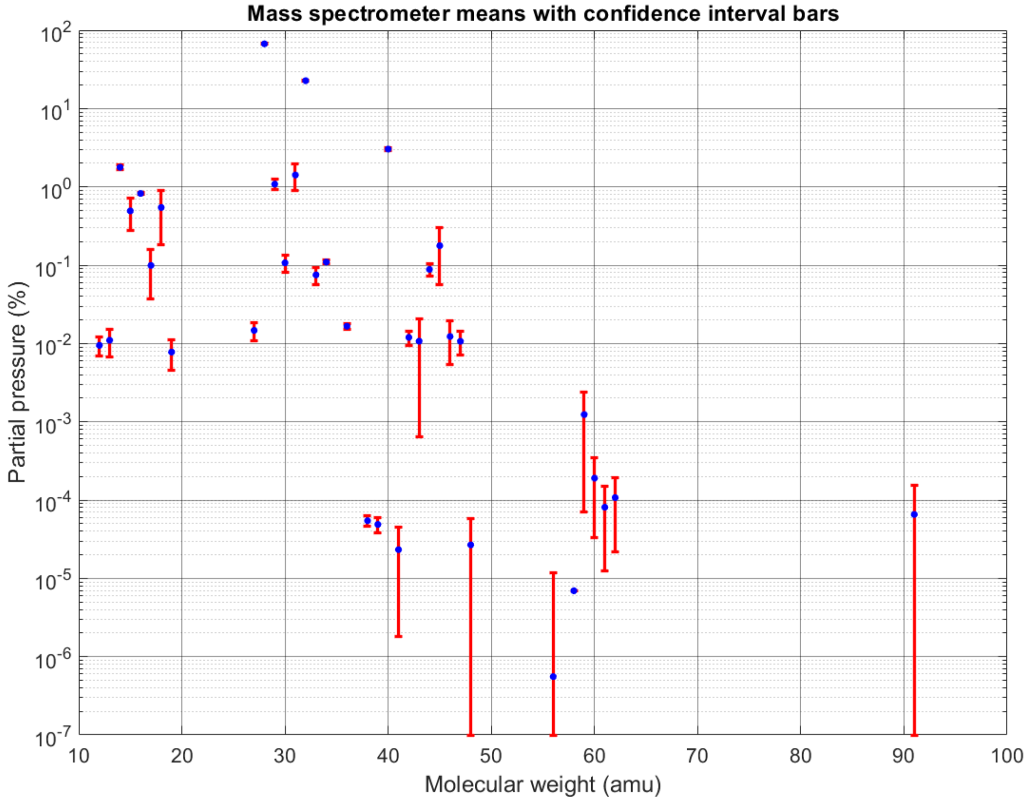

Figure 6.13: Plot of partial pressure averages for masses and confidence intervals

The analysis of these samples also produced an FITR spectrum for each that was re-processed by subtracting the background spectrum of each respective test from the sample spectrum. The FTIR spectra of each sample were then plotted onto one graph with all spectra overlaid. When analyzing the spectra, the peak locations appeared consistent throughout the tests, and the relative heights for each spectrum also were generally consistent. The graph showing FTIR spectra from all of the tests and the baseline air spectrum can be seen in Figure 6.14.

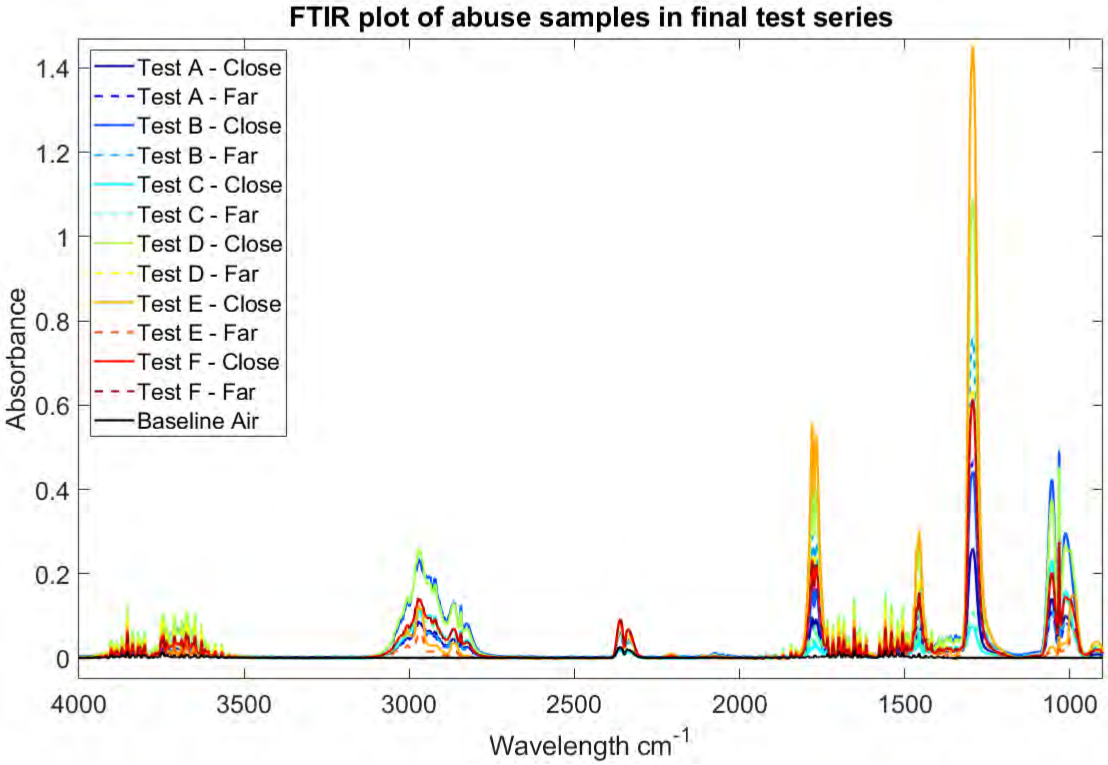

Figure 6.14: FTIR plot of spectra from samples in the final test series

The average MS and FTIR data for these tests were then used to find species possibilities and to find the most likely chemical composition for the samples. First, using the same databases used for the air sample (the NIST and PubChem databases), species possibilities were found for all of the molecular weights found from the MS data. Then, species were eliminated if they were found to be a possible species for the molecular weight, but no known mass spectrum was found in the databases. This was done because the data from these species were not available to be compared to the collected data, and therefore the species was ignored. The list of species possibilities and their molecular weights can be found in Appendix A.

Next, a series of eliminations were made for the species possibilities based on different criteria. The boiling point of each species was used as the first criterion. If the species had a boiling point above 200 °C, it was eliminated because the sample was only heated to 180° during the chemical analysis process. Lastly, species were eliminated based on chemical composition. Knowing the general components that may be present in the cell, species were eliminated if they contained elements besides: lithium (electrolyte salt), phosphorous (electrolyte salt), fluorine (electrolyte salt), carbon (electrolyte solvents and anode material), hydrogen (electrolyte solvents), oxygen (electrolyte solvents and cathode material), cobalt (cathode material), manganese (cathode material), nickel (cathode material), copper (cell component), and aluminum (cell component). Other elements assumed to be in the cell due to air are nitrogen and argon.

Once species were eliminated based on these criteria, existing FTIR spectra were found from NIST for the remaining species. These species were imported into the Essential FTIR (eFTIR) software [26] and used as an FTIR database for analysis in the software. FTIR spectra for each of the potential electrolyte solvent components were also added to the database. Using the eFTIR software, the Test 10 close sample FTIR spectrum was analyzed using a Correlation Coefficient search algorithm. For the correlation coefficient, a matching number was calculated for each spectrum with a match of 1.0 meaning a perfect correlation and a -1.0 meaning a perfect anti-correlation [26]. This coefficient was calculated in the software using Equation 6.1, with x and y representing the data on each the sample and database spectrum, and with $\bar{x}$ and $\bar{y}$ representing the means of the spectra data.

$$r = \frac{(x-\bar{x})(y-\bar{y})}{\sqrt{\sum(x-\bar{x})^2 \sum(y-\bar{y})^2}} \tag{6.1}$$

From this analysis, a table of species from the database and their correlation coefficient was produced. This analysis calculated coefficients for spectra from: the built-in database in the software, the species manually added for the potential species list, and the species listed as possible electrolyte components from the battery MSDS (ethylene carbonate, propylene carbonate, dimethyl carbonate, and diethyl carbonate). The five species with the highest coefficients were investigated, and it was found from the coefficient and visual comparison of spectra that the best match for the sample spectrum was dimethyl carbonate (DMC - $C_3H_6O_3$). The other four species did not match the sample spectrum at all, so it was assumed that only DMC from the list was present. DMC is one of the listed possible components of the electrolyte solvent from the MSDS for the used cells [36], so the presence of DMC is believable. The other possible electrolyte components from the MSDS did not have good correlation coefficients, and after visual comparison of each spectrum and the sample spectrum, they were ruled out as possibilities. Because the spectrum of DMC and the sample spectrum aligned so well, the other species listed from the correlation coefficient analysis were ignored. This species had a correlation coefficient of 0.5461, which is not a great match, but from visual comparison, the spectra appeared fairly consistent with most of the peaks in the spectrum. The spectrum used for the analysis (close sample of Test 10) was plotted against the spectrum of DMC with the y-value scaled down by 4.543 to closer match the intensity of the sample spectrum peaks. The two spectra are shown in Figure 6.15.

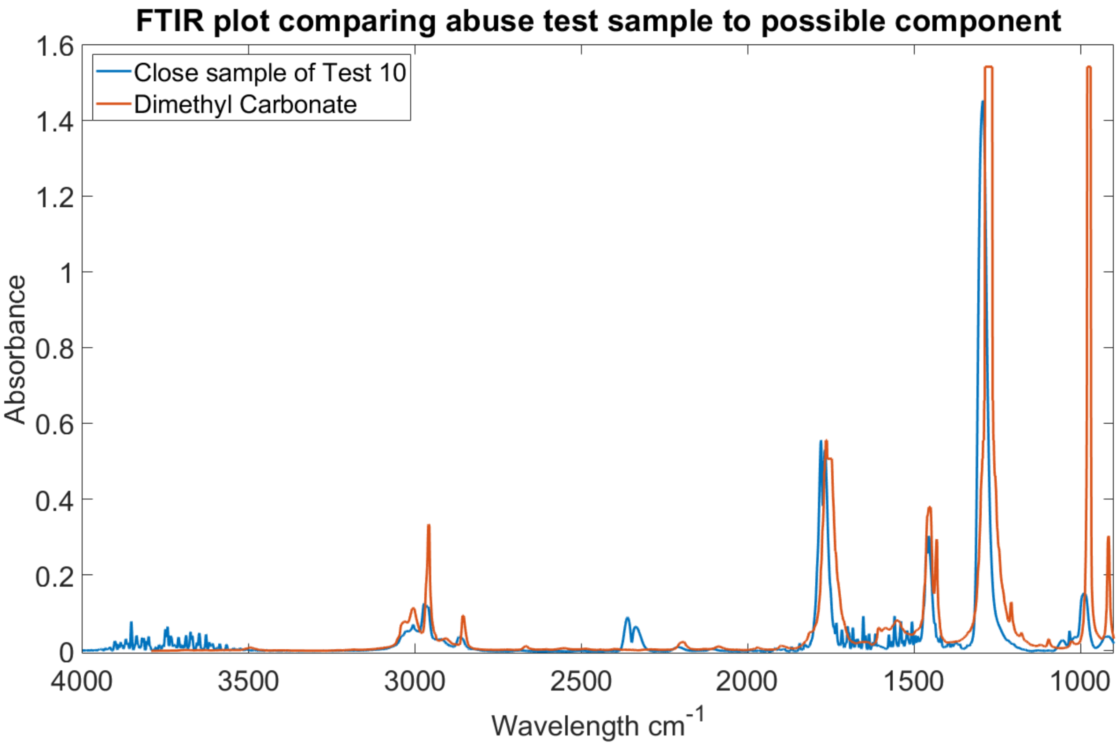

Figure 6.15: FTIR spectra of test sample and dimethyl carbonate

A synthesized spectrum for the sample was created using this analysis result and the detected species in the baseline air test. Because the sample was taken in air, it was assumed that the species present in the air sample were also components in the abuse test samples. Therefore, a synthesized spectrum was created using the SpectraGryph software using scaled spectra of CO_2, water, and dimethyl carbonate. The synthesized spectrum and a spectrum from one of the abuse tests is shown in Figure 6.16.

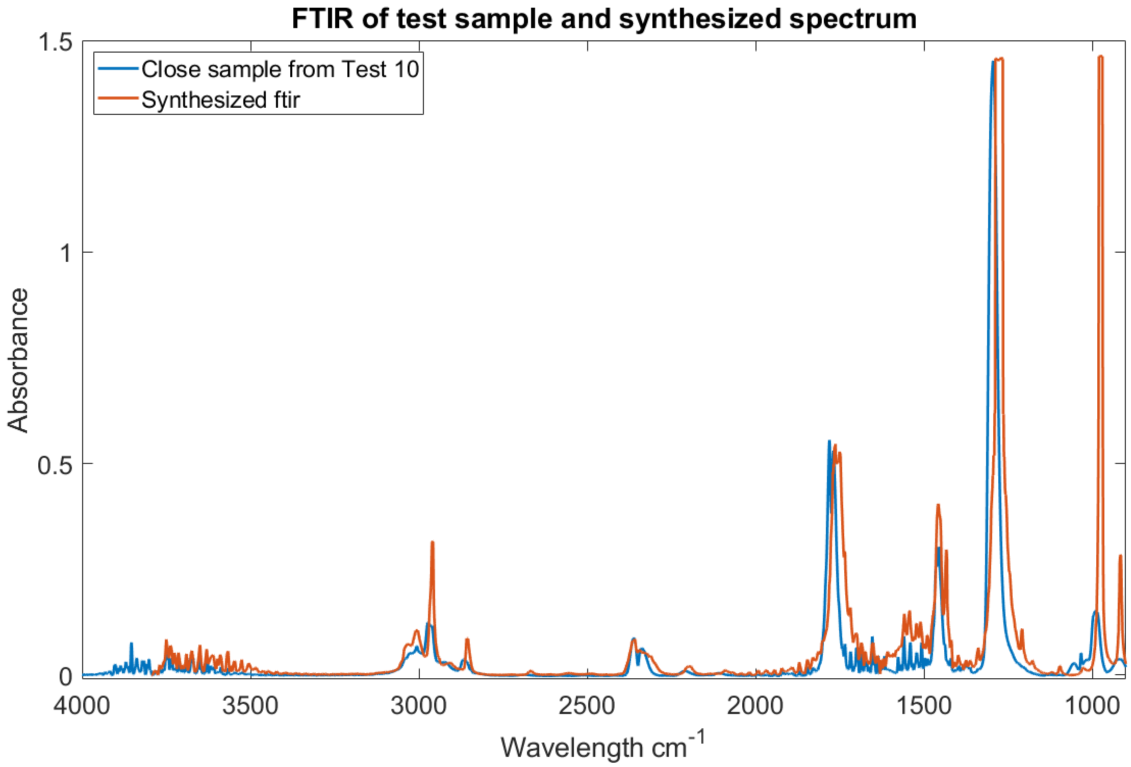

Figure 6.16: FTIR spectra of a test sample and synthesized spectrum

Once the main species possibilities were determined (nitrogen, oxygen, argon, CO_2, methane, water, and dimethyl carbonate), the species were compared to the mean MS data from the samples to determine the partial pressures of each species. The species that were detected in the baseline air sample (N_2, O_2, Ar, CO_2, and Methane) were used as the beginning of analysis for the abuse test analysis. The partial pressure for the main peaks of each species was used in combination with the relative abundances of the other peaks to determine partial pressures relating to all of the peaks for each species. The ratios of air species were compared to those of the species in the abuse test. Most of the species had good agreement with the air species, except for methane. Therefore, the methane partial pressure was adjusted to agree with the air. After the analysis of the species and relative abundances for air species, water and dimethyl carbonate were analyzed. Once partial pressures were determined, the remainder of the detected partial pressures were calculated. The tabulated list of relative abundances and partial pressures for these first species is shown in Tables 6.10 and 6.11.

Using this analysis, final partial pressures for the determined species were found. The species present - nitrogen, oxygen, argon, carbon dioxide, methane, water and dimethyl carbonate - were determined to have partial pressures of 68.96%, 23.32%, 3.038%, 0.6073%, 0.03283%, 0.6523%, and 1.698% respectively.

Next, the confidence interval for the partial pressure for each species was determined. This was calculated by determining the confidence interval for every peak in each species. Due to multiple molecular weights being peaks in multiple species, the confidence interval was scaled for each peak. The partial pressure determined for the peak in that species was divided by the average partial pressure measured at that molecular weight. This would determine the portion of partial pressure that represented the peak in that species. Then, this value was multiplied by the confidence interval value to find the scaled confidence interval (CI). These values are listed in Tables 6.10 and 6.11 with each species' partial pressures and peaks. The final summed confidence intervals for each species are tabulated and shown in Table 6.12.

Table 6.10: Species in abuse test data, their relative abundances and partial pressures

Species	MW of peak (amu)	Final relative abundance (%)	Final partial pressure (%)	95% Confidence interval (%)
Nitrogen	28	100.0	67.08	±0.8129
	14	1.870	1.254	±0.08087
	29	0.9391	0.6299	±0.09565
Oxygen	32	100.0	22.70	±0.6066
	16	2.727	0.6190	±0.09913
Argon	40	100.0	3.037	±0.1209
	36	0.01228	3.4e-4	±3.0e-5
Carbon dioxide	44	100.0	0.05084	±9.18e-3
	28	9.810	4.99e-3	±6.0e-5
	16	9.610	4.89e-3	±1.8e-4
	45	0.02739	1.4e-5	±9.5e-6
	29	1.0e-3	5e-7	±8e-8
Methane	16	100.0	0.01569	±5.7e-4
	15	88.79	0.01393	±6.16e-3
	14	20.42	3.20e-3	±2.1e-4
Water	18	100.0	0.5444	±0.3613
	17	17.53	0.09545	±0.05933
	16	0.90	4.90e-3	±1.78e-4
	19	1.396	7.60e-3	±3.16e-3
Dimethyl carbonate	15	100.0	0.4793	±0.2118
	45	37.03	0.1775	±0.1216
	29	70.45	0.3376	±0.05127
	31	69.06	0.3310	±0.1218
	59	0.2577	1.24e-3	±1.16E-3
	30	22.37	0.1072	±0.02691
	14	12.11	0.05804	±3.74e-3
	44	7.820	0.03748	±6.77e-3
	33	10.16	0.04869	±0.01251
	28	8.840	0.04237	±5.1e-4
	62	0.02241	1.1e-4	±8.5e-5
	60	0.03974	1.9e-4	±1.6e-4
	61	0.01690	8.1e-5	±6.9e-5
	16	2.930	0.01404	±5.1e-4
	46	2.563	0.01228	±6.92e-3
	13	2.292	0.01198	±4.193E-3
	32	1.940	9.30e-3	±2.5e-4
	43	2.232	0.01070	±0.01006

Table 6.11: Species in abuse test data, their relative abundances and partial pressures continued

Species	MW of peak (amu)	Final relative abundance (%)	Final partial pressure (%)	95% Confidence interval (%)
Dimethyl carbonate cont'd	17	1.10	5.27e-3	±3.28e-3
	42	0.36	1.73e-3	±3.5e-4
	91	0.01366	6.5e-5	±9.1e-5
	47	2.224	0.01066	±1.8e-5
	18	0.27	1.29e-3	±8.6e-4
	34	0.18	8.6e-4	±4.4e-5
	41	4.853E-3	2.3e-5	±2.1e-5
	19	0.05	2.4e-4	±1.0e-4
	40	0.05	2.4e-4	±9.5e-6

Table 6.12: Species in abuse test data, their summed partial pressures, confidence intervals, and the upper and lower bounds from the confidence interval

Species	Summed partial pressure (%)	Summed confidence interval	Upper bound of partial pressure (%)	Lower bound of partial pressure (%)
Nitrogen	68.96	0.9894	69.95	67.97
Oxygen	23.32	0.7058	24.02	22.61
Argon	3.038	0.1209	3.159	2.917
Carbon dioxide	0.6073	9.43e-3	0.07016	0.05130
Methane	0.03283	6.94e-3	0.03976	0.02589
Water	0.6523	0.4239	1.076	0.2284
DMC	1.698	0.5851	2.284	1.113

Comparing the final partial pressures of these species to those of air, certain assumptions can be made. Because many of the species that are in both agree within the confidence intervals or the partial pressure for the abuse test is less than those of air, the species that are vented out of the cell are assumed to be water and DMC. The ratios of these were calculated based on the partial pressures of the two species. The ratios were calculated by adding the partial pressures and finding the portion that each species makes up. This was completed for the mean values, the upper bounds, and the lower. These ratios are shown in Table 6.13. These ratios were used as the values entered in the reduced-order model.

Table 6.13: Species vented out of cell and ratios of each species

Species	Ratio from mean values (%)	Ratio from upper values (%)	Ratio from lower values (%)
Water	27.75	32.03	17.02
DMC	72.25	67.97	82.98

6.3 Cleaning validation test results

To test the cleaning process, a cleaning validation sample was collected. The sample cylinder that was used for all the tests was cleaned using the same process used before testing. Once the cleaning was complete, the cylinder was attached to the sampler and pulled to vacuum. Then, the sampler was opened to sample the air in the testing system to be compared to the original baseline air test and to the abuse samples. The sample was analyzed using the same methods as used for all previous samples.

The FTIR spectrum from the cleaning validation experiment was plotted against: the test sample spectrum with the highest intensities (close sample of Test 9), a spectrum from the first test in the final test series (far sample of Test 6), and the spectrum from the baseline air. This plot of overlayed spectra can be seen in Figure 6.17.

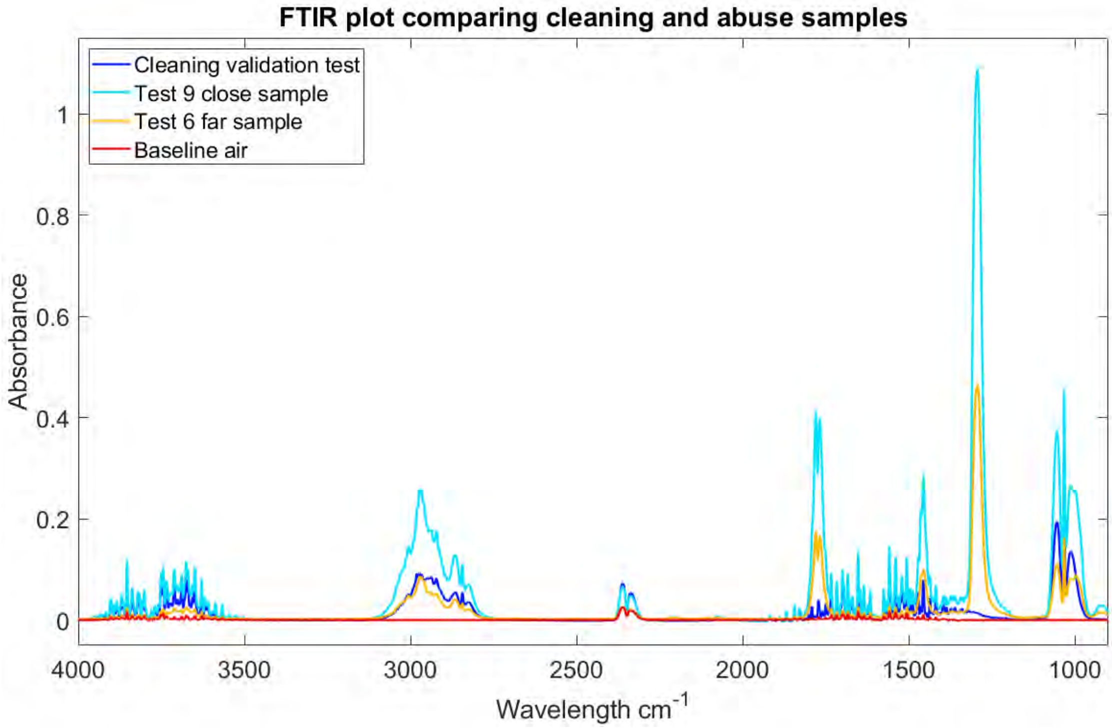

Figure 6.17: Comparison of cleaning validation test spectrum to abuse test spectra and air spectrum

It can be seen that the intensity of peaks in the cleaning validation spectrum is higher at some wavelengths than those of the far sample for Test 6. Although the peak intensities of the cleaning validation spectrum are less than those of the Test 9 spectrum, the cleaning validation spectrum shows that there was a build-up of material on the inside of the sample cylinders and that the cleaning process was not fully effective. The contamination is residual material from previous tests, which may impact the detected materials in subsequent tests. The cleaning reduced the build-up of these contaminants but did not fully clean the cylinder. Although there are peaks in spectrum from Test 6 that have lower intensities than that of the cleaning validation test, the location of the peaks was consistent throughout all of the samples. This means that the species in the test samples were seen to be consistent. Furthermore, the relative height of the peaks were fairly consistent in each test spectrum. This means that the partial pressure and composition of the species should not change despite the inefficiency of cleaning, because the values are calculated based on the total measured pressure for that sample. Therefore, the ratios determined for the vented species were kept the same for testing with the model.

6.4 Reduced-order model results

For the testing with the reduced-order model, tests were first run with the ratios determined from the mean partial pressures. This testing produced data for 1 cell venting 72.25% DMC and 27.75% water into a range of volumes. The data produced showed times for each volume at which the system becomes flammable (if it ever does) and at which the upper flammability limit had been surpassed and the volume is no longer flammable (if this ever occurs). This was then completed for the ratios from both the upper and lower bounds with the confidence intervals. The same data were obtained for both of these tests, and the data was plotted for all three tests. It can be seen from the results that the scenario simulated in the model, with the assumptions used The plot of the flammability map for the three tests with lower and upper flammability data is shown in Figure 6.18. In the

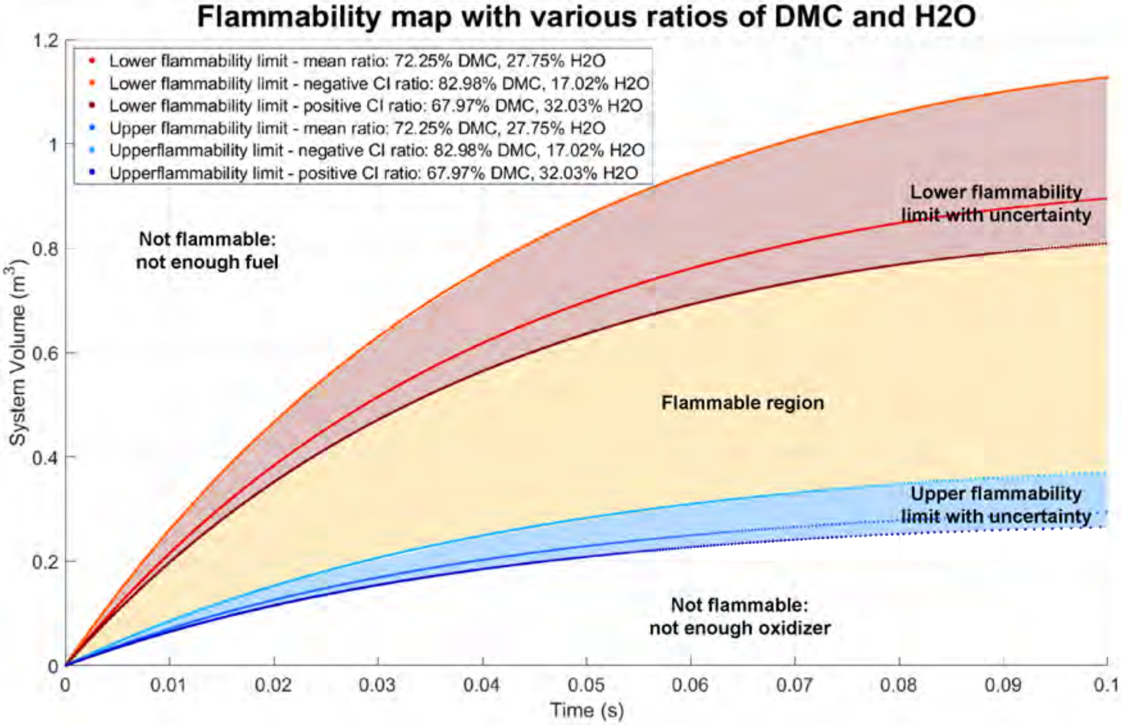

Figure 6.18: Flammability map for 1 cell venting ratios of DMC and water with variation from confidence intervals

CHAPTER 7

CONCLUSIONS AND FUTURE WORK

A reduced-order model was developed in MATLAB to simulate the thermal runaway and failure event of a lithium-ion battery. The model allows the user to specify the scenario in which the cell fails by defining the system volume, parameters, and vented gas chemistry. The results produced from the simulation include a flammability profile versus time for the scenario which can also be calculated for a range of volumes.

Experimental abuse testing was completed with varying cell heating rates until the desired vent rupture failure was observed. A series of abuse tests was conducted with constant test parameters to observe statistical differences in the vented gas composition. The samples taken from the tests were analyzed using FTIR and MS for chemical composition. The species detected in the samples included air species (N_2, O_2, Ar, CO_2, and CH_4) as well dimethyl carbonate, which was determined to be the liquid electrolyte solvent component, and water. The testing method was determined to be an effective method in determining the general composition of the vented gases from the failing cell.

Using the determined ratios of species vented from the failing cell (water and DMC) as well as the ratios using the confidence interval values, a flammability map for these cell failures was created for this failure scenario through the reduced-order model. From the flammability map, it can be seen that even with the range of partial pressures, no volume above 1.1275 m^3 becomes flammable, and that no volume over 0.3695 m^3 surpasses the upper flammability limit. The results are a basis for safety assessment that can be built upon in the future.

7.1 Future work

Analysis using chemical techniques such as Raman spectroscopy or nuclear magnetic resonance (NMR) spectroscopy on the abuse samples would provide a more comprehensive understanding of the chemical composition of the vented gases. Raman spectroscopy would provide vibrational data similar to FTIR with different sensitivity [11], while NMR produces data relating to the interaction of the species with electromagnetic radiation [20]. Thermogravimetric Analysis (TGA) on the baseline electrolyte would produce data for the breakdown of the sample as a function of temperature. This analysis would produce a set of data to compare to the results of the collected samples.

Other sets of abuse experiments with cells of different chemistry would further validate the experimentation method and assist in the risk assessment of other scenarios. This work focused on lithium-ion batteries with lithium nickel cobalt manganese oxide cathode chemistry, but repeating abuse tests using LIB's with another cathode chemistry (i.e., lithium nickel cobalt aluminum oxide) could provide flammability assessment of other kinds of cells. This would expand the information of flammability hazards relating to LIB's and assist in safety. The cells here were all of the 18650 size, but future work could also vary the cell geometry.

The effects of time and physical distance in the abuse experiments should also be studied. The experiments completed for this work focused on the statistical differences in the data from the collection and analysis methods rather than effects of variables such as time after venting and distance from the cell that the sample was taken. Conducting experiments with different time and distance variables would provide a better understanding of the full flammability environment dynamics as well as the evolution of the environment.

REFERENCES

[1] American Society of Heating, Refrigerating, and Air-Conditioning Engineers. *2021 ASHRAE Handbook: Fundamentals*, 2021.

[2] J. B. Bates. Fourier transform infrared spectroscopy. *Science*, 191(4222):31–37, January 1976.

[3] Claus Borgnakke and Richard E. Sonntag. *Fundamentals of Thermodynamics*. John Wiley and Sons, Inc., 2013.

[4] Peter Brimblecombe. *Air composition & Chemistry*. Press Syndicate of the University of Cambridge, 2nd edition, 1996.

[5] NIST Mass Spectrometry Data Center and William E. Wallace. *NIST Chemistry WebBook, NIST Standard Reference Database Number 69, Eds. P.J. Linstrom and W.G. Mallard*, chapter Mass Spectra. National Institute of Standards and Technology, https://doi.org/10.18434/T4D303, (retreived July-October 2022).

[6] NIST Mass Spectrometry Data Center and William E. Wallace. *NIST Chemistry WebBook, NIST Standard Reference Database Number 69, Eds. P.J. Linstrom and W.G. Mallard*, chapter Infrared Spectra. National Institute of Standards and Technology, https://doi.org/10.18434/T4D303, (retreived July-October 2022).

[7] Changki Choi, Deokhan Kim, Pyeong-Yeon Lee, Wooki Na, and Jonghoon Kim. Analysis of safety for lithium-ion battery with risk assessment of thermal runaway according to SOC. In *International Conference on Electrical Machines and Systems*, November 2021.

[8] H. F. Coward and G. W. Jones. Limits of flammability of gases and vapors. Technical report, Accession Number: AD0701575, United States Department of the Interior, 1952.

[9] Chhabil Dass. *Fundamentals of Contemporary Mass Spectrometry*. John Wiley and Sons, Inc., 2007.

[10] Tuula Hakkarainen, Esko Mikkola, Jan Laperre, Francis Gensous, Peter Fardell, Yannick Le Tallec, Claudio Baiocchi, Keith Paul, Margaret Simonson, Caronline Deleu, and Edwin Metcalfe. Smoke gas analysis by fourier transform infrared spectroscopy - summary of the safir project results. *Fire and Materials*, 24:101–112, 2000.

[11] Daniel C. Harris and Michael D. Bertolucci. *Symmetry and Spectroscopy: An Introduction to Vibrational and Electronic Spectroscopy*. Dover Publications, Inc., 1978.

[12] Muthukrishnan Kaliaperumal, Milindar S. Dharanendrakumar, Santosh Prasanna, Kaginele V. Abhishek, Ramesh Kumar Chidambaram, Stefan Adams, Karim Zaghib, and M. V. Reddy. Cause and mitigation of lithium-ion battery failure—a review. *Materials*, 14(5676), 2021.

[13] S. Kim, J. Chen, T. Cheng, A. Gindulyte, J. He, S. He, Q. Li, B. A. Shoemaker, P. A. Thiessen, B. Yu, L. Zaslavsky, J. Zhang, and E. E. Bolton. Pubchem in 2021: new data content and improved web interfaces. *Nucleic Acids Res.*, 49(D1):D1388–D1395, 2019.

[14] Kenneth A. Kobe and R. Emerson Lynn Jr. The critical properties of elements and compounds. *Chemical Reviews*, 52:117–236, February 1953.

[15] Joshua Lamb, Christopher J. Orendorff, E. Peter Roth, and Jill Langendorf. Studies on the thermal breakdown of common li-ion batteryelectrolyte components. *Journal of The Electrochemical Society*, 10(162):A2131–A2135, 2015.

[16] Peter J. Larkin. *IR and Raman Spectroscopy: Principles and Spectral Interpretation*. Elsevier, 2011.

[17] Stephen Y. Lin and Carton W. Dence. *Methods in Lignin Chemistry*. Springer-Verlag, 1992.

[18] Binghe Liu, Yikai Jia, Chunhao Yuan, Lubing Wang, Xiang Gao, Sha Yin, and Jun Xu. Safety issues and mechanisms of lithium-ion battery cell upon mechanicalabusive loading: A review. *Energy Storage Materials*, 24:86–112, 2020.

[19] Richard E. Lyon and Richard N. Walters. Energetics of lithium ion battery failure. *Journal of Hazardous Materials*, 318:164–172, 2016.

[20] Roger S. Macomber. *A Complete Introduction to Modern NMR Spectroscopy*. John Wiley & Sons, Inc., 1998.

[21] Arumugam Manthiram. A reflection on lithium-ion battery cathodechemistry. *Nature communications*, 11(1550), 2020.

[22] Frank Austin Mier. Measurement of 18650 format lithium ion battery vent mechanism flow parameters. MS thesis, New Mexico Institute of Mining and Technology, May 2018.

[23] Frank Austin Mier. *Fluid Dynamics of Lithium Ion Battery Venting Failures*. PhD thesis, New Mexico Institute of Mining and Technology, August 2020.

[24] MKS Instruments. *Process Eye Professional and EasyView*, August 2005.

[25] Emily Moore. *Fourier transform infrared spectroscopy (FTIR): methods, analysis, and research insights*. Nova Science Publishers, Inc., 2016.

[26] Operant LLC. *Essential FTIR*, 15th edition, 2014.

[27] Fernanda Stuani Pereira, Eduardo Ribeiro deAzevedo, Eirik F. da Silva, Tito José Bonagamba, Deuber L. da Silva Agostíni, Alviclér Magalhães, Aldo Eloizo Job, and Eduardo R. Pérez González. Study of the carbon dioxide chemical fixation - activation by guanidines. *Tetrahedron*, 64:10097–10106, 2008.

[28] Bruce E. Poling, John M. Prausnitz, and John P. O'Connell. *The Properties of Gases and Liquids*. McGraw-Hill, 5th edition, 2001.

[29] Russel Rhodes. Explosive lessons in hydrogen safety. *Ask Magazine*, 2011.

[30] E. Peter Roth, Chris C. Crafts, Daniel H. Doughty, and James McBreen. Advanced technology development program for lithium-ion batteries: Thermal abuse performance of 1860 li-ion cells. Report, SAND2004-0584, Sandia National Laboratories, March 2004.

[31] Francis Rouessac and Annick Rouessac. *Chemical Analysis: Modern Instrumentation Methods and Techniques*. John Wiley and Sons, Inc., 2nd edition, 2007.

[32] G. S. Settles. *Schlieren and Shadowgraph Techniques: Visualizing Phenomena in Transparent Media*. Springer-Verlag, 2001.

[33] Sigma Aldrich. *IR Spectrum Table and Chart*, 2022, https://www.sigmaaldrich.com/US/en/technical-documents/technical-article/analytical-chemistry/photometry-and-reflectometry/ir-spectrum-table.

[34] Neil S. Spinner, Christopher R. Field, Mark H. Hammond, Bradley A. Williams, Kristina M. Myers, Adam L. Lubrano, Susan L. Rose-Pehrsson, and Steven G. Tuttle. Physical and chemical analysis of lithium-ion battery cell-to-cellfailure events inside custom fire chamber. *Journal of Power Sources*, 279:713–721, 2015.

[35] R. Spotnitz and J. Franklin. Abuse behavior of high-power, lithium-ion cells. *Journal of Power Sources*, 113:81–100, 2003.

[36] Techtronic Industries Power Equipment. *Technical Data Sheet: Ryobi Lithium-Ion Battery Pack*, May 2016.

[37] L.G. Wade. *Organic Chemistry*. Pearson Prentice Hall Inc., 6th edition, 2006.

[38] Qingsong Wang, Binbin Mao, Stanislav I. Stoliarov, and Jinhua Sun. A review of lithium ion battery failure mechanisms and fire prevention strategies. *Progress in Energy and Combustion Science*, 73:95–131, 2019.

[39] Yong Zhou, Jiangtao Wu, and Eric W. Lemmon. Thermodynamic properties of dimethyl carbonate. *Journal of Physical and Chemical Referecne Data*, 40(043106), 2011.

APPENDIX A

ALL SPECIES POSSIBILITIES FOR MS ANALYSIS

The final species possibilities for the masses detected in the abuse test samples are:

Mass 12:
- No species possibilities known

Mass 13:
- No species possibilities known

Mass 14:
- Nitrogen ion

Mass 15:
- Borohydride ion

Mass 16:
- Methane
- Oxygen ion

Mass 17:
- Ammonia
- Hydroxyl ion

Mass 18:
- Water

Mass 19:
- Hydronium ion
- Fluorine ion

Mass 27:
- Hydrogen cyanide

Mass 28:
- Carbon monoxide
- Nitrogen
- Ethylene
- Diborane
- Borohydride ion

Mass 29:
- No species possibilities known

Mass 30:
- Nitric oxide
- Ethane
- Formaldehyde

Mass 31:
- Methylamine

Mass 32:
- Sulfur
- Oxygen
- Silane
- Methyl alcohol
- Hydrazine

Mass 33:
- No species possibilities known

Mass 34:
- Hydrogen sulfide
- Phosphine
- Methyl fluoride

Mass 36:
- Hydrogen chloride

Mass 38:
- No species possibilities known

Mass 39:

- No species possibilities known

Mass 40:

- Argon
- Cyclopropene
- Allene
- Propyne

Mass 41:

- Methyl isocyanide
- Acetonitrile

Mass 42:

- Ketene
- Propene
- Cyclopropane

Mass 43:

- No species possibilities known

Mass 44:

- Carbon dioxide
- Nitrous oxide
- Acetaldehyde
- Ethylene oxide
- Propane

Mass 45:

- Formamide
- Dimethylamine
- Ethylamine

Mass 46:

- Nitrogen dioxide
- Formic acid
- Ethanol

Mass 47:

- No species possibilities known

Mass 48:

- Methanethiol

Mass 58:

- Glyoxal
- Propanal
- Cyclopropanol
- Trimethylene oxide
- Acetone
- Propylene oxide
- Butane
- Isobutane

Mass 59:

- Acetaldoxime
- Acetamide
- Propylamine

Mass 60:

- Carbonyl sulfide
- Thiirane
- Methyl formate
- Acetic acid
- Urea
- Isopropyl alcohol
- Ethylenediamine

Mass 61:

- Methyl nitrite
- Cyanogen chloride

Mass 62:

- Boric acid
- Ethanethiol
- Dimethyl sulfide

Mass 91:

- Hydrazinecarbothioamide

APPENDIX B

WIRING DIAGRAM FOR TEST SETUP

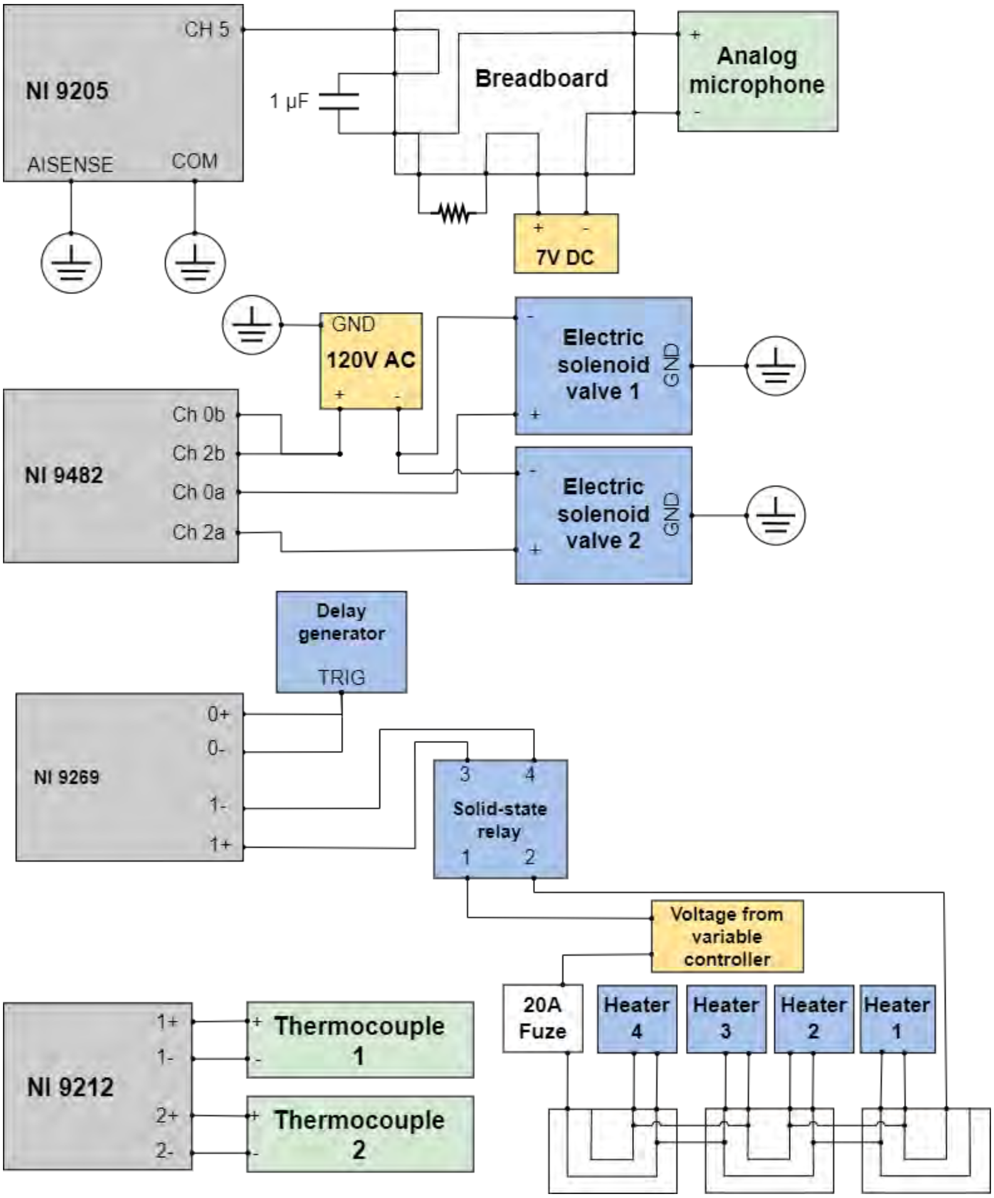

APPENDIX C

REDUCED-ORDER MODEL FOR LITHIUM-ION BATTERY VENTING SIMULATION

Written by Simone Hill
Last updated on: November 29, 2022

```
clc;
clear all;
close all;
```

Set up the Import Options and import the data

```
opts = spreadsheetImportOptions("NumVariables", 10);

% Specify sheet and range
opts.Sheet = "Sheet1";
opts.DataRange = "A2:J19";

% Specify column names and types
opts.VariableNames = ["Species", "LFL", "UFL", "R", "Cp", "Cv", "rho", "mw", "Class", "Formula"];
opts.VariableTypes = ["string", "double", "double", "double", "double", "double", "double", "double", "categorical", "string"];

% Specify variable properties
opts = setvaropts(opts, ["Species", "Formula"], "WhitespaceRule", "preserve");
opts = setvaropts(opts, ["Species", "Class", "Formula"], "EmptyFieldRule", "auto");

% Import the data
ChemSpecFlam = readtable("C:\Users\Simone\MATLAB Drive\SNL\ChemSpecFlam.xlsx", opts, "UseExcel", false);
```

Clear temporary variables

```
clear opts
```

System Variables

```
%System volume(s) (m^3)
Vol = (0.0001:0.0001:0.0405)';
%Calculating system mass with density of air (kg)
Mass = Vol * 1.205;
%Initial stagnation pressure (Pa)
P0i =  2.158 *10^6;
%Stagnation temperature (K)
Ti = 398.15;
%Number of cells in system
Cells = 1;
%Time increment
dt = 0.00001;
%Atmospheric pressure (Pa)
Patm = 101.3*10^3;
```

```
%Defining exit area for battery (m^2)
Ae = 8.967*10^(-6);
%Defining exit mach number of cell
Me = 1;
%Defining volume of battery cell (m^3)
BatVol = 1.52*10^(-6);

%Time cutoff (s)
endtime = 100 *10^(-3);
%Defining list of species from data sheet
SpecList = [ChemSpecFlam.Species];
%Defining info of species from data sheet
SpecInfo = [ChemSpecFlam(:,2:end)];
```

Species Determination

```
%Getting species from user input
[Spec,tf] = listdlg('ListString',SpecList);
%Getting indexes for chosen species
Index = Spec';
%Getting names of Species selected
Spec = ChemSpecFlam.Species(Spec);
%Getting gas properties of selected species
R = ChemSpecFlam.R(Index);
Cp = ChemSpecFlam.Cp(Index);
Cv = ChemSpecFlam.Cv(Index);
Rho = ChemSpecFlam.rho(Index);
MW = ChemSpecFlam.mw(Index);
LFL = ChemSpecFlam.LFL(Index);
UFL = ChemSpecFlam.UFL(Index);
Class = ChemSpecFlam.Class(Index);

%Determining inert species selected and properties of them
InSpec = find(Class=="I");
Spec_In = Spec(InSpec);
R_In = R(InSpec);
Cp_In = Cp(InSpec);
Cv_In = Cv(InSpec);
Rho_In = Rho(InSpec);
MW_In = MW(InSpec);
Class_In = Class(InSpec);
%Determining oxidizing species selectedand properties of them
OxSpec = find(Class=="O");
Spec_Ox = Spec(OxSpec);
R_Ox = R(OxSpec);
Cp_Ox = Cp(OxSpec);
```

```
Cv_Ox = Cv(OxSpec);
Rho_Ox = Rho(OxSpec);
MW_Ox = MW(OxSpec);
Class_Ox = Class(OxSpec);
%Determining flammable species selected and properties of them
FlSpec = find(Class=="F");
Spec_Fl = Spec(FlSpec);
R_Fl = R(FlSpec);
Cp_Fl = Cp(FlSpec);
Cv_Fl = Cv(FlSpec);
Rho_Fl = Rho(FlSpec);
MW_Fl = MW(FlSpec);
Class_Fl = Class(FlSpec);
LFL = LFL(FlSpec);
UFL = UFL(FlSpec);
```

Density adjustment

Adjusting density of each species based on temperature. Using P=(rho)(R_u)(T) to find initial pressure with density at room temperature and 25C for temp. Then finding new density assuming constant pressure and new temp

```
T_room = 298.15;
for i=1:1:length(Spec_In)
    P_temp = T_room*8.314*Rho_In(i);
    Rho_In(i) = P_temp/(Ti*8.31);
end
for i=1:1:length(Spec_Ox)
    P_temp = T_room*8.314*Rho_Ox(i);
    Rho_Ox(i) = P_temp/(Ti*8.31);
end
for i=1:1:length(Spec_Fl)
    P_temp = T_room*8.314*Rho_Fl(i);
    Rho_Fl(i) = P_temp/(Ti*8.31);
end
```

```
Ratio_In = zeros(length(Spec_In));
Ratio_Ox = zeros(length(Spec_Ox));
Ratio_Fl = zeros(length(Spec_Fl));
%Determing ratios of species from user input
for i=1:1:length(Spec_In)
    prompt = append('Input ratio (in decimal form) for', Spec_In(i));
    Ratio_In(i) = str2double(inputdlg(prompt));
end
for i=1:1:length(Spec_Ox)
    prompt = append('Input ratio (in decimal form) for', Spec_Ox(i));
    Ratio_Ox(i) = str2double(inputdlg(prompt));
```

```
end
for i=1:1:length(Spec_Fl)
    prompt = append('Input ratio (in decimal form) for', Spec_Fl(i));
    Ratio_Fl(i) = str2double(inputdlg(prompt));
end
```

Gas properties for the mixture

Universal gas constant (J/mol*K)

```
R_un = 8.314;

%Initializing mixture properties
%Molar mass of mixture
M = 0;
%Density of mixture
Rho_Mix = 0;
%Specific gas constant of mixture
R_Mix = 0;
%Specific heat sums
Cp_sum = 0;
Cv_sum = 0;
%Specific heat ratio of mixture
K_Mix = 0;

Rho_Mix = 0;
R_Mix = 0;
Gamma_Mix = 0;
for i = 1:1:length(Spec_In)
    %Calculating Rho for gas mixture
    Rho_Mix = Rho_Mix  + (Rho_In(i)*Ratio_In(i));
    %Calculating M for gas mixture
    M = M + (MW_In(i) * Ratio_In(i));
    %Calculating specific heat sums
    Cp_sum = Cp_sum + (Cp_In(i) * Ratio_In(i));
    Cv_sum = Cv_sum + (Cv_In(i) * Ratio_In(i));
end
for i = 1:1:length(Spec_Ox)
    %Calculating Rho for gas mixture
    Rho_Mix = Rho_Mix  + (Rho_Ox(i)*Ratio_Ox(i));
    %Calculating M for gas mixture
    M = M + (MW_Ox(i) * Ratio_Ox(i));
    %Calculating specific heat sums
    Cp_sum = Cp_sum + (Cp_Ox * Ratio_Ox(i));
    Cv_sum = Cv_sum + (Cv_Ox * Ratio_Ox(i));
end
```

```
for i = 1:1:length(Spec_Fl)
    %Calculating Rho for gas mixture
    Rho_Mix = Rho_Mix  + (Rho_Fl(i)*Ratio_Fl(i));
    %Calculating M for gas mixture
    M = M + (MW_Fl(i) * Ratio_Fl(i));
    %Calculating specific heat sums
    Cp_sum = Cp_sum + (Cp_Fl * Ratio_Fl(i));
    Cv_sum = Cv_sum + (Cv_Fl * Ratio_Fl(i));
end

%Calculating specific gas constant (J/mol*K)
R_Mix = R_un / M;
%Calculating specific heat ratio based on weigthed sums of each
K_Mix = Cp_sum / Cv_sum;
MoverT = zeros(length(Mass),endtime/dt,length(Spec));
```

Running Simulation

```
%Runs for each system volume defined
MassOx = zeros(length(Spec_Ox));
for m =1:length(Mass)
    % Initializing time, a flag, and counter
    time = 0;
    flag = 0;
    counter = 1;
    flamcounter = 0;
    unflamcounter = 0;

    %Setting stagnation pressure to initial stagnation pressure
    P0 = P0i;
    %Calculating initial pressure ratio
    PRatio = P0 / Patm;

    %Determining which Cd value to use in further calculations
    %based on the value of pressure ratio
     if PRatio > 3.2
        Cd = 0.95;
    elseif PRatio < 2.2
        Cd = 0.75;
    else
        Cd = 0.75 + ((PRatio-2.2)/5);
    end

    %Defining empty matrices
    GasMass_In = zeros(length(Spec_In));
    GasMass_Ox = zeros(length(Spec_Ox));
```

```
GasMass_Fl = zeros(length(Spec_Fl));
MassRatio = zeros(length(Spec_Fl));
%Initializing total mass variable
TotMass = 0;
%Calculating initial mass ratio for each species
MassOx(m) = Mass(m);
for s = 1:1:length(Spec_Fl)
    MassRatio = 100 * GasMass_Fl(s) / Mass(m);
end

%Calculating inital mass flow
MassFlow = Cd*(P0/sqrt(R_Mix*Ti))*Ae*sqrt(K_Mix)...
    *Me*(1+((K_Mix-1)/2)*Me^2)^((K_Mix+1)/(2-(2*K_Mix)));

%System runs for 3 ms based on Mier's dissertation (2020)
while time < endtime
    %Calculating change in pressure
    dP = -MassFlow * R_Mix * Ti * dt / BatVol;
    %Calculating new stagnation pressure
    P0 = P0 + dP;
    %Logging stagnation pressure at current time
    PoverT(counter) = P0;
    %Calculating new pressure ratio
    PRatio = P0 / Patm;

    %Determining value of Cd to be used based on
    %current pressure ratio
    if PRatio > 3.2
        Cd = 0.95;
    elseif PRatio < 2.2
        Cd = 0.75;
    else
        Cd = 0.75 + ((PRatio-2.2)/5);
    end

    %Calculating new mass flow rate
    MassFlow = Cd*(P0/sqrt(R_Mix*Ti))*Ae*sqrt(K_Mix)...
        *Me*(1+((K_Mix-1)/2)*Me^2)^((K_Mix+1)/(2-(2*K_Mix)));
   %Calculating mass of mixture entering the system
   dm = MassFlow * Cells * dt;
   TotMass = TotMass + dm;

   %Updating the mass of each oxidizer species
   for o=1:1:length(Spec_Ox)
       GasMass_Ox(o) = GasMass_Ox(o) + (dm*Ratio_Ox(o));
       MassOx(m) = MassOx(m) + GasMass_Ox(o);
```

```
    end
    %Updating the mass of each inert species
    for i=1:1:length(Spec_In)
        GasMass_In(i) = GasMass_In(i) + (dm*Ratio_In(i));
    end

    for x = 1:1:length(Spec_Fl)
         %Updating the mass of each flammable species
        GasMass_Fl(x) = GasMass_Fl(x) + (dm * Ratio_Fl(x));
        %Calculating new mass ratios for each flammable gas
        MassRatio(x) = 100 * GasMass_Fl(x) / (MassOx(m));
        MoverT(m,counter,x) = MassRatio(x);
        %Comparing each mass ratio to the species' flammability limits
        if MassRatio(x) >= LFL(x)
            if flag(x) == 0
                FlamTime(m,x) = time;
                flag(x) = 1;
                flamcounter = flamcounter + 1;
                %fprintf('The system')
            elseif flag(x) == 1
                if MassRatio(x) >= UFL(x)
                    UnFlamTime(m,x) = time;
                    flag(x) = 2;
                    unflamcounter = unflamcounter +1;
                    %fprintf('System unflam')
                end
            end
        end
    end
    %Increasing time by specified time increment
    time = time + dt;
    %Increasing counter
    counter = counter + 1;
end
    flag = 0;
    %Setting flam and unflam times to 0 if none of the
    %species ever reach their LFL, and setting only
    %unflam times to 0 if none of the species reach
    %their UFL
    if flamcounter == 0
        FlamTime(m,:) = 0;
        UnFlamTime(m,:) = 0;
    elseif flamcounter > 0
        if unflamcounter == 0
            UnFlamTime(m,:) = 0;
        end
```

```
        end
        %Setting final time of that run for that mass
        finalt(m,1) = time;
        if flamcounter == 0
            break
        end
end
```

Plotting simulation results

```
 %Plotting mass ratio versus time for each volume
times = linspace(0,endtime,(endtime/dt));
for y = 1:1:length(Spec)
    figure
    for x=1:1:length(FlamTime) -1
        plot(times,MoverT(x,1:length(times),y),'DisplayName',append(num2str(Vol(x)),' m^3'))
        hold on
    end
    set ( gca,'FontSize',16 )
    legend('Location','northwest','FontSize',20)
    xlabel('Time (s)','FontSize',18)
    ylabel('Mass Ratio','FontSize',18)
    title(append('Mass Ratio of ',Spec(y),' for Different System Volumes'),'FontSize',22)
    hold off
end

 %Tabulating data from simulation to be plotted
 LastFlamTime = FlamTime(length(FlamTime)-1);
 secondlast = FlamTime(length(FlamTime)-2);
 timelim = (2*LastFlamTime) - secondlast;

PlotFlam = FlamTime(FlamTime~=0);
PlotUnFlam = UnFlamTime(UnFlamTime~=0);
VolFlam = Vol(FlamTime~=0);
VolUnFlam = Vol(UnFlamTime~=0);

PlotFlamt = linspace(0,time);
pFlam = polyfit(PlotFlam,VolFlam,2);
pFlamp = polyval(pFlam,PlotFlamt);

plotUnFlamt = linspace(0,time);
pUnFlam = polyfit(PlotUnFlam,VolUnFlam,4);
pUnFlamp = polyval(pUnFlam,plotUnFlamt);
x2 = [PlotFlamt,fliplr(PlotFlamt)];
FlamRegion = [pFlamp,fliplr(pUnFlamp)];
```

```
tryplot = fit(PlotFlam,VolFlam,'exp2','Upper',[1000 1000]);
tryplot2 = fit(PlotUnFlam,VolUnFlam,'exp2');

%Plotting flammability and nonflammability times as a function of volume
figure,
p1(1) = plot(tryplot);
hold on
p1(2) = scatter(PlotFlam,VolFlam,2,'filled');
hold on
p1(3) = plot(tryplot2);
hold on
p1(4) = scatter(PlotUnFlam,VolUnFlam,2,'filled');
hold on

set(p1(1),'color',[0.1294 0.588 0.953],'linewidth',3);
set(p1(2),'MarkerFaceColor','b');
set(p1(3),'color',[0 0.784 0.325],'linewidth',3);
set(p1(4),'MarkerFaceColor',[0.08 0.28 0.08]);

test1 = [PlotFlam, fliplr(PlotFlam)];
testeq1 = (tryplot.a)*exp(tryplot.b*PlotFlam) + tryplot.c*exp(tryplot.d*PlotFlam);
testeq2 = (tryplot2.a)*exp(tryplot2.b*PlotFlam) + tryplot2.c*exp(tryplot2.d*PlotFlam);
inbetween = [testeq1, fliplr(testeq2)];
fill(test1,inbetween,'g');

set ( gca,'FontSize',19 )
xlim([0  timelim])
ylim([0 Vol(length(FlamTime))])
xlabel('Time (s)','FontSize',20)
ylabel('System Volume (m^3)','FontSize',20)
title('Flammability Map for 1 Cell','FontSize',28)
legend('Lower Flammability Limit Data','Lower Flammability Limit Curve Fit',...
    'Upper Flammability Limit Data','Upper Flammability Limit Curve Fit','Location','southeast');
```

Published with MATLAB® R2020b

APPENDIX D

TEST PLAN FOR LITHIUM-ION ABUSE EXPERIMENTS

NEW MEXICO TECH
ENERGETIC MATERIALS RESEARCH AND TESTING CENTER
1001 South Road • Socorro • NM • 87801 • telephone: 575.835.5312 • facsimile: 575.835.5630 • **www.emrtc.nmt.edu**
EMRTC - Committed to Excellence in the Fields of Energetic Materials Research, Testing and Training since 1947.

TEST PLAN

Lithium ion battery abuse testing and vacuum grab sampling

New Mexico Tech Mechanical Engineering Department
Dr. Michael Hargather
Michael.Hargather@nmt.edu

Author: Simone Hill
(575)956-8966
Simone.Hill@student.nmt.edu

Fund: MRBA50

Date: 08/02/2022

Lithium ion battery abuse testing and vacuum grab sampling

Research Project Summary:

Lithium ion batteries have a well-known tendency to fail violently under abuse conditions which can result in venting of flammable material. Understanding the chemical composition of the vented material can aid in evaluating safety associated with individual battery cells and battery packs when venting occurs. To capture the vented electrolyte material, vacuum grab samplers were built and will be used.

A testing setup was designed and constructed to control and vent the flammable environment surrounding the failing cell. The entire system is controlled and observed remotely using a LabVIEW VI in the control room. A venting system is installed in the opposite side of the enclosure from the battery. A 3" aluminum cube was machined to act as a heating chamber for the battery. The block holds one 18650 format lithium ion battery, four cartridge heaters, and two thermocouples. The cartridge heaters are controlled using a PID controller that is powered on using a National Instruments Relay controlled through LabVIEW. Thermocouples are also read with LabVIEW.

The grab samplers consist of a pneumatic actuated ball valve, a check valve, a stainless steel sample cylinder, and a regular ball valve connected in line in the order listed with appropriate adapters. A pressure transmitter is also in line to read absolute pressure in the sample cylinder and outputs values to LabVIEW. Two of these samplers were built and will both be used during all tests sampling either simultaneously or in sequence. Before testing, aa vacuum pump is used to pull vacuum in the sample cylinders. During a cell failure, aa microphone detecting an acoustic signal will trigger the grab sampling process whichwhich will open an pneumatic valve allowing flow into the sample cylinders. After power is turned off to the solenoid the sample cylinder will be closed, capturing the desired sample.

After each test, sample cylinder with check valve, and ball valve will be disconnected from pneumatic valve. The cylinders will then be transported out of EMRTC to Dr. Gayan Rubasinghege's Lab in Lopez on campus. After each test, the sample cylinders will be cleaned with a three-step process. First, cylinders will be flushed out thoroughly using Reverse Osmosis (RO) water. The cylinders will be sealed with the water and shaken vigorously. The cylinders will then be opened and the water will be emptied out. The same process is then completed using methanol. Then, the cylinders will be attached to each sampler. The battery test enclosure will be cleaned after each test to remove any residue.

To validate testing procedure, isolated vent caps will be ruptured using compressed carbon dioxide in place of the batteries. These tests will take place before any battery abuse testing. All other components of the test will be consistent with the battery abuse tests, except for the aluminum block will be removed and replaced with a mount for the vent caps, and the PID controller, cartridge heaters, and thermocouples will not be used.

Energetic Materials, Chemicals, or Hazardous Materials Involved:

- 18650 size lithium ion batteries (1 per abuse test)

Lithium ion battery abuse testing and vacuum grab sampling

- Methanol (cylinder cleaning)
- Compressed carbon dioxide (validation vent cap tests)
- BH-38 non-flammable degreaser (as needed for testing enclosure cleaning)

Location of Operations:

- Chemistry Lab 7 Control room for test control
- Chemistry Lab 7 testing room for test operation

Material Storage Requirements:

- Live batteries will be stored in the lockable flammables cabinet in the control room of L7
- Compressed gas cylinders will be stored with protective caps installed and chained to the optical table in the testing room of L7.
- All other chemicals will be stored in the lockable flammables cabinet in the control room of L7

Disposal Requirements:

- Abused/failed batteries, gloves, and soiled paper towels from tests will be placed in sealed bags within a satellite waste barrel. Batteries are to be stored within their own individual bag without other waste present. All bags are to be labeled with the hazards and specific cathode type present within the battery. Waste containers will be properly marked as "Hazardous Waste", contents, and hazards. Containers will be transported to campus and disposed of.

Required Personnel:

- All testing requires a lead test operator responsible for operations within the testing room.
- Tests will be facilitated by a data recorder who is responsible for controlling the LabVIEW based data acquisition program. The data recorder will double as a safety observer as they will not handle batteries or compressed gas during testing.
- Required to have 1 safety observer in the EMRTC Chem-Lab building while performing vent mechanism testing.
- Required to have 1 safety observer in L7 during grab sampling testing.
- Typical tests will have 2 people present: the test operator and the safety observer.
- Researcher and any assistants will complete test setup in both the control room and testing room of Lab 7
- When test is setup, all personnel will remain in the control room of Lab 7 with both doors to the testing room closed

Personal Protective Equipment (PPE):

- Safety glasses will be worn by all personnel present in the test chamber and control room during any testing.
- Ear plugs of muffs will be worn by all personnel during all vent mechanism testing.

Lithium ion battery abuse testing and vacuum grab sampling

- A lab coat and disposable gloves will be worn by any personnel involved in removing the failed battery
- See Attachment 2

Equipment Needed:

- Testing enclosure
- Aluminum battery mount
- Vacuum Grab Samplers
- Vacuum pump
- air compressor
- Electric solenoid valvest
- Microphone
- PID Controller and Solid State Relay
- Battery vent cap burst testing fixture
- National Instruments cDAQ
- Desktop computer in control room of L7
- High speed camera, laptop, light source, and Stanford Research Systems Digital Delay Generator
- Nitrile gloves
- Safety goggles
- Leather/heat resistant gloves

Planned Test Matrix:

- Varied placement of grab samplers within the testing enclosure
- Varied time after venting to sample
- Simultaneous and sequential sampling with the grab samplers
- Varied time of valve open

Planned Testing Schedule or Duration of Project:

Vent cap mechanism testing will be ongoing as remaining equipment arrives and test setup is within its validation phase. Hazardous operations will only be conducted during normal work hours (M-F, 8am-4:30pm). Battery abuse testing will begin when validation phase has concluded. Battery testing is to be performed within normal working hours, and tests will be started before 4:30 PM to ensure appropriate testing time without running late in the evening. Testing schedule and dates will also be communicated to ensure testing is on the EMRTC testing schedule.

References:

Include all references pertinent to the project (DELETE THOSE NOT NEEDED)

- SOP 101, Health and Safety
- SOP 103, Industrial Safety
- SOP 104, Laboratory Safety and Operations

Lithium ion battery abuse testing and vacuum grab sampling

- SOP 402, Emergency Action Plan
- SOP 403, Risk Management
- SOP 404, Hazardous Waste

Attachments:

1. Job Hazard Analysis
2. PPE Selection
3. Safety Data Sheets
4. Testing Procedure

Lithium ion battery abuse testing and vacuum grab sampling

Reviewed and Accepted List

Engineer/Project Manager	Print Name Signature	Date
Ordnance	Print Name Signature	Date
Instrumentation	Print Name Signature	Date
Field Supervisor	Print Name Signature	Date
Quality Control Engineer	Print Name Signature	Date
Associate Director	Print Name Signature	Date
Director	Print Name Signature	Date

The above blocks need to be signed off on only if they are pertinent to the project
(e.g. Field Supervisor signs off if there are TRO’s involved)

Lithium ion battery abuse testing and vacuum grab sampling

Test Plan Revision

Reason for revision:											
		Engineer Signature:									
		Date:									
Safety:		Ord:		Inst:		Field:		QA:		Dir:	
Reason for revision:											
		Engineer Signature:									
		Date:									
Safety:		Ord:		Inst:		Field:		QA:		Dir:	
Reason for revision:											
		Engineer Signature:									
		Date:									
Safety:		Ord:		Inst:		Field:		QA:		Dir:	
Reason for revision:											
		Engineer Signature:									
		Date:									
Safety:		Ord:		Inst:		Field:		QA:		Dir:	
Reason for revision:											
		Engineer Signature:									
		Date:									
Safety:		Ord:		Inst:		Field:		QA:		Dir:	

Attachment 1

Job Hazard Analysis

Attachment 2

PPE Selection

Attachment 3

Safety Data Sheets

Attachment 4

Testing Procedure

Lithium ion battery abuse testing and vacuum grab sampling

Testing Procedure/Checklist:

1. Test Setup:
    - 1.1 Ensure all connections for sensor and hoses are secure
    - 1.2 Turn on power supply and set voltage for pressure transducers to 15.0 V, and voltage for microphone to 7.0 V
    - 1.3 Ensuring regulator is turned all the way down, turn on air compressor until tank pressure reaches 120 psi
    - 1.4 Clean testing enclosure windows

2. Schlieren Setup:
    - 2.1 Power on computer, camera, and Stanford Delay Generator
    - 2.2 Open Photron Software on camera control computer
    - 2.3 Ensure clean alignment of imaging setup
    - 2.4 Set variables: resolution, frame rate, shutter speed
    - 2.5 Ensure settings on Stanford Delay Generator: External trigger, rising (Check this), voltage level of 1.0 V

3. Cleaning Sample Cylinders:
    - 3.1 Put on gloves
    - 3.2 Obtain 2 sample cylinders and ensure one end is sealed on each
    - 3.3 Clean cylinders one at a time:
        - 3.3a Pour 20-30 mL of Reverse Osmosis (RO) water into open end of cylinder
        - 3.3b Seal the cylinder
        - 3.3c Shake cylinder vigorously for 5 seconds
        - 3.3d Open one end of cylinder and pour out RO water into a sealed container to later dispose
        - 3.3e Pour 25 mL of methanol into the open end of one cylinder
        - 3.3f Seal the cylinder
        - 3.3g Swirl methanol in sealed cylinder for 5 seconds, ensuring every area of internal surface is thoroughly coated
        - 3.3h Shake cylinder vigorously for 10 seconds
        - 3.3i Unseal one end
        - 3.3j Careful pour remaining methanol into seal amber waste bottle to later transport to campus to dispose of in Dr. Rubasinghege's chemistry lab
        - 3.3k Place cylinder with unsealed end down into cylinder stand
        - 3.3l Repeat steps 3.a. – 3.g. for the second cylinder
        - 3.3m Leave cylinders to drain for 2 minutes
    - 3.4 Once cylinders are dry, attach the check valve on the cylinder to the pneumatic valve mounted on the sampler stands using thread sealant tape

4. Abuse testing:
    - 4.1 Open LabVIEW VI and ensure connection with DAQ and each module
    - 4.2 Ensure all variables are set accurately
    - 4.3 Based on current trial from testing matrix, define sample time after failure, sample duration time, and time between samples
    - 4.4 Begin running VI

4.5 Place safety signs on both doors and around bay door
4.6 Turn on cameras for test monitoring and begin recording on all three systems
4.7 Turn on venting system and run ventilation out bay door; venting system will run for entirety of test
4.8 Coat each cartridge heater (4 in total) in thermal paste and insert into heater each hole in aluminum block mount
4.9 Coat each thermocouple (2 in total) in thermal paste and inset into each thermocouple hole in aluminum block mount
4.10 Based on current trial from testing matrix, place grab samplers at desired locations
4.11 Pull vacuum in sample cylinders:
  4.11a Connect hose from vacuum pump to quick-connect end of one sampler, and open ball valve
  4.11b Turn on vacuum pump until low pressure is reached
  4.11c Close ball valve and turn off vacuum pump
  4.11d Disconnect hose from quick-connect
4.12 Disconnect quick-connect from one sampler and attach to the other using more thread sealant tape if needed
4.13 Repeat steps 11a-11d for second sampler
4.14 Open regulator valve on air compressor to 100-105 psi and ensure switch on compressor is on to keep tank pressure between 120 and 150 psi
4.15 Obtain one 18650 format battery and carefully remove red plastic cover
4.16 Apply a thin coat of thermal paste to the cell and insert into the front of the aluminum block mount
4.17 Replace window of testing enclosure and secure in place
4.18 If using schlieren:
  4.18a Using camera control computer, take a snapshot for later analysis and save into folder
  4.18b Ready the computer in software
4.19 Return to control room and ensure all doors to the testing room are closed
4.20 Run grab sampling sequence in VI
  4.20a In LabVIEW, set minimum temperature to 171°C and maximum temperature to 172°C, but DO NOT turn "heating" switch on
  4.20b Determine average microphone current reading (i.e., -2.4) and set the microphone cutoff to the absolute value of the reading minus 0.25 (i.e., for a reading of -2.4, cutoff should be set at 2.15)
  4.20c Stop and start LabVIEW VI
  4.20d Turn on grab sampling sequence and heating switches in VI. This begins heating the aluminum 18650 mounting block and cell in the block using four cartridge heaters and monitoring system
  4.20e Monitor temperature of two thermocouples and estimated temperature of the cell waiting until failure, which should occur after 125°C
  4.20f When thermal runaway begins, disk in vent cap within the cell will break and an analog microphone will detect the break and trigger the next steps
    4.20g When failure is detected, system will wait a set time and then send power to the two electric solenoid valves which directs the air from the compressor to the pneumatic valves allowing them to open

- 4.20h Air will be pulled into the sample cylinder through the open pneumatic valves from the vacuum in the cylinder
- 4.20i After a set time, power will be cut from the electric solenoid valves and the air will be redirected out of a muffler which then closes the pneumatic valves and seals the cylinders
- 4.20j Turn heating off to stop heating the block allowing it to begin cooling
- 4.20k Grab sampling sequence is then complete

4.21 After failure and samples occur, researcher must until thermocouples read 93℃ before re-entering testing room
4.22 Once in testing room, turn air compressor regulator off and box fan on
4.23 Wait to proceed until thermocouples read 60℃
4.24 While wearing thermally protective gloves, carefully remove failed cell from the mounting block and follow disposal procedure listed in research plan
4.25 Carefully remove sample cylinders from samplers, ensuring they are sealed prior to removal
4.26 Place cylinders into transport container
4.27 Turn venting system off
4.28 Stop LabVIEW VI
4.29 Turn off power supply
4.30 Transport cylinders to Dr. Rubasinghege’s laboratory on campus

The main hazard of these tests is the flammability environment created by the failure of the cell

5. IN THE EVENT OF SYSTEM IGNITING:

5.1 All personnel remain in the control room with both of the doors to the testing room closed
5.2 Turn off grab sampling sequence and heating switches to allow mounting block to begin cooling
5.3 Assess situation through all security cameras and identify location of fire
5.4 If safe to enter testing room on far end, safety operator will take fire extinguisher into test room and attempt to extinguish fire
5.5 Allow system to vent out through hood and out the bay doors until battery has finished venting gases and it is safe
5.6 Once safe, enter testing room turn air compressor regulator and venting system off
5.7 While wearing gloves, carefully remove failed cell from the mounting block and follow disposal procedure listed in research plan
5.8 Inspect sample cylinders and pneumatic valves for any damage
5.9 If no damage is present, carefully remove sample cylinders from samplers and begin testing process again from initial cleaning on page 9

6. IN THE EVENT OF CELL NOT VENTING:

6.1 All personnel remain in the control room with both of the doors to the testing room closed
6.2 Remain with grab sampling sequence and heaters on at 161℃ for up to 5 minutes
6.3 If cell fails within 5 minutes, resume testing procedure at step 21
6.4 If cell does not fail, turn off heating switch in VI

6.5 Wait to proceed until thermocouples read 60°C
6.6 Then, wearing a lab coat, face shield, and thermally protective gloves, enter testing room and obtain disposal bucket containing sand
6.7 Carefully remove cell from mounting block and place into sand in disposal container
6.8 Ensure cell is fully covered in sand
6.9 Reseal disposal bucket and place outside of bay door